NORSAR

ROYAL NORWEGIAN COUNCIL FOR SCIENTIFIC AND INDUSTRIAL RESEARCH

NORSAR Scientific Report No. 1–86/87

SEMIANNUAL TECHNICAL SUMMARY

1 April – 30 September 1986

L.B. Loughran (ed.)

Kjeller, November 1986

UNCLASSIFIED
SECURITY CLASSIFICATION OF THIS PAGE

REPORT DOCUMENTATION PAGE

1a. REPORT SECURITY CLASSIFICATION UNCLASSIFIED	1b. RESTRICTIVE MARKINGS NOT APPLICABLE
2a. SECURITY CLASSIFICATION AUTHORITY NOT APPLICABLE	3. DISTRIBUTION/AVAILABILITY OF REPORT APPROVED FOR PUBLIC RELEASE DISTRIBUTION UNLIMITED
2b. DECLASSIFICATION/DOWNGRADING SCHEDULE NOT APPLICABLE	
4. PERFORMING ORGANIZATION REPORT NUMBER(S) SCIENTIFIC REPORT 1-86/87	5. MONITORING ORGANIZATION REPORT NUMBER(S) SCIENTIFIC REPORT 1-86/87
6a. NAME OF PERFORMING ORGANIZATION NTNF/NORSAR 6b. OFFICE SYMBOL (If applicable) GSD	7a. NAME OF MONITORING ORGANIZATION HQ/AFTAC/TGX
6c. ADDRESS (City, State and ZIP Code) POST BOX 51 N-2007 KJELLER, NORWAY	7b. ADDRESS (City, State and ZIP Code) PATRICK AFB, FL 32925-6001
8a. NAME OF FUNDING/SPONSORING ORGANIZATION DEFENCE ADVANCED RESEARCH PROJECT AGENCY 8b. OFFICE SYMBOL (If applicable)	9. PROCUREMENT INSTRUMENT IDENTIFICATION NUMBER CONTRACT NO. F08606-86-C-0004
8c. ADDRESS (City, State and ZIP Code) 1400 Wilson Blvd Arlington, VA 22209-2308	10. SOURCE OF FUNDING NOS. PROGRAM ELEMENT NO.: R&D PROJECT NO.: NORSAR PHASE 3 TASK NO.: SOW TASK 5.0 WORK UNIT NO.: SEQUENCE NUMBER 003A2
11. TITLE (Include Security Classification) SEMIANNUAL TECHNICAL SUMMARY 1 APR-30 SEPT 86 (UNCLASSIFIED)	
12. PERSONAL AUTHOR(S) L.B. LOUGHRAN (ED.)	
13a. TYPE OF REPORT SCIENTIFIC SUMMARY 13b. TIME COVERED FROM 1 APR TO 30 SEP 86	14. DATE OF REPORT (Yr., Mo., Day) NOV 86 15. PAGE COUNT 117
16. SUPPLEMENTARY NOTATION NOT APPLICABLE	

17. COSATI CODES			18. SUBJECT TERMS (Continue on reverse if necessary and identify by block number)
FIELD	GROUP	SUB. GR.	
8	11		NORSAR, NORWEGIAN SEISMIC ARRAY

19. ABSTRACT (Continue on reverse if necessary and identify by block number)

This Semiannual Technical Summary describes the operation, maintenance and research activities at the Norwegian Seismic Array, (NORSAR) for the period 1 April - 30 September 1986.

20. DISTRIBUTION/AVAILABILITY OF ABSTRACT UNCLASSIFIED/UNLIMITED ☒ SAME AS RPT. ☐ DTIC USERS ☐	21. ABSTRACT SECURITY CLASSIFICATION UNCLASSIFIED
22a. NAME OF RESPONSIBLE INDIVIDUAL CAPT JAMES A. ROBB	22b. TELEPHONE NUMBER (Include Area Code) (305) 494-7665 22c. OFFICE SYMBOL AFTAC/TGX

DD FORM 1473, 83 APR EDITION OF 1 JAN 73 IS OBSOLETE.

UNCLASSIFIED
SECURITY CLASSIFICATION OF THIS PAGE

UNCLASSIFIED

19. (cont.)

The NORSAR Detection Processing system has been operated through the reporting period with an average uptime of 99.3 per cent. A total of 2218 seismic events have been reported by NORSAR in the period. The performance of the continuous alarm system and the automatic bulletin transfer by telex to AFTAC have been satisfactory. Processing of requests for full NORSAR/NORESS data on magnetic tape has progressed without problems.

An investigation into further potential improvements in the NORSAR array processing system has taken place. From analysis results, some of which have been reported in earlier Semiannual Reports, it has been found to be worthwhile to implement full 20 Hz processing of NORSAR data, which will involve installing 8 Hz analog filters, new detection processor coding and new event processor coding.

Field maintenance activity has included regular preventive maintenance at all subarrays and occasional corrective actions as required. No special problems have been noted in the performance of the field installations. In addition, field maintenance personnel have participated in experiments involving the High Frequency Seismic Element (together with Sandia representatives), as well as noise measurements and reconnaissance for selecting a site for a possible new small array.

We have developed a method for obtaining phase velocity and azimuth using broadband f-k analysis, and compared the results to the monochromatic f-k analysis used in the RONAPP program. The method has been applied to a set of 10 mining explosions in Western Norway. The broadband azimuth results are consistent within 1-2 degrees, whereas the single-frequency results show a scatter of 5-10 degrees. Moreover, it has been possible, using the broadband method, to obtain a complete separation between the Sn and Lg phases, based on phase velocity measurements.

In a continuation of our studies of 3-component processing techniques, we have investigated whether or not the observed displacement response from regional Sn-phases is well suited for three-component slowness vector estimation. The success of such processing depends on our ability to predict the displacement pattern. In our theoretical calculations, these patterns have, however, shown strong model dependency, and will therefore be difficult to predict reliably.

A study of the usefulness of horizontal components in detection and phase identification has been carried out, using a data base of 17 seismic events at local and regional distances. Using incoherent beamforming, there is a clear gain in including all horizontal and vertical instruments together, especially for Sn detection. The amplitude ratio between vertical and radial components has been shown to be a promising criterion for phase identification. Averaging data for 4 3-component NORESS instruments, we found that 25 out of 29 secondary phases (Sn and Lg) could be correctly classified.

We have undertaken a study to determine how the noise suppression characteristics can best be exploited in the detection of regional and teleseismic phases at NORESS. For a sequence of events, we have applied the seven bandpass filters currently in use in the online processing (1.0-3.0 Hz, 1.5-3.5 Hz, 2.0-4.0 Hz, 2.5-4.5 Hz, 3.0-5.0 Hz, 4.0-8.0 Hz, 8.0-16.0 Hz) and computed SNR for beams using different subgeometries and compared it to average single sensor SNR. The main results for P-detection are as follows:

- The advantage in applying a number of digital filters has been confirmed.

- There is, for each filter band, one array subgeometry that provides the best SNR. In all cases processed, a subgeometry different from the full array provides the largest SNR.

- The achievable beamforming gain relative to single sensor ranges from 10 to 17 dB, and is highest at frequencies between 2 and 5 Hz. At frequencies above 3 Hz, steered beams are necessary to achieve 10 dB gain.

An automatic algorithm has been implemented to compute and store noise spectra from NORESS and the HFSE once every hour. The spectra comprise individual channels as well as beams based on subgeometries of NORESS. The preliminary results earlier reported have been further confirmed. Thus: during weekends and holidays, the noise level is very stable at all frequencies, whereas cultural noise during weekdays causes some significant diurnal variations. These are only minor (± 2 dB or less) below 2 Hz, increasing slightly up to 5 Hz and becoming very strong around 6 Hz (± 10 dB). At frequencies above 8 Hz, the variations are again modest (typically ± 3 dB). The noise peak around 6 Hz has been found to originate from a sawmill 15 km away from NORESS. We have also found indications that the volume of water flow in nearby rivers can influence the noise level significantly.

We have also used the automatic spectral generation program to conduct studies of noise suppression on NORESS beams, using different subarray configurations. The noise suppression characteristics are quite stable over time, and show no strong dependency on the noise level (e.g., suppression during nighttime and daytime is similar, even though the actual noise level is quite variable). The studies have confirmed that

(a) better than $\sqrt{N}$ suppression can be consistently achieved at selected frequencies and subconfigurations and (b) at selected frequencies a subgeometry can outperform the full array. We have in particular conducted a comprehensive analysis of a 1-week interval, using hourly computed noise spectra on NORESS single sensors and subgeometry beams (infinite velocity). The results, based upon more than 5,000 noise spectra, are summarized as follows:

(i) Full array geometry (A0, A, B, C, D rings, 25 instruments)

Noise suppression of $\sqrt{N}$ (14 dB for N = 25) is consistently achieved in the band 2.5-20.0 Hz.

(ii) A0, C, D geometry (17 instruments, $\sqrt{N} \sim 12$ dB)

Noise suppression greater than 14 dB is achieved in the band 1.5-3.0 Hz. This subgeometry is superior to the full array for all frequencies below 3 Hz.

(iii) A_0, B, C geometry (13 instruments, $\sqrt{N} \sim 11$ dB)

Noise suppression greater than 14 dB is achieved in the band 3.0-5.5 Hz.

(iv) A_0, A, B geometry (9 instruments, $\sqrt{N} \sim 9.5$ dB)

Noise suppression does not match that of the full array, but still averages 11 dB in the band 6.0-20.0 Hz.

AFTAC Project Authorization	:	T/6141/B/PMP
ARPA Order No.	:	4138
Program Code No.	:	0F10
Name of Contractor	:	Royal Norwegian Council for Scientific and Industrial Research
Effective Date of Contract	:	1 October 1985
Contract Expiration Date	:	30 September 1986
Project Manager	:	Frode Ringdal (02) 71 69 15
Title of Work	:	The Norwegian Seismic Array (NORSAR) Phase 3
Amount of Contract	:	$ 686,546.00
Contract Period Covered by the Report	:	1 Apr - 30 Sep 1986

This research was supported by the Advanced Research Projects Agency of the Department of Defense and was monitored by AFTAC, Patrick AFB, FL 32925, under contract no. F08606-86-C-0004.

NORSAR Contribution No. 372

TABLE OF CONTENTS

I. SUMMARY

This Semiannual Technical Summary describes the operation, maintenance and research activities at the Norwegian Seismic Array (NORSAR) for the period 1 Apr - 30 Sep 1986.

The uptime of the NORSAR online detection processor system has averaged 99.3 per cent during the reporting period, which is slightly higher than for the previous half-year period. The array communications system has generally shown a reliable performance. A total of 2218 seismic events were reported in the NORSAR monthly seismic bulletins in this period, giving a daily average of 12.1 events.

During this reporting period an investigation into further potential improvements in the NORSAR array processing system has taken place. From analysis results, some of which have been reported in earlier Semiannual Reports, it has been found to be worthwhile to implement full 20 Hz processing of NORSAR data, which will involve installing 8 Hz analog filters, new detection processor coding and new event processor coding.

Field maintenance activity has included regular preventive maintenance at all subarrays and occasional corrective actions as required. No special problems have been noted in the performance of the field installations. In addition, field maintenance personnel have participated in experiments involving the High Frequency Seismic Element (together with Sandia representatives), as well as noise measurements and reconnaissance for selecting a site for a possible new small array.

The research activity is summarized in section VII. Section VII.1 discusses the stability of various f-k estimation techniques. Section VII.2 presents a three-component analysis of secondary phases, while the applicability of horizontal components for detection and phase discrimination is assessed in Section VII.3. In Section VII.4 the topic of optimum beam deployment for NORESS P-wave detection is discussed. Sections VII.5 - VII.7 present various NORESS noise spectral studies, including system description (VII.5), beam suppression (VII.6) and noise level characteristics (VII.7).

II. OPERATION OF ALL SYSTEMS

II.1 Detection Processor (DP) Operation

There have been 72 breaks in the otherwise continuous operation of the NORSAR online system within the current 6-month reporting interval. The uptime percentage for the period is 99.3 as compared to 98.8 for the previous period.

Fig. II.1.1 and the accompanying Table II.1.1 both show the daily DP downtime for the days between 1 April and 30 September 1986. The monthly recording times and percentages are given in Table II.1.2.

The breaks can be grouped as follows:

a)	Hardware failure	3
b)	Stops related to program work or error	1
c)	Hardware maintenance stops	6
d)	Power jumps and breaks	4
e)	TOD error correction	36
f)	Communication lines	23

The total downtime for the period was 30 hours and 4 minutes. The mean-time-between-failures (MTBF) was 2.5 days, as compared to 2.4 for the previous period.

J. Torstveit

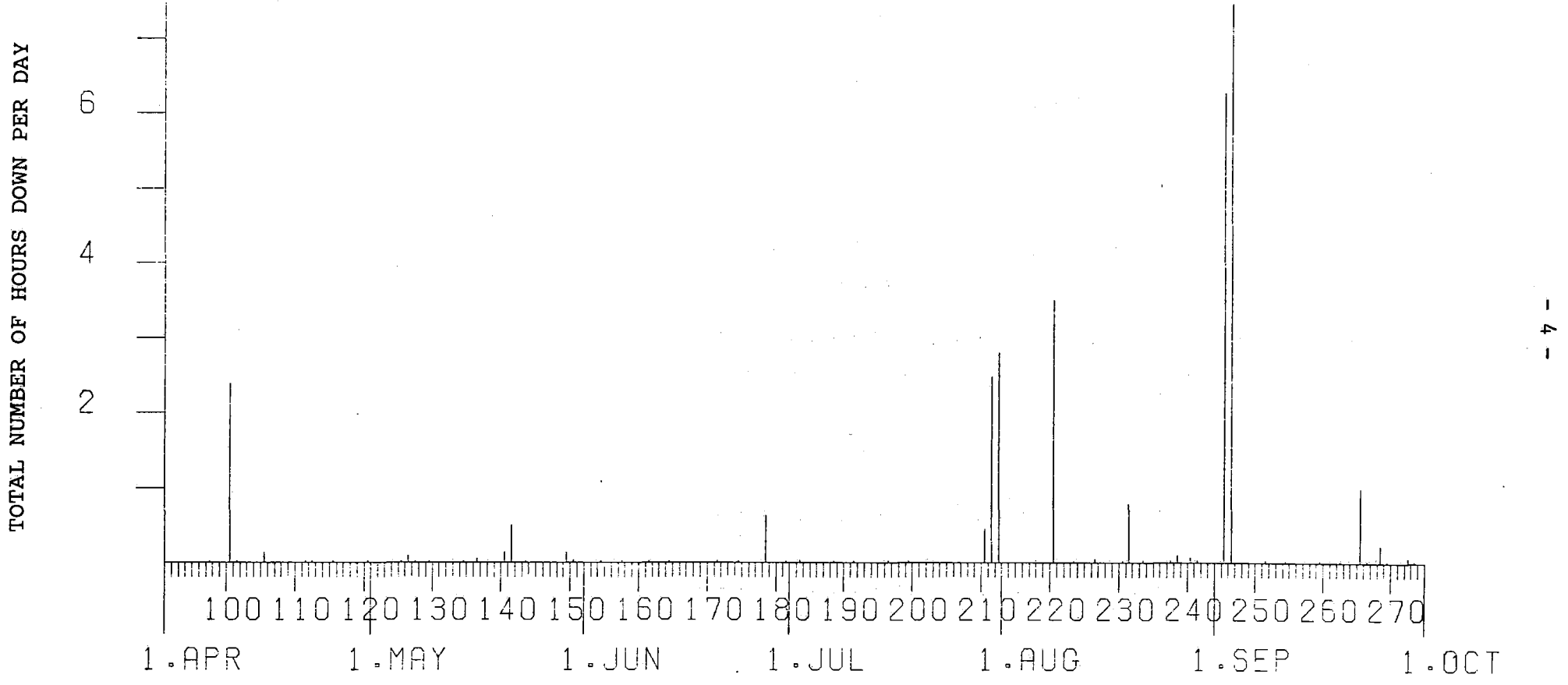

Fig. II.1.1 Detection Processor downtime in the period 1 Apr - 30 Sep 1986.

LIST OF BREAKS IN DP PROCESSING THE LAST HALF-YEAR

DAY	START		STOP		COMMENTS.....
97	6	2	6	3	TOD RETARED 65MS
100	8	28	10	51	CE MAINTENANCE DISK
101	6	2	6	3	TOD RETARED 25MS
105	6	0	6	3	TOD RETARED 26MS
105	12	12	12	17	CE MAINTENANCE CPU A
111	6	2	6	3	TOD RETARED 33MS
112	9	9	9	10	LINE FAILURE
115	6	1	6	2	TOD RETARED 26MS
115	6	13	6	14	LINE FAILURE
120	10	23	10	24	TOD RETARED 40MS
125	6	22	6	23	TOD RETARED
126	6	32	6	33	TOD RETARED
126	13	47	13	48	TOD RETARED
126	13	47	13	50	LINE FAILURE
127	11	21	11	22	LINE FAILURE
129	6	1	6	2	TOD RETARED 26MS
134	6	0	6	1	LINE FAILURE
136	6	51	6	54	TOD RETARED 15MS
140	6	1	6	2	TOD RETARED 26MS
140	12	45	12	52	SYSTEM FAILURE
141	11	50	12	20	POWER FAILURE
143	9	46	9	47	TOD RETARED 30MS
149	12	25	12	33	POWER FAILURE
150	6	0	6	2	TOD RETARED 34MS
154	11	3	11	4	LINE FAILURE
157	6	14	6	15	TOD RETARED
161	6	30	6	31	TOD RETARED 30MS
164	6	1	6	2	TOD RETARED 20MS
171	12	2	12	3	TOD RETARED 26MS
174	6	4	6	5	TOD RETARED 47MS
178	6	12	6	47	MODCOMP FAILURE
178	9	16	9	19	LINE FAILURE
181	7	12	7	13	TOD RETARED 26MS
183	6	3	6	4	TOD RETARED 14MS
183	12	2	12	3	LINE FAILURE
188	6	14	6	15	TOD RETARED 33MS
191	6	1	6	2	TOD RETARED 23MS

DAY	START		STOP		COMMENTS.....
196	6	36	6	37	TOD RETARED 33MS
199	6	3	6	4	TOD RETARED 25MS
210	7	11	7	12	LINE FAILURE
210	14	44	15	10	DISK FAILURE
211	14	0	16	0	DISK SERVICE
211	20	27	20	56	DISK FAILURE
212	10	0	12	48	DISK SERVICE
220	14	58	18	28	POWER BREAKE
223	6	19	6	20	TOD RETARED 160MS
226	5	54	5	55	TOD RETARED 25MS
226	8	40	8	42	LINE FAILURE
230	7	33	7	34	TOD RETARED 25MS
231	10	24	11	10	DISK SERVICE
231	13	4	13	5	LINE FAILURE
233	6	0	6	2	TOD RETARED 25MS
237	6	1	6	2	TOD RETARED 25MS
237	20	23	20	24	LINE FAILURE
238	6	43	6	49	LINE FAILURE
240	6	14	6	16	TOD RETARED 25MS
240	13	1	13	3	LINE FAILURE
241	11	54	11	56	LINE FAILURE
245	12	30	12	31	LINE FAILURE
245	12	37	12	38	LINE FAILURE
245	17	45	24	0	LINE FAILURE
246	0	0	7	28	LINE FAILURE
251	6	3	6	5	TOD RETARED 35MS
254	6	1	6	2	TOD RETARED 24MS
259	6	0	6	2	TOD RETARED 30MS
262	6	1	6	2	TOD RETARED 25MS
265	8	10	9	10	SERVICE MODCOMP
266	6	1	6	2	TOD RETARED 24MS
268	7	12	7	13	LINE FAILURE
268	9	7	9	20	POWER FAILURE
269	6	1	6	2	TOD RETARED 24MS
272	7	8	7	12	LINE FAILURE
273	12	44	12	45	LINE FAILURE
273	12	56	12	57	LINE FAILURE

Table II.1.1 Daily DP downtime in the period 1 Apr - 30 Sep 1986.

Month	DP uptime hours	DP uptime %	No. of DP breaks	No. of days with breaks	DP MTBF* (days)
APR	717.37	99.6	10	8	2.7
MAY	742.98	99.9	13	11	2.2
JUN	719.25	99.9	9	8	3.0
JUL	738.16	99.2	11	8	2.6
AUG	739.37	99.4	14	10	2.1
SEP	704.78	97.9	15	12	1.8
		99.3	72	57	2.5

* Mean-time-between-failures = total uptime/no. of up intervals.

Table II.1.2 Online system performance, 1 Apr - 30 Sep 1986.

II.2 Data communications

Automatic telex transmission of NORSAR DPX/EPX and NORESS detection lists to AFTAC has proceeded normally in the period. NORESS bulletins have been transmitted daily (weekdays only, with weekends included in following Monday's bulletin) to the CSS via ARPANET throughout the period. The performance of these transmissions has been satisfactory.

Processing requests by AFTAC for complete NORSAR/NORESS data files covering selected time intervals has progressed normally during the period. Such data are currently copied to magnetic tapes in standard formats, and the tapes are mailed through the APO system. NORSAR also regularly handles requests for NORSAR, NORESS and HFSE data from various U.S. Government contractors.

Table II.2.1 reflects the performance of all communications systems in the NORSAR array during the reporting period. The most affected systems have been 02C and 04C. The other systems have also been affected, although less frequently.

The most common reason for the irregularities has been defective/ damaged cables, faulty equalizers, attenuated lines (causing reduced level to modems), lightning (specially 04C, 06C), and faulty modem cards. In addition, scheduled maintenance activities and corrective actions initiated here at the NDPC and the subarrays created error figures.

Summary

Apr 86 02B was out of operation 20 to 22 and 25 April due to a faulty cable between Hamar and the subarray.

A failing equalizer at Lillehammer telestation caused outages 1 and 2 May.

The other communications systems were most reliable.

May 86 A bad cable, unstable equalizer and a failing modem were the main reasons for 02B, 02C and 04C performance reduction in May.

Jun 86 Apart from a period with reduced performance at 04C (week 23, 24), the communications system performance may be characterized as most reliable for June.

10 and 11 June 04C was visited and input level to the subarray was found too low (-30.0 dBm) and fluctuating. The NTA found a defective equalizer at the telestation in Elverum. Correct input level to the subarray was obtained after replacement, and C-loop (digital loop) back to normal operation.

Jul 86 Apart for lightning affecting 02C (week 31), most reliable performance also in July.

Aug 86 All communications systems except 01B and 02B affected in August.

01A. A bad cable caused reduced performance. NTA/Hamar repaired the cable 29 August.

02C. In connection with "spikes" on all channels, NTA/ Lillestrøm notified 11 August. NTA/Hamar and Lillehammer found a damaged cable between Mesnalien and Hornsjø. NTA/ Hamar finished the repair 28 August.

03C. Week 34 and 35 this subarray was affected frequently. Low level on the communications path toward Kjeller (-30.0 dBm). B- and C-loop also failed. As NTA was not able to take immediate action, as they were busy the actual date, the communications system remained in this status throughout the month.

04C. The subarray was affected by the end of week 34, and remained so also week 35 due to low level toward Kjeller. Level adjusted to accepted level 27 August by NTA/Hamar, and system resumed operation.

06C. A damaged cable caused spikes in data week 33 and 34. NTA/Hamar repaired the cable, which had been damaged by lightning.

Sep 86 Scheduled cable work carried out by NTA/Lillestrøm outside LFK (Air Force Supply Command) on 2 September affected all systems longer than planned. Instead of an estimated couple of hours outage, the systems remained down until the next morning at approx. 0730 GMT. Besides, 03C was unreliable, as sporadic outages occurred specially weeks 38 and 39. A bad contact somewhere along the communications path was assumed to have caused the irregularities. When the subarray was visited 25 September all connections related to the communications system were checked for possible bad connections. The B/C-loop which had been out of order for a while was repaired. The subarray was left fully operational, under control of the Input Command Words (ICWs) from Kjeller. On 29 September the 03C communications system again failed.

O.A. Hansen

Sub-array	APR 86 (5) (31.3-4.5)	MAY 86 (4) (25.5-1.6)	JUN 86 (4) (2-29.6)	JUL 86 (5) (30.6-3.8)	AUG 86 (4) (4-31.8)	SEP 86 (4) (1-28.9)	Average ½ yr
01A	0.068	0.009	0.006	0.051	1.320	3.141	0.766
01B	*4.820	0.009	0.002	0.090	0.078	2.694	1.282
02B	*3.680	*7.146	0.002	0.019	0.028	2.692	2.261
02C	*5.374	*36.615	0.001	0.196	*51.360	3.138	16.114
03C	0.015	0.003	0.002	0.026	*20.989	*21.510	7.091
04C	0.034	1.551	0.642	0.089	*6.269	3.140	1.954
06C	0.081	0.002	0.001	3.601	*8.024	3.582	2.549
AVER	2.010	6.476	0.094	0.582	12.581	5.700	4.574
Less	01B,02B 02C	02B,02C	-	06C	*02C,03C **02C-06C	03C	02C
	0.161	1.874	-	0.079	*3.144/**0.475	3.065	2.650

* see item II.2 regarding figures with asterisks

Table II.2.1 Communications performance. The numbers represent error rates in per cent based on total transmitted frames/week (1 Apr - 30 Sep 1986).
Note that the percentages refer to times when data were recorded at Kjeller; therefore this table must be seen in conjunction with Table II.1.2.

III. ARRAY PERFORMANCE

Event Processor Operation

In Table III.1 some monthly statistics of the Event Processor operation are given:

	Teleseismic	Core Phases	Sum	Daily
APR 86	273	55	328	10.9
MAY 86	450	59	509	16.4
JUN 86	309	128	437	14.6
JUL 86	295	90	385	12.4
AUG 86	236	68	304	9.8
SEP 86	200	55	255	8.5
	1763	455	2218	12.1

Table III.1 Event Processor Statistics, April - September 1986.

B. Paulsen

IV. IMPROVEMENTS AND MODIFICATIONS

During this reporting period we have investigated further the potential for improvements in the NORSAR array processing system. The results obtained for the NORESS array, and for NORSAR SPZ channels with 8 Hz analog filter, show that the large array should have a potential for better processing capability both for teleseismic and regional events.

The NORSAR recording system store the short period data at a 20 Hz sample rate, whereas as real-time processing is done using 10 Hz data. The analog anti-aliasing filter cuts data above 4.75 Hz, which is of course a result from designing the array for teleseismic detection. From our analysis results, some of which have been reported in earlier Semiannual Reports, we have found it worthwhile to implement full 20 Hz processing of NORSAR data. This involves installing 8 Hz analog filters, new detection processor coding and new event processor coding.

Today the NORSAR data is received by the MODCOMP Classic processor, where filtering and subarray beamforming is also done. The raw 20 Hz data plus 10 Hz filtered subbarray beams are transmitted to the NORSAR processor (IBM 4341). Here, array beam detection processing and data recording is done, as well as event processing and plotting. All processing is done using 10 Hz data. The event processor beampacking procedure uses time delay corrections observed at the subarray level, with a resolution of 10 Hz.

In the process of converting to 20 Hz processing, we have identified two main tasks.

a. Rewriting the detection processor task to perform beamforming and filtering at a 20 Hz rate.

b. Collect a new data base of time delay corrections for event location using a new beam set.

During the planning of software for these processes, a considerable effort has been devoted to the design of the programs. We are in a situation where rather specialized software has previously been implemented both for NORSAR and NORESS processing. The code for these systems can not easily be adopted for other arrays or other computer systems. We therefore recognize the need for a software design that fulfills some basic criteria, like:

a. The processing tools used on the data (filtering, beamforming, detection processing,...) must be coded in high level language, it must follow defined rules for code documentation and the code must not be tied to particular instrumentation parameters.

b. The data collecting routines may use system efficient program tools, but must interface array processing tools via standard parameters.

Looking at the NORSAR detection system and the NORESS RONAPP system, we find the following infinite processing loop:

1. Get next data buffer. (Finite length, time right after former buffer).
2. Filter the data. (Have to use some of the former data buffer).
3. Form a finite number of beams. (Some of former buffer used). Use a preset beam configuration list with preset delays.
4. Do STA/LTA processing on each beam.
5. Use rules for declaring a detection.

6. If detection, optionally use other array processing tools (e.g., f-k analysis).
7. Report and present plot of detection if any.
8. Go to 1.

Looking at many other processing schemes (like interactive analyst review of detected events), we find a similar pattern. We specify a time for data and get a data buffer (1), we optionally filter the data (2), we adopt some processing on the data (processing tool, 4,5,6,7), but we do not go into an infinite loop.

Let us define these two processing schemes as continuous and singular processing. Let us also define the terms online and offline processing: Online processing is defined as a system that collects and processes data from the instruments in near real time. Offline is defined as a process where the array data are read in from the system's data recording medium and subsequently processed. Presently, the NORSAR detection processing system is in this sense online. The NORESS detection processing system (RONAPP) is in this sense offline. The data recording tasks of both systems are online.

The array processing systems must in both cases, online or offline, be able to process one second of data using less than one second of elapsed time, in order to keep up with continuous operation.

It is clearly desirable to develop one common software package to process either NORSAR, NORESS or any other array or even single instrument, both in continuous and singular mode. We must then specify the necessary parameters that define an operation, and divide the computer programs into smaller routines that perform commonly used processes. Such routines will be called array signal processing tools. The different tools are easily classified for continuous or singular processing. Filtering, beamforming, STA and LTA are processing measures

that must be programmed for both modes of operation, whereas f-k analysis is a typical singular operation.

We have elsewhere in this report, and earlier reports, seen the results from the DISPAT program (Harris and Kværna, NORSAR Sci. Rep. No. 2-84/85). This program is typically written for singular operations, but tools have been tested, using this package, that may be suited for implementation in the array processing systems. We have therefore begun the process of defining "rules" for the tools, i.e., we will develop software such that there is one and only one routine for each tool, and we will find the same routine in packages of the DISPAT type of program and in offline array processing systems, both for singular and continous operations.

So far we have adopted this concept in three parts of the "array processing loop". We have defined which parameters that describe the reading of a data buffer, and we have developed these programs both for NORSAR and NORESS data. There will be only one data buffer input routine. Today this routine reads NORSAR, NORESS and HFSE data from tape, online disk and disk files, and may run in an offline processing mode. Moreover, we have developed the programs for generating filters and filter a data buffer both for singular and continuous operation.

We are currently working with general programs for presenting the instrument data. This work has been done in conjunction with the process of developing a new time delay data base for NORSAR beams, using 20 Hz data and using all present instruments (42). For this purpose we need a good analyst's tool for reviewing computed delays.

During the process of developing the data buffer routines, we have also studied the NORSAR line communication problems more closely. We have identified that ICW/ODW reported errors may generate spikes in the data and hence false detections, as described in NORSAR Sci.rep.no. 2-85/86. Results from new data routines that repeat a

former sample if an error is notified, show that the data quality can be significantly improved.

We note that adopting this concept means that it will be necessary to run the array detection system in an offline mode. This may not mean a large processing delay, since data can in many cases be read back very quickly. E.g., for NORSAR, recording is done on disk, and an offline detection package may run with a time delay equal to the length of the data buffer. If 10 seconds of data buffer is selected, the detection system does not need to be more than 11 - 12 seconds behind real time.

The benefits of the above approach relative to running in the online mode are, e.g., that processing can be stopped and resumed at any time, and that it is easy to perform reruns over specific time intervals using different parameters. Moreover, using the general data buffer read routines, and processing tools following the rules, we may theoretically use data from any array, any medium (disk, disk file, tape, communication link), and even several arrays, in the processing packages.

Examples of the programs developed so far are shown in Figs. IV.1-4. The one general input routine reads data from the NORSAR, NORESS and HFSE recording systems, stores the data in internal buffers and presents the data to the general plot routine. We have defined rules for setting up data buffers to such an extent that in fact the actual variable names are the same for different programs, i.e., when looking at different array processing tools (subroutines) there are a set of predefined variable names (FORTRAN arrays), which mean the same, and are organized in the same way in different programs. This means that

we can present our data to for example DISPAT, and use the data directly, e.g., to obtain spectra as shown in Fig. IV.2.

By implementing the plot routine used in Figs. IV.1,3 and 4, the user has at once an interactive tool available where the data traces on the plot can be manipulated with. The results from such manipulations can optionally be presented to the calling program. In Fig. IV.3 , the user has selected DELAYS with a graphics cursor control, and he has pointed out individual arrival times. Then on Fig. IV.4 , the traces have been plotted with corresponding time delays. This may then be used as a starting point for iterative cross-correlation in order to determine the time delay anomalies for a given array beam relative to the best plane wave fit.

With respect to the NORSAR 20 Hz upgrade, we have set up the following implementation plan:

1. Based on new array signal processing tools, implement NORSAR offline detection system using 20 Hz data, and run it in parallel with the present on-line detection system.

After acceptance of part 1,

2. Complete the upgrading of subarray electronics with 8 Hz filters.

3. Remove subarray beamforming and filtering from MODCOMP.

4. Remove the 'old' NORSAR detection system, thus retaining only the new off-line system, (this must of course be run in a close to real-time mode).
   Keep the present online recording system.

5. Implement a new time delay correction data base, and use this to improve the detection processor beam delays.

6. Replace the present NORSAR Event Processing system with a new array processing package based on the general approach outlined here and incorporating the new time delay correction data base.

J. Fyen

References

Harris, D.B. and T. Kværna (1985): Interactive analysis program for use with NORESS data, Semiannual Technical Summary, 1 Oct 84 - 31 Mar 85, NORSAR Sci. Rep. No. 2-84/85, Kjeller Norway.

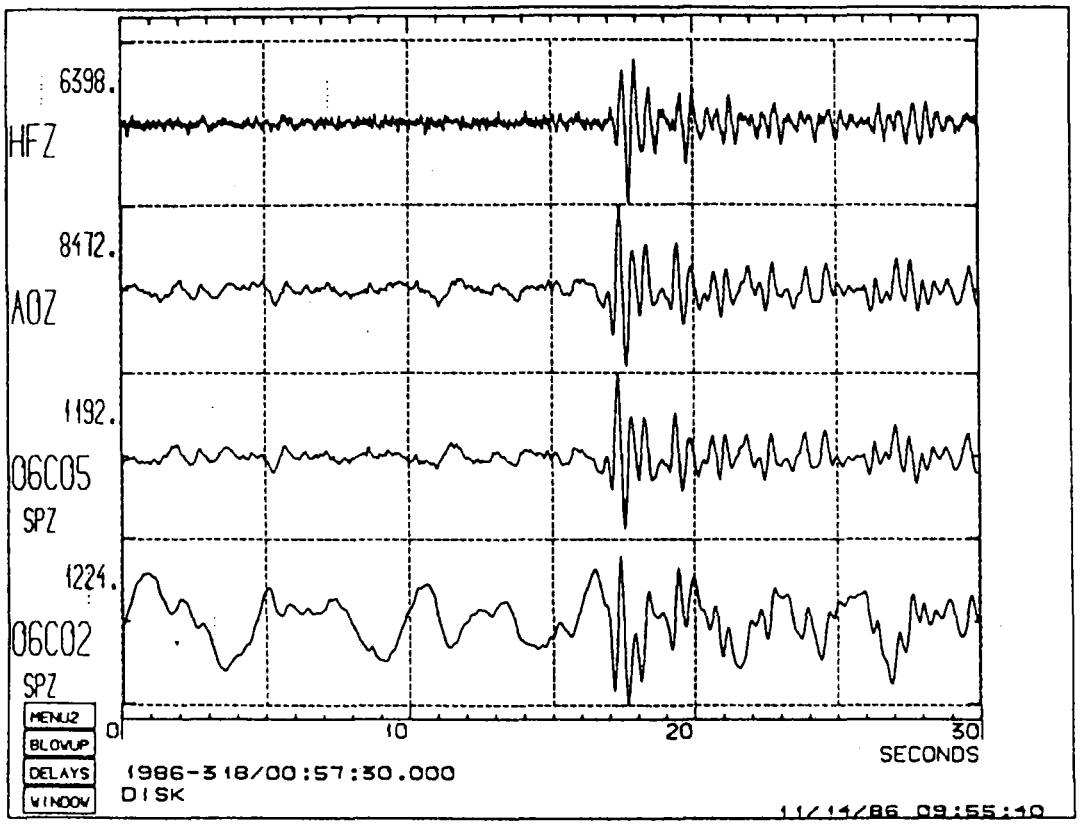

Fig. IV 1. Example of a teleseismic event recorded by NORSAR 06C02 and 06C05, NORESS AOZ and HFSE-Z. All instruments are located at the NORESS vault. 06C02 is a HS-10 instrument with 4.75 Hz cutoff frequency sampled at 20 HZ. 06C05 is a HS-10 instrument sampled at 20 Hz, but with analog filters designed to give an instrument response close to the NORESS GS-13 instrument. AOZ and HFZ is data taken from the same GS-13 instrument. AOZ is sampled at 40 Hz, and HFZ is sampled at 125 Hz.

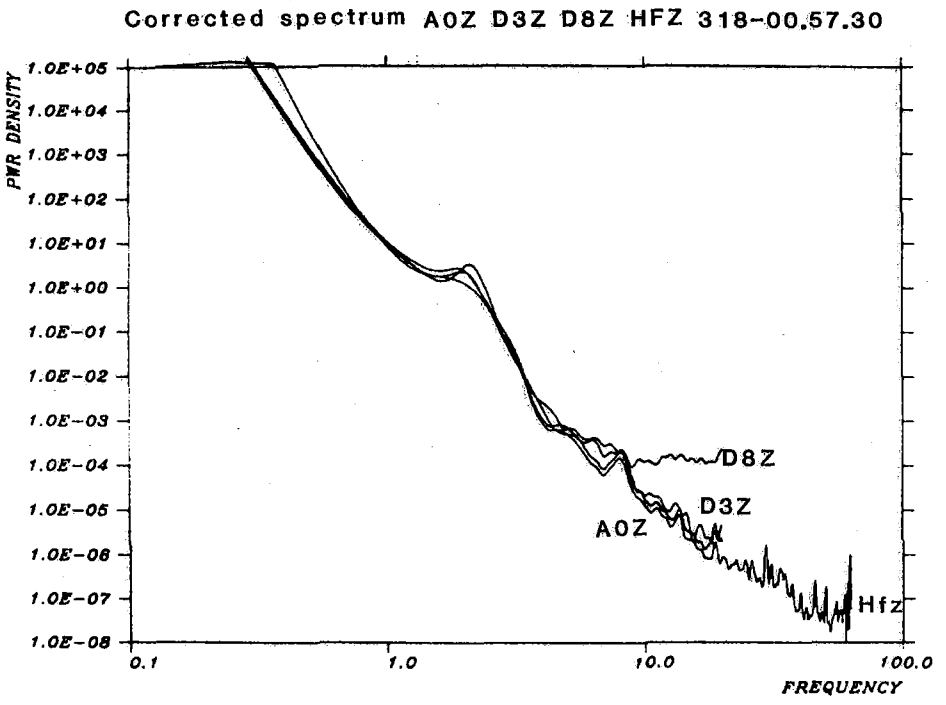

Fig. IV.2 DISPAT power spectra of the event in Fig. IV.1. The spectra are based on 20 seconds of signal for HFZ, A0Z, D3Z and D8Z, respectively. The spectra have been corrected for instrument response. The power density unit is nm^2/Hz.

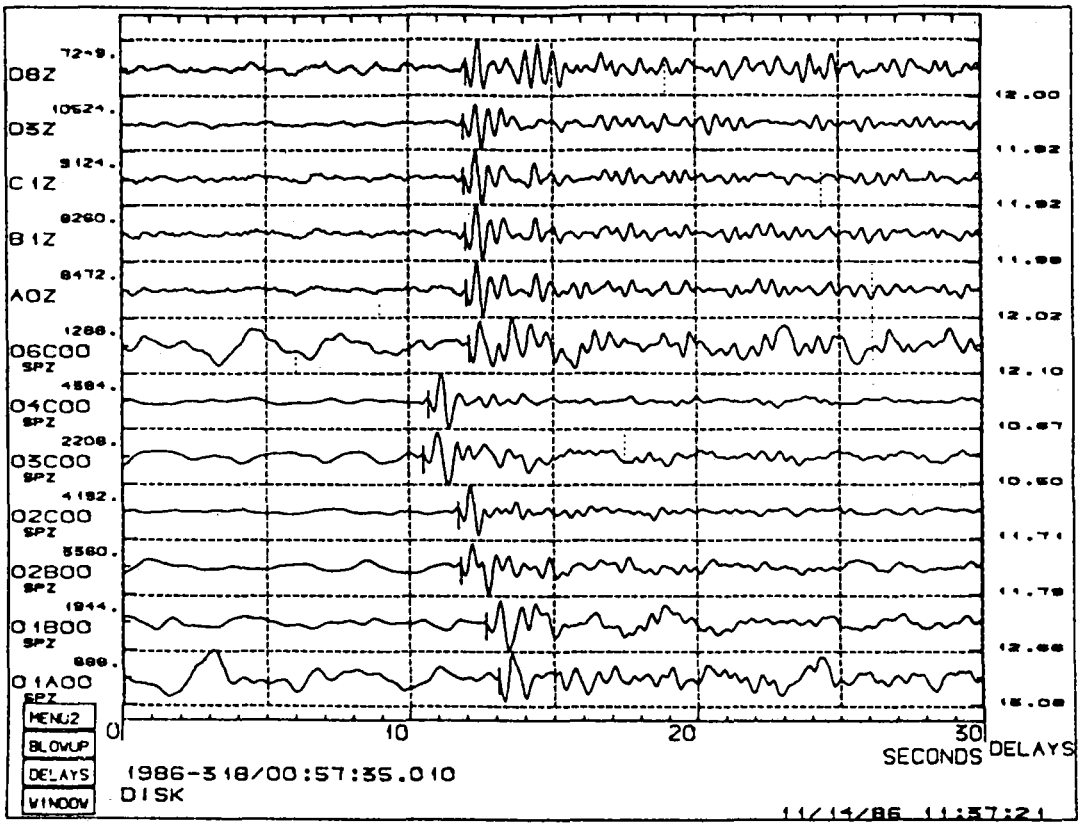

Fig. IV.3 Example of use of the plot routine. (QTPLOT). The analyst has selected the option DELAYS on the plot menu. As the marker is used, the selected values are plotted.

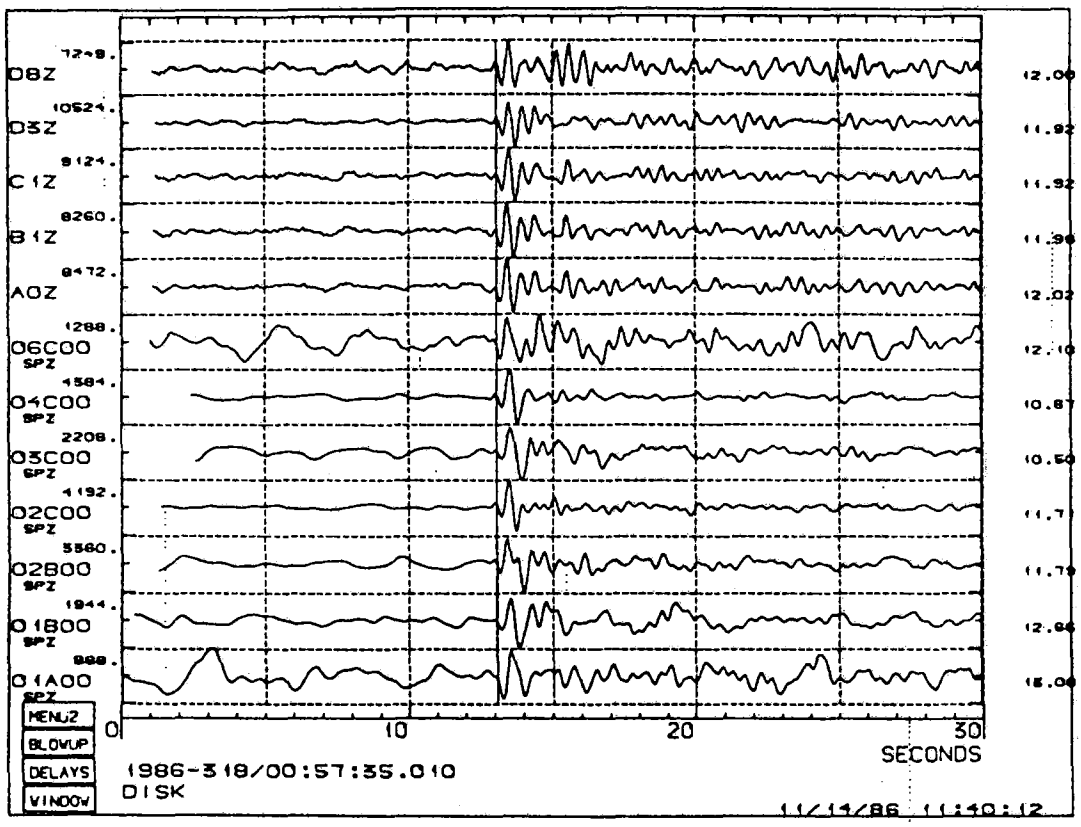

Fig. IV.4 Same data as in Fig. IV.3, but with the channels delayed according to the selected arrival times.

V. MAINTENANCE ACTIVITIES

V.1 Activities in the field and at the Maintenance Center

The NMC staff has been engaged in a wide range of tasks during the period, comprising corrective/preventive maintenance of NORSAR/NORESS, HF-experiments (together with Sandia representatives), as well as noise measurements and reconnaissance for selecting a site for a possible new small array.

At the NDPC NORSAR communications circuits (comprising modems and lines) have been supervised/monitored. The NORSAR subarray electronics have been checked and monitored on a routine basis.

A summary of the activities performed during the period is given in Table V.1.

For completeness we list activities carried out on both systems, i.e., NORSAR and NORESS.

Subarray/ area	Task	Date
02B (Tel.)	Replaced defective power regulator at the receiving station	18 Apr
NORESS	CID OF moved to site A3	1 Apr
	CID 22 moved to site C2	"
	Satellite transmitter frequency adjusted	27 Apr
	Transmitter frequency checked	28 Apr
NDPC/ Kjeller	Daily SP/LP data check. SP/LP calibration weekly	April
	SP-channels evaluated OFFLINE by means of "CHANEV SP" program.	
	A/D converters checked for correct reproduction of numbers within a given range by means of a "MISNO" program.	
	Long period seismometers with parameters outside specifications adjusted.	
NORESS	Frequency test with Medley, England	14 May
	Visit to the array after lightning had blown fuses in the mains transformer	22 May
	Modem fault caused by lightning located	24 May
	Faulty voltage charger located	29 May
NDPC/ Kjeller	Daily/weekly checks and monitoring. LP seismometer adjustments	May
04C	EW Mass Pos. and Free Period Remote Centering Devices (RCDs) replaced	10 Jun
	Line input level (-33.0 dBm) measured. NTA adjusted to -19.5 dBm.	11 Jun
	EW Free Period adj. SP-channel 1-4 gain adj.	
01A	Mass Pos. and Free Period all LP instruments adjusted. SP-channel 1,2,3 and EW gain adj.	23 Jun
04C	Mass Pos., Vert., NS and Free Period EW adjusted. SP-channel gain 2,4 and all LP channels adjusted	24 Jun
06C	Mass Pos. and Free Period all LP seismometers adjusted. SP-channel gain 1,3,4 and all LP channels adjusted.	30 Jun

Subarray/ area	Task	Date
01A, 04C 06C	LPV/CTV lids and WHV covers painted. CTV batteries cleaned, checked and filled with water. LPV/CTV cleaned inside	June
NORESS	Hub visited in connection with modem/multiplexer check	5 Jun
NDPC/ Kjeller	Daily/weekly checks and monitoring, incl. verifying the RSA/ADC's ability to reproduce all possible numbers within a given range (5 subarrays), by means of the OFFLINE program "MISNO"	
01B, 02B 02C, 03C	Corrective/preventive program which started 10 June finished for the remaining subarrays.	July
	SP/LP channel gain and LP-seismometer mass pos. adjustment on channels/instruments outside specifications	
04C, 05	Cable trace pointed out	
NORESS	Time of day clock repaired	2 Jul
NDPC/ KJeller	LP/SP data checked daily and weekly calibration "MISNO" program 03C, 04C and 06C run	July
06C	Internal LPV maintenance, incl. LPV tanks which were opened and painted.	5-12 Aug
01B	Channel gain SP01, 04 and NS,EW adjusted	13 Aug
	Mass Pos. (MP) NS and EW adjusted.	
	Tank NS seismometer opened and seismometer readjusted	
01B	RA-5 amplifier SP05 replaced. Top of LPV/CTV painted	14 Aug
NORESS	Several HF experiments together with Mr. Kromer of Sandia carried out	15-30 Aug
NMC	A complete 3-channel SP-outfit prepared for Blåsjø	
NDPC/ Kjeller	Daily SP/LP data check; weekly SP/LP calibration	Aug

Subarray/ area	Task	Date
NMC	Final preparation of Blåsjø 3-channel SP outfit	Sept
Karasjok/ Finnmark	Noise measurements and reconnaissance	7-10 Sept
Blåsjø	Installation of the equipment prepared at the NMC	15-19 Sept
Karasjok/ Finnmark	Selection and marking of all seismometer points	19-22 Sept
03C	Visit to the subarray in connection with communications line/modem check and SP01 cable	25 Sept
NDPC/ Kjeller	Daily SP/LP check; weekly SP/LP calibration. SP-channel evaluation (-03 C) by means of CHANEV SP program	Sept

Table V.1 Activities in the field and at the NORSAR Maintenance Center, including NDPC activities related to the NORSAR array, April - September 1986.

V.2 Improvements and modifications (NORSAR array)

No changes during the reporting period.

V.3 Array status

As of 30 September 1986 the following channels deviated from tolerances:

01A	01	8 Hz filters
	02	"
	04	attenuated 30 dB
01B	05	
02C	08	
03C	08	
04C	01	
06C	05	8 Hz filter
	08	

O.A. Hansen

VI. DOCUMENTATION DEVELOPED

Bache, T.C., S.R. Bratt and H. Bungum (1986): High-frequency P-wave attenuation along five teleseismic paths from Central Asia, Geophys. J. R. Astr. Soc., 85, 505-522.

Havskov, J. and H. Bungum: Source parameters for earthquakes in the northern North Sea, submitted for publication.

Husebye, E.S., S.F. Ingate and E. Thoresen (1986): Seismic arrays for everyone, In: A.U. Kerr (ed.), The VELA Program, A Twenty-Five Year Review of Basic Research, DARPA, 526-545.

Loughran, L.B. (ed.): Semiannual Technical Summary, 1 October 1985 - 31 March 1986, NORSAR Sci. Rep. No. 2-85/86, Kjeller, Norway.

Mykkeltveit, S. (1986): A new regional array in Norway: Design work and results from analysis of data from a provisional installation, In: A.U. Kerr (ed.), The VELA Program, A Twenty-Five Year Review of Basic Research, DARPA, 546-553.

Paulsen, R.: NORESS Online System, NORSAR Technical Report No. 1/86, Kjeller, Norway.

Ringdal, F. (1986): Study of magnitudes, seismicity and earthquake detectability using a global network, In: A.U. Kerr (ed.): The VELA Program, A Twenty-Five Year Review of Basic Research, DARPA, 611-624.

L.B. Loughran

VII. SUMMARY OF TECHNICAL REPORTS/PAPERS PREPARED

VII.1 Stability of various f-k estimation techniques

Experience with real-time NORESS processing has shown that estimates of phase velocity and azimuth of regional phases usually contain a fair amount of uncertainty. Thus, the median azimuth difference between P and Lg of the same event in RONAPP was found to be 5 degrees for a set of 132 Western Norway events (Mykkeltveit, 1985). In some cases, the difference exceeded 10 degrees, and although this performance is sufficiently good for phase association purposes, there is clearly a possibility of significant errors in locating the event under such circumstances.

Kværna and Doornbos (1986) described a method to estimate the slowness vector using arrays of either vertical or 3-component seismometers. They compared the performance of various algorithms (e.g., beamforming versus maximum likelihood, single frequency vs wide-band) for the P phases of a set of 5 events from approximately the same location (Leningrad region). Their conclusion was that conventional f-k processing of vertical sensor data provided more stable estimates than estimates obtained by similar processing of three-component arrays or sensors.

In this paper we pursue this investigation further, by concentrating on conventional f-k estimation (single frequency and wide band) for a suite of reference events of known origin. We have selected a set of 10 chemical explosions from a dam construction site (Blåsjø) in southern Norway:

Site coordinates:	59.31°N 6.95°E
True azimuth from NORESS:	240.19 degrees
Distance from NORESS:	301.2 km

The size of the explosions are typically 50 tons TNT. All of the events have a high SNR at NORESS; thus noise interference in the slowness vector estimates is minimal.

A list of the reference events is given in Table VII.1.1. An example of NORESS recordings (Event 1) produced by RONAPP is shown in Fig. VII.1.1. The spectra for P, S_n, Lg and the preceding noise are displayed in Fig. VII.1.2.

Fig. VII.1.3 shows the results of f-k analysis of the P_n phase for each of the 10 events. Four different methods have been chosen for frequency selection:

a) Narrow band - variable frequency

The frequency f_o selected for each event is the dominant frequency of the signal as determined by the cycle count method in RONAPP.

b) Broadband - variable frequency

Processing is done in the band $[f_o - f_o/4, f_o + f_o/4]$ where f_o is the dominant frequency.

c) Narrow band - 7.0 Hz

In this case the frequency has been kept fixed (f_o = 7.0 Hz) for all events.

d) Broadband 5.25 - 8.75 Hz

This is analogous to b) but with f_o = 7.0 Hz kept fixed for all events.

It is clear from the figure that by far the most stable result is obtained by method d). As seen in Table VII.1.2, the mean azimuth is

estimated at 242.19 deg, and the maximum spread around the mean is only ±1 degree.

We also conducted f-k processing of the S_n and Lg phases of the 10 events, using the fixed frequency band approach, i.e., corresponding to c) and d). Fig. VII.1.4 shows the results for the single frequency case (4 Hz), plotted together with the P_n results from c) above. We notice that the azimuth spread is larger for the two secondary phases. There is a clear distinction between the estimated phase velocities of the primary and secondary phases, and the S_n phase velocities tend to be larger than those of Lg.

In Fig. VII.1.5, a similar plot is presented corresponding to the broadband, fixed frequency approach (cf. d) above). We now see a clear phase velocity separation among all three phase types. In addition, estimated azimuths are generally consistent, although the scatter is somewhat larger for S_n and Lg than for P_n. Table VII.1.3 gives the detailed results for estimating the slowness vectors of the S_n and Lg phases, corresponding to the broadband case.

We also conducted some experiments, changing slightly the windowing positioning used for the f-k analysis and also in assessing the effects of introducing elevation correction for the NORESS seismometers. These did not produce any significant changes in the overall results, and do not appear to be factors of critical importance.

In conclusion, the broadband f-k estimation approach clearly provides the most stable estimates of azimuths and apparent velocities based on the data and methods applied in this investigation. It is particularly encouraging that we were able to obtain consistent separation between the S_n and Lg phases, based on phase velocity measurements alone. It must be noted, however, that all of the events processed had high signal-to-noise ratios, and the performance of the method at low SNR

is at present more uncertain. It also appears that the fixed frequency band approach is preferable in processing and comparing a suite of events from the same general area. However, the "best" frequency band to process will be regionally dependent, and criteria for selecting such bands need to be further developed.

T. Kværna
F. Ringdal

References

Kværna, T. and D.J. Doornbos (1986): An integrated approach to slowness analysis with arrays and three-component stations. Semiann. Tech. Summary, 1 Apr - 30 Sep 1986, NORSAR Sci. Rep. No. 2-85/86, Kjeller, Norway

Mykkeltveit, S. (1985): Evaluation of NORESS real-time processing performance: Case study for 132 Western Norway/North Sea events, Final Technical Report, 1 Apr - 30 Sep 1985, NORSAR Sci. Rep. No. 1-85/86, Kjeller, Norway.

Event Name	Date	Origin time	SNR P-phase	Magnitude M_L
BL1	06/04/85	03.13.59	209.6	2.3
BL2	06/07/85	14.42.39	62.7	2.0
BL3	06/19/85	13.03.53	20.2	2.5
BL4	06/27/85	08.45.37	17.0	2.1
BL5	06/28/85	15.42.12	33.4	2.0
BL6	07/02/85	12.55.59	16.3	2.1
BL7	07/03/85	20.28.01	25.1	2.4
BL8	07/05/85	03.59.29	45.6	2.3
BL9	07/16/85	17.33.12	115.8	2.5
BL10	07/29/85	13.55.18	42.0	2.8

Table VII.1.1 List of events used in this study. The table specifies event date, origin time, signal-to-noise ratio of the P-phase as computed by RONAPP and local magnitude (M_L). All of the events are located near the Blåsjø site 59.3°N, 6.95°E.

Broad-band, Pn-phase without elevation correction

VELMEAN	AZMEAN	THETA	PROB	SA	SB	SXMEAN	SYMEAN
7.99	242.19	-3.42	0.95	0.005640	0.001879	-0.110649	-0.058369

Event	Phase	Start	Stop	Freq	Delta	Azimuth	Velocity	Pmax
BL1	P	29.5	32.5	7.0	1.75	241.55	8.2107	0.6201
BL2	P	29.5	32.5	7.0	1.75	241.70	8.0854	0.5999
BL3	P	29.7	32.7	7.0	1.75	243.35	7.9359	0.5988
BL4	P	29.0	32.0	7.0	1.75	242.65	7.9497	0.5611
BL5	P	29.4	32.4	7.0	1.75	241.43	8.0618	0.5713
BL6	P	28.6	31.6	7.0	1.75	242.46	7.9134	0.5770
BL7	P	29.1	32.1	7.0	1.75	242.78	7.7779	0.5539
BL8	P	29.0	32.0	7.0	1.75	242.11	8.0143	0.6006
BL9	P	29.0	32.0	7.0	1.75	242.13	7.9139	0.6007
BL10	P	29.5	32.5	7.0	1.75	241.65	8.1300	0.6561

Explanation of variables:

Velmean : Mean velocity of 10 events from Sxmean and Symean.
Azmean : Mean azimuth of 10 events from Sxmean and Symean.
Theta : Rotational angle of the confidence ellipse.
Prob : Probability limit of the confidence ellipse.
Sa : Semi-axis of confidence ellipse.
Sb : Semi-axis of confidence ellipse.
Sxmean : Mean value of Sx.
Symean : Mean value of Sy.

Event : Event number.

Phase : Phase (E-means elevation correction).
Start : Start of data interval after start of disk-file.
Stop : Stop of data interval after start of disk-file.
Freq : Center analysis frequency.
Delta : Half-bandwidth of frequency band.
Azimuth : Estimated azimuth.
Velocity: Estimated velocity.
Pmax : Normalized power of estimated slowness peak

Table VII.1.2 Estimation results for the Pn phase using the broad-band f-k method with a fixed frequency band.

Broad-band, Sn-phase without elevation correction

VELMEAN	AZMEAN	THETA	PROB	SA	SB	SXMEAN	SYMEAN
4.71	238.35	-41.57	0.95	0.023276	0.004850	-0.180698	-0.111388

Event	Phase	Start	Stop	Freq	Delta	Azimuth	Velocity	Pmax
BL1	S	63.0	66.0	4.0	1.00	239.25	4.7096	0.3302
BL2	S	63.0	66.0	4.0	1.00	239.38	4.6098	0.4635
BL3	S	63.2	66.2	4.0	1.00	240.89	4.6896	0.4960
BL4	S	62.5	65.5	4.0	1.00	237.74	4.7903	0.4719
BL5	S	62.9	65.9	4.0	1.00	239.75	4.6864	0.4632
BL6	S	62.1	65.1	4.0	1.00	236.02	4.7033	0.3768
BL7	S	62.6	65.6	4.0	1.00	239.43	4.6683	0.4710
BL8	S	62.5	65.5	4.0	1.00	235.38	4.8004	0.4906
BL9	S	62.5	65.5	4.0	1.00	241.46	4.6534	0.4938
BL10	S	63.0	66.0	4.0	1.00	233.92	4.8209	0.4538

Part 1

Broad-band, Lg-phase without elevation correction

VELMEAN	AZMEAN	THETA	PROB	SA	SB	SXMEAN	SYMEAN
3.96	238.86	-26.01	0.95	0.013890	0.004894	-0.216135	-0.130595

Event	Phase	Start	Stop	Freq	Delta	Azimuth	Velocity	Pmax
BL1	LG	69.0	72.0	4.0	1.00	240.73	3.9287	0.5114
BL2	LG	69.0	72.0	4.0	1.00	239.15	3.9551	0.5657
BL3	LG	69.2	72.2	4.0	1.00	240.47	3.8741	0.5300
BL4	LG	68.5	71.5	4.0	1.00	238.19	3.9711	0.6067
BL5	LG	68.9	71.9	4.0	1.00	238.06	4.0199	0.5901
BL6	LG	68.1	71.1	4.0	1.00	237.03	4.0670	0.5250
BL7	LG	68.6	71.6	4.0	1.00	238.45	3.9672	0.5610
BL8	LG	68.5	71.5	4.0	1.00	238.73	3.9348	0.5509
BL9	LG	68.5	71.5	4.0	1.00	239.20	4.0127	0.5987
BL10	LG	69.0	72.0	4.0	1.00	238.47	3.9202	0.5215

Part 2

Table VII.1.3 **Estimation results as in Table VII.1.2, but corresponding to the Sn phase (Part 1) and the Lg phase (Part 2).**

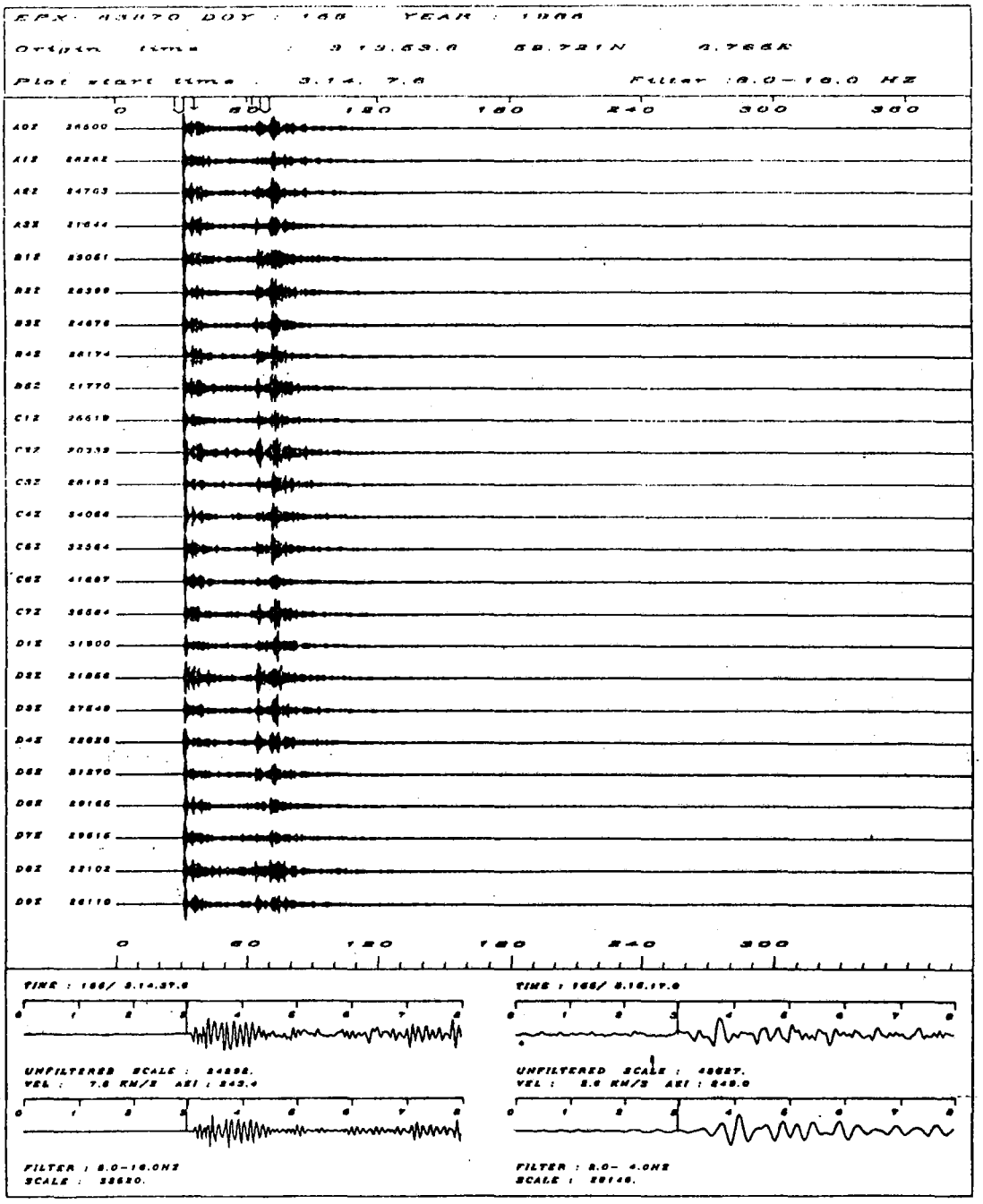

Fig. VII.1.1 NORESS waveform plots for Event 1 of Table VII.1.1. The large arrows mark the onsets of P and Lg, respectively. At the bottom, the P and Lg beams are shown in an expanded scale. Note the difference in frequency contents of the two phases.

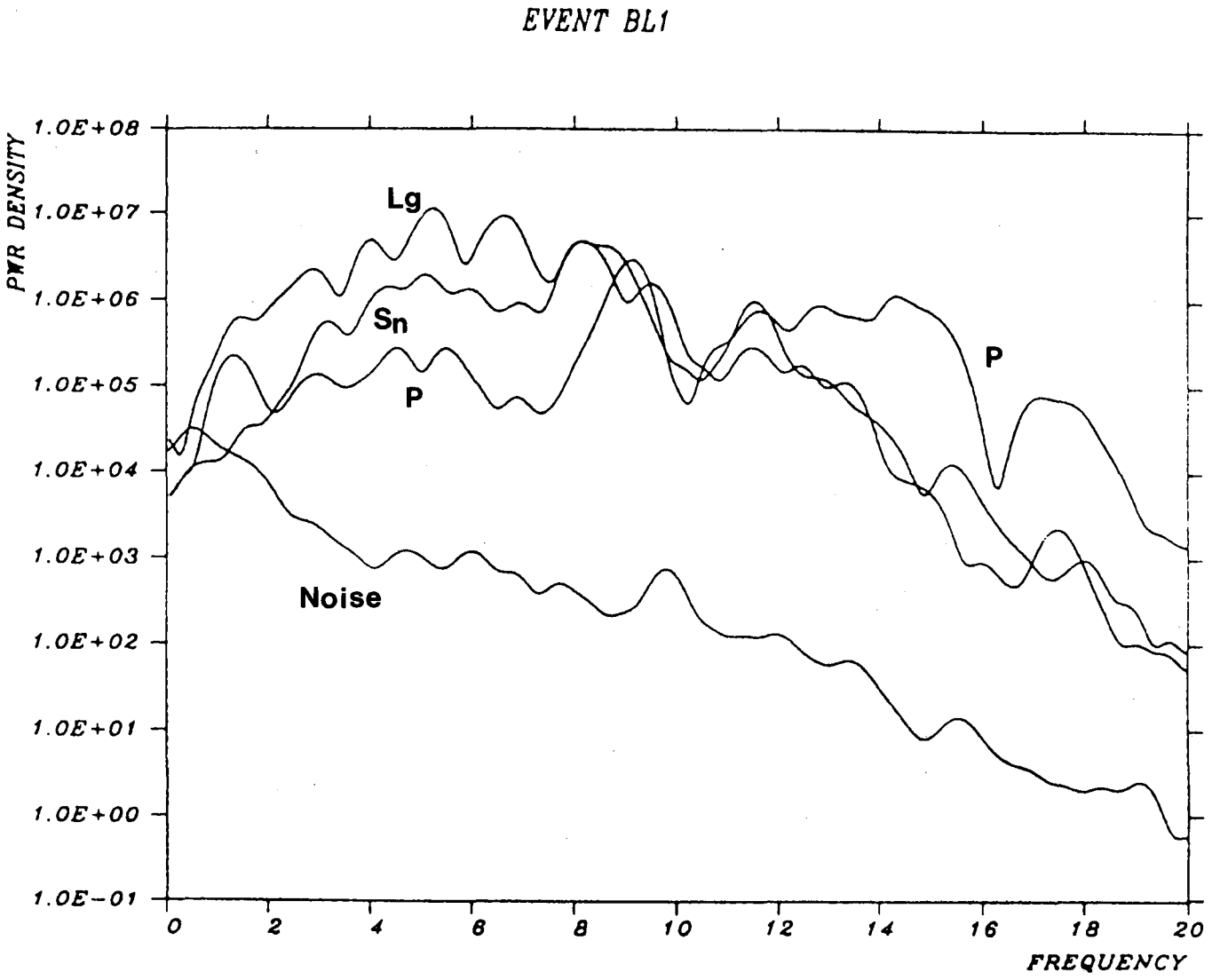

Fig. VII.1.2 Power density spectra of the P, S_n and Lg phases of Event 1, as recorded by NORESS instrument AOZ. The noise spectrum prior to P is also shown.

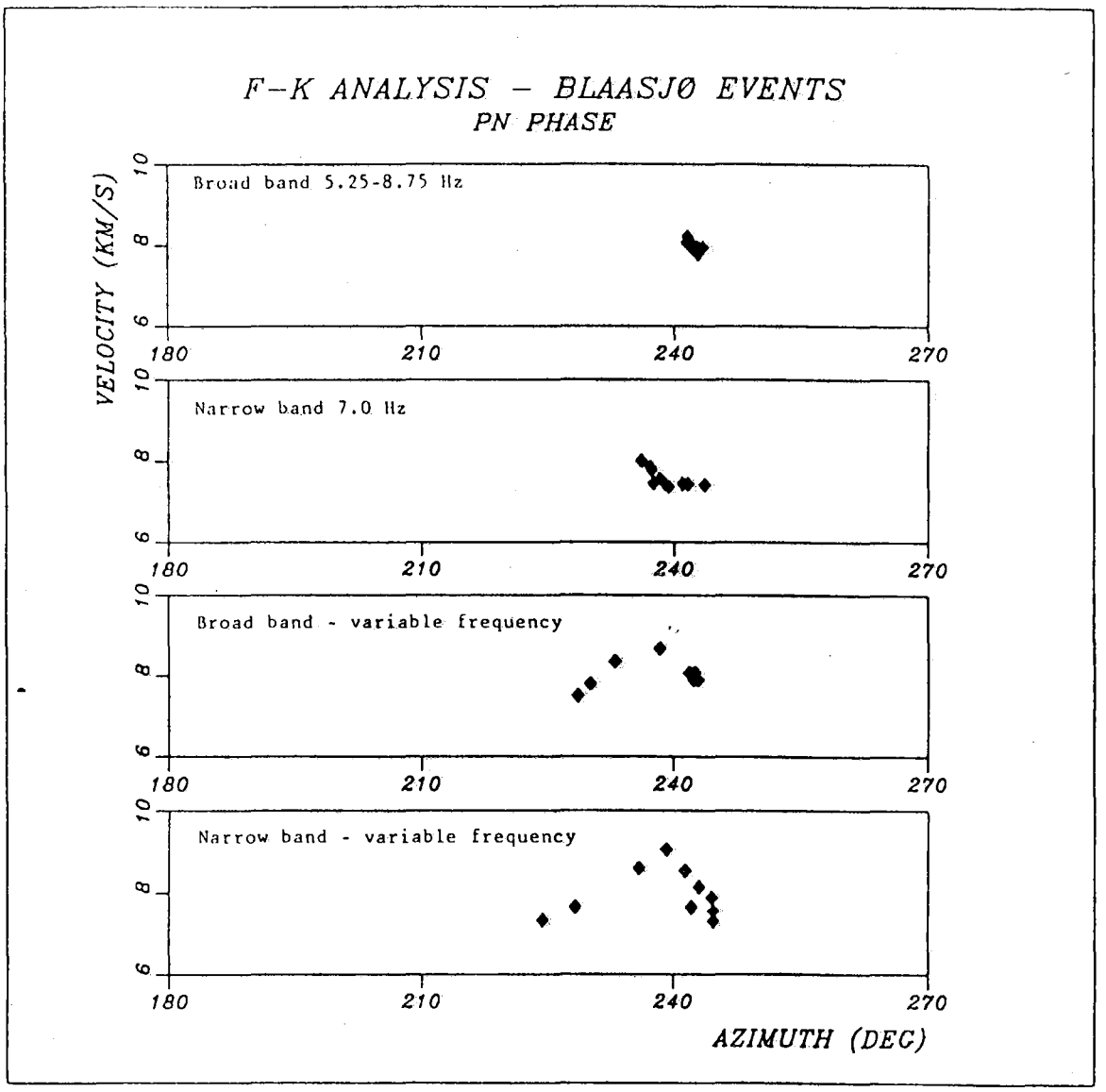

Fig. VII.1.3 Processing results (azimuth and phase velocity) for the Pn phase of the 10 events in the data base. Results using four different approaches, as described in the text, are shown. Note the excellent consistency of the results for the broadband case shown on top.

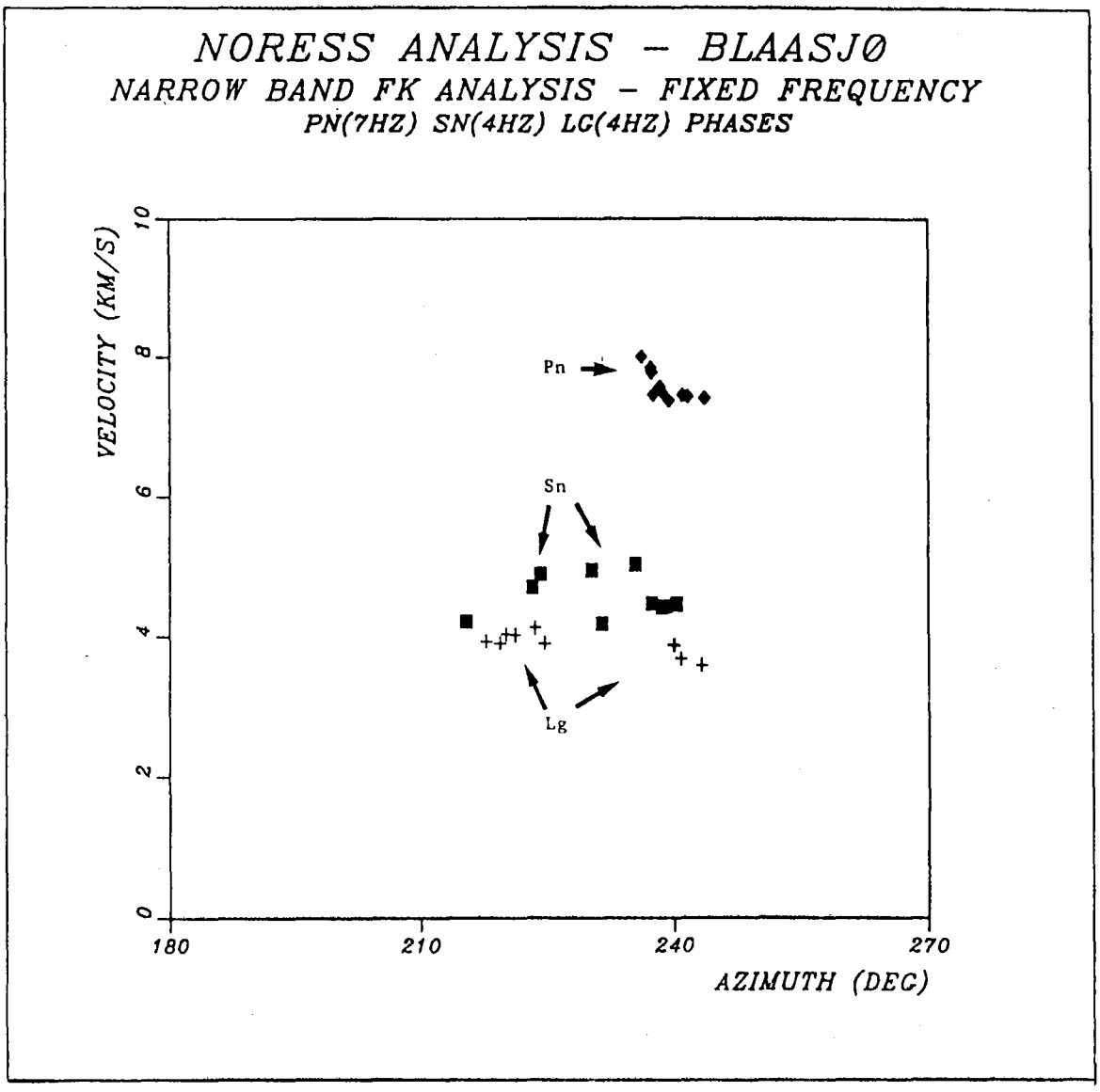

Fig. VII.1.4 Results using monochromatic f-k analysis of Pn, Sn and Lg phases of the 10 events. The processing frequency has been kept fixed for all events, but is higher (7 Hz) for Pn than for Sn and Lg (4 Hz).

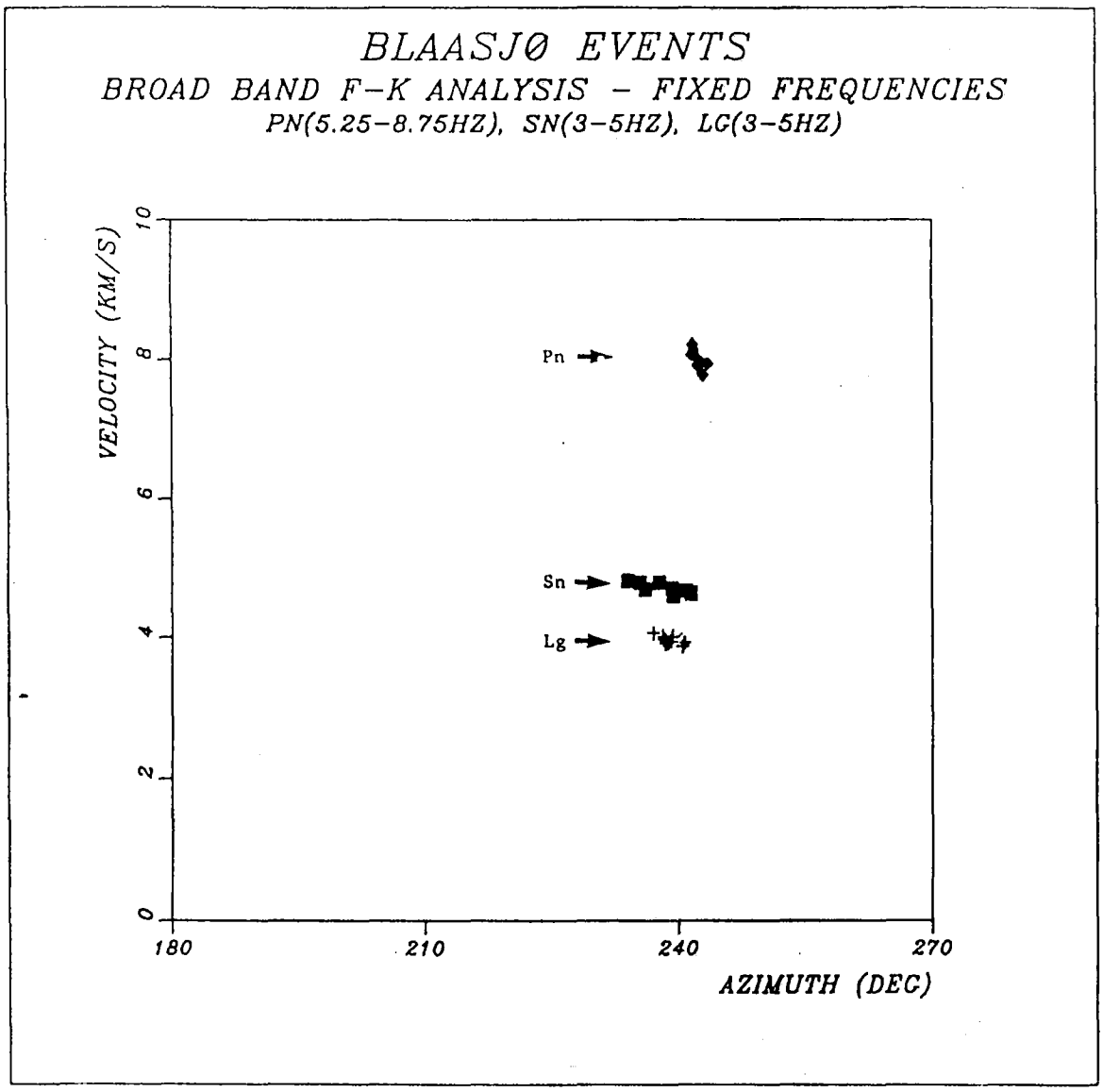

Fig. VII.1.5 Results using broadband f-k analysis of Pn, Sn and Lg phases of the 10 events. The processing frequencies have been kept fixed, as indicated in the plot. Note in particular that there is a clear phase velocity separation between each of the three phase types.

VII.2 On three-component analysis of secondary phases

In a previous report we discussed the relative performance of arrays and three-component stations in the analysis of regional P phases (Kværna and Doornbos, 1986). An important aspect of this analysis is the determination of a covariance matrix $\underline{\underline{C}}$ of the form

$$C_{nm}(\underline{s}) = \int F_n(\omega,\underline{s})\, F_m^*(\omega,\underline{s})\, d\omega/2\pi \qquad (1)$$

where the signals have been phase shifted for slowness $\underline{s}$:

$$F_n(\omega,\underline{s}) = F_n(\omega)\, \exp(i\omega \underline{s}\cdot\underline{x}_n)$$

and $F_n(\omega)$ is the Fourier spectrum at channel n. Using $\underline{\underline{C}}$ of eq. (1), the generalization of conventional beamforming is given by the normalized response

$$P(\underline{s}) = \underline{g}^+ \underline{\underline{C}}\, \underline{g} \;/\; \{|\underline{g}|^2 \,\mathrm{tr}\, \underline{\underline{C}}\} \qquad (2)$$

where $\underline{g}$ is the predicted displacement vector for slowness $\underline{s}$. The generalization of optimum beamforming methods proceeds similarly, but eq. (2) is sufficient for our present purpose.

Eq. (2) involves no explicit assumption about the phase type, and so may be applicable in the analysis of secondary phases as well. The success of such an analysis depends on our ability to predict the vector $\underline{g}$ in eq. (2). Put another way, it depends on the ability to match the covariance matrix $\underline{\underline{C}}$, since

$$\underline{g}^+ \underline{\underline{C}}\, \underline{g} = \mathrm{tr}(\underline{\underline{C}}\, \underline{\underline{G}}) \;, \quad \underline{\underline{G}} = \underline{g}\, \underline{g}^+$$

In this regard we note the following points: (1) The particle displacement of S is relatively complicated even in simple models. The fact that in its simplest form, plane wave S motion is polarized in a plane implies that from the observed direction of S motion at a given time one cannot uniquely infer the slowness vector; the solution vec-

tors span the plane perpendicular to the direction of S motion. Only when the SV/SH ratio is known can a unique solution be obtained. This is not usually the case. The problem is aggrevated when interaction with the surface and near-surface structure is taken into account (see below). (2) For a single component array of sensors, the $\underline{g}$ vector in eq. (2) is constant and the operation (2) is trivial. For a three-component sensor, $\underline{g}$ represents the predicted displacement vector for slowness $\underline{s}$. The prediction is model-dependent. For example, $\underline{g}$ will be frequency independent if a uniform half-space model is used to account for surface interaction. In the real earth this is usually not the case, not even for P waves. Fig. VII.2.1 shows the results of an analysis of three-component records from the broadband station in NORESS. The records give the P wave from an event in the Hindu Kush (Fig. VII.2.1a). The slowness solutions, in the form of apparent velocity and azimuth (Fig. VII.2.1b), show significant dispersion violating the assumption of frequency independent $\underline{g}$. The correct values are near the SP solution for apparent velocity, and near the LP solution for azimuth. This suggests that relatively small-scale lateral structure is the dominant source of azimuth bias, whereas the apparent velocity for P is mostly affected by large-scale vertical structure. Indeed, a simple modification of the uniform half-space model by introducing a discontinuity between the upper and lower crust at 15 km depth, does produce velocity dispersion of the observed order of magnitude (Fig. VII.2.2). The calculations in this and other one-dimensional models are based on a stripped version of Kennett's (1983) reflectivity algorithm. (The required modifications were made by Kennett during a visit to NORSAR this summer.) Of course, this and other models introduced here are not meant to have any significance other than that they give an indication of the required scale of inhomogeneity.

For short-period S there is little difference between the response of the two-layer crustal model and that of a uniform half space (as is the case for short-period P). The uniform half-space response for SV gives a ratio of horizontal to vertical displacement, for slowness p:

$$u_h/u_v = (1/\beta^2 - 2p^2)/(2p\sqrt{1/\alpha^2-p^2}) \qquad (3)$$

where α and β are the P and S velocity, respectively.

The SV particle motion for the uniform half-space model is plotted in Fig. VII.2.3. Note that the regional S_n phase has an apparent velocity of about 4.5-5.0 km/s, hence $p \approx 0.20$-0.22 s/km, and the predicted motion is elliptical with the long axis vertical. However, the observed response is quite different. Fig. VII.2.4 displays the 3 components of a typical regional S_n phase. The response is dominated by horizontal motion. The particle motion of S_n from three different events is plotted in Fig. VII.2.5, showing almost rectilinear SV motion with the long axis horizontal.

It is well known that S interacts strongly with crustal inhomogeneity, and three-dimensional models are certainly required to account for the observed effects. However, even simple modifications of a one-dimensional model can produce dramatic effects. Fig. VII.2.6 displays the SV particle motion when adding a thin (200 m) low-velocity layer on top of the crust. The effect of the layer is to change the long axis of SV motion from vertical to horizontal for a wide range of slowness encompassing the slowness of S_n. The modification does not affect the P motion. It is emphasized again that the model has no significance other than to indicate the required scale of inhomogeneities. The result suggests that 3-component data of regional S are unsuitable for slowness analysis. At best one can infer the azimuth

apart from a 180° ambiguity, and only if the SV/SH ratio is known. On the other hand, due to the response characteristics should horizontal components have potential for detection of S_n.

T. Kværna
D.J. Doornbos

References

Kennett, B.L.N. (1983): Seismic Wave Propagation in Stratified Media, 342 pp. Cambridge Univ. Press.

Kværna, T. and D.J. Doornbos (1986): An integrated approach to slowness analysis with arrays and three-component stations. Semiann. Tech. Summary, 1 Oct 85 - 32 Mar 86, NORSAR Sci. Rep. No. 2-85/86.

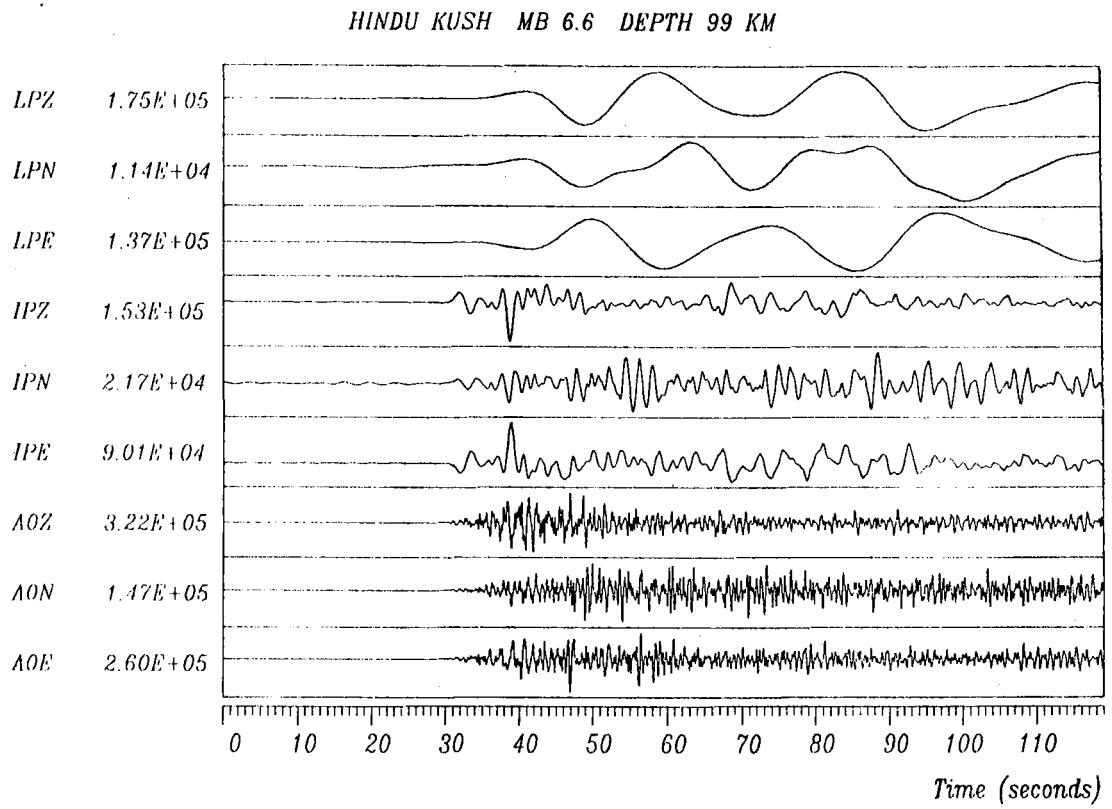

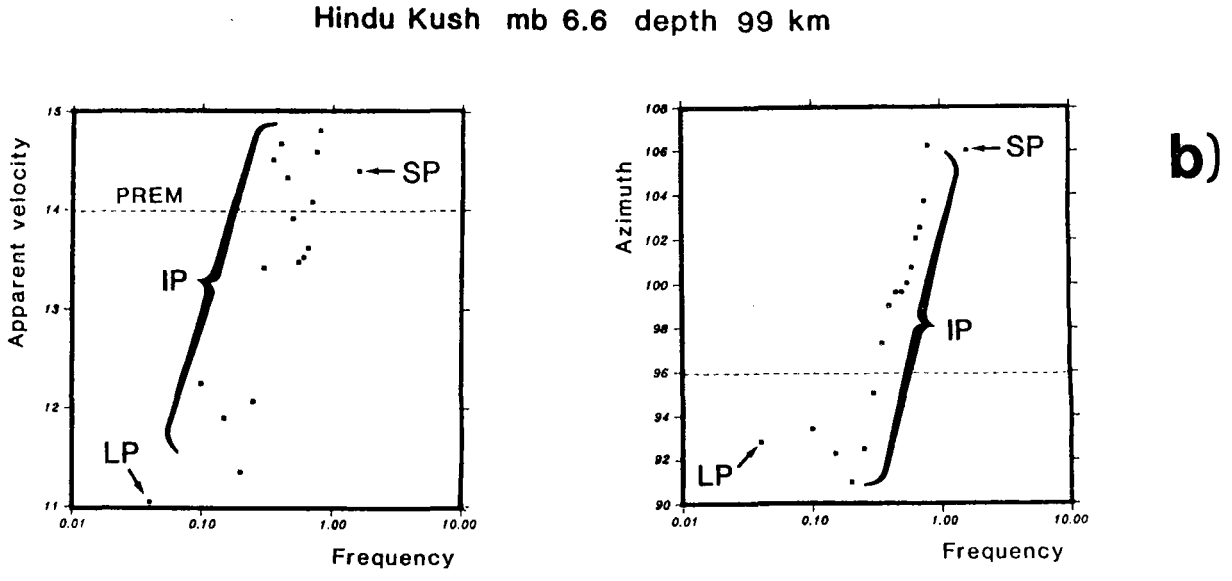

Fig. VII.2.1 a) P wave from event in Hindu Kush recorded in three different frequency bands of the broadband station in NORESS.

b) Slowness solutions as a function of frequency, using uniform half space model with v_p = 6.0 km/s, v_s = 3.46 km/s. Slowness vector decomposed in apparent velocity and azimuth.

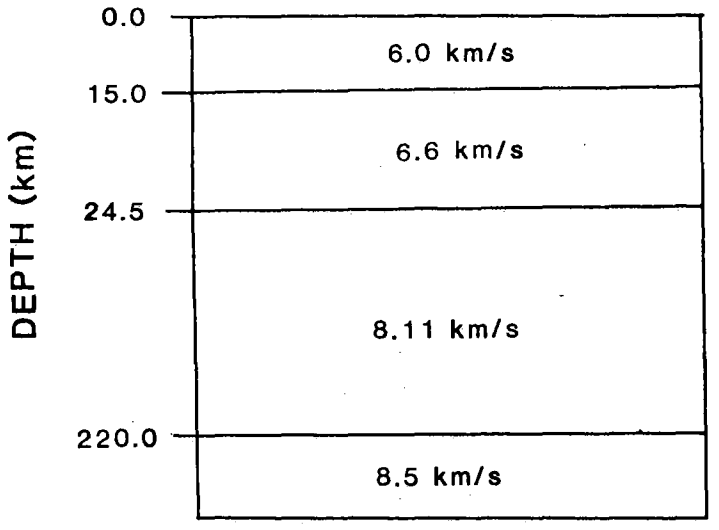

a)

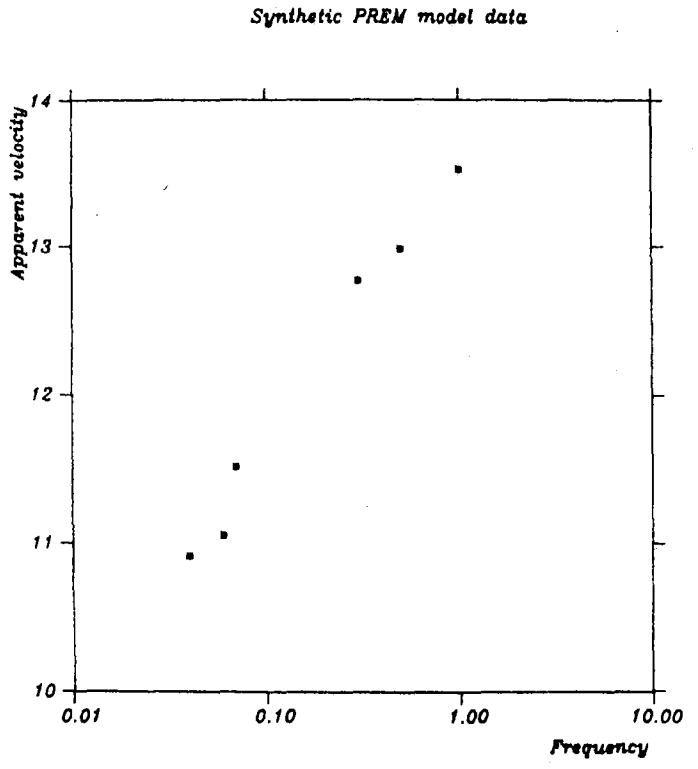

b)

Fig. VII.2.2 a) Crustal model used to generate synthetic broadband P.
b) Slowness solutions when applying the uniform half-space model (v_p = 60 km/s, v_s = 3.46 km/s) to the synthetic data generated in model in a).

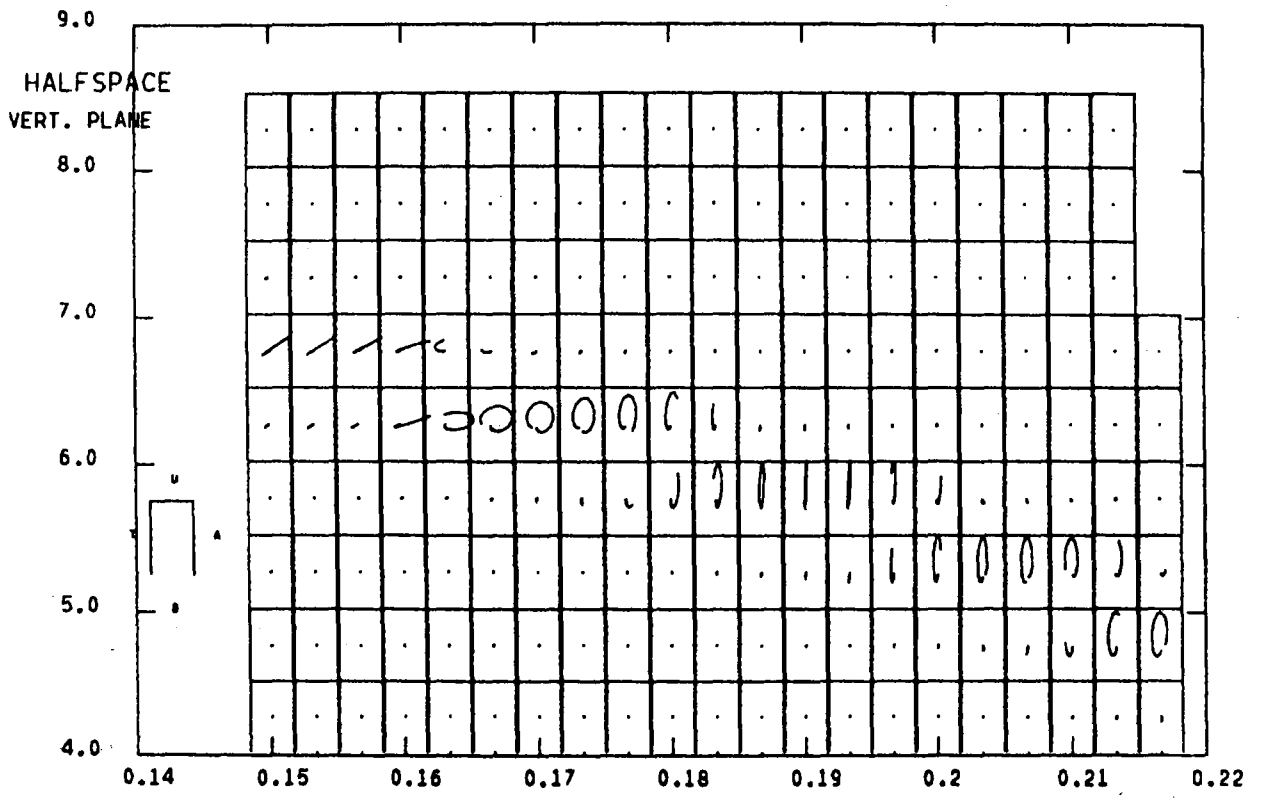

Fig. VII.2.3 Particle displacement as a function of slowness and time. Synthetic data represent the response of the uniform half space to incident plane SV wave.

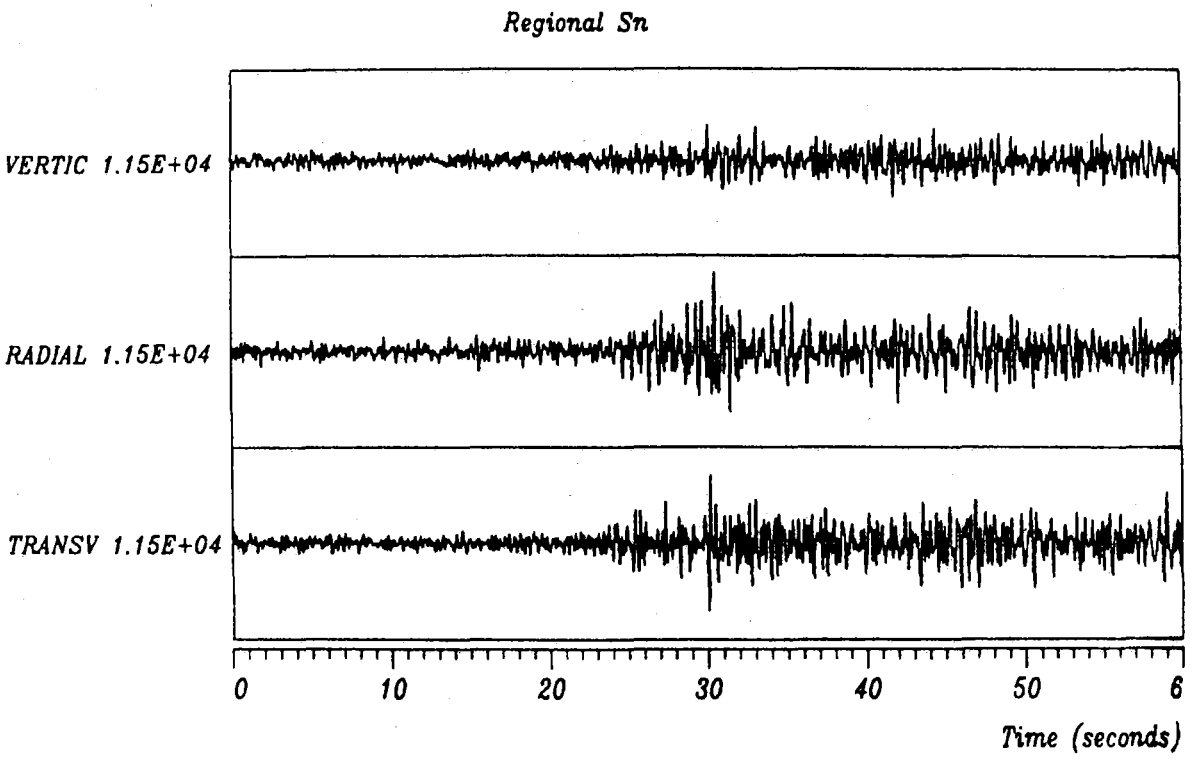

Fig. VII.2.4 Typical three-component seismograms of regional S_n. All traces are scaled to the same value.

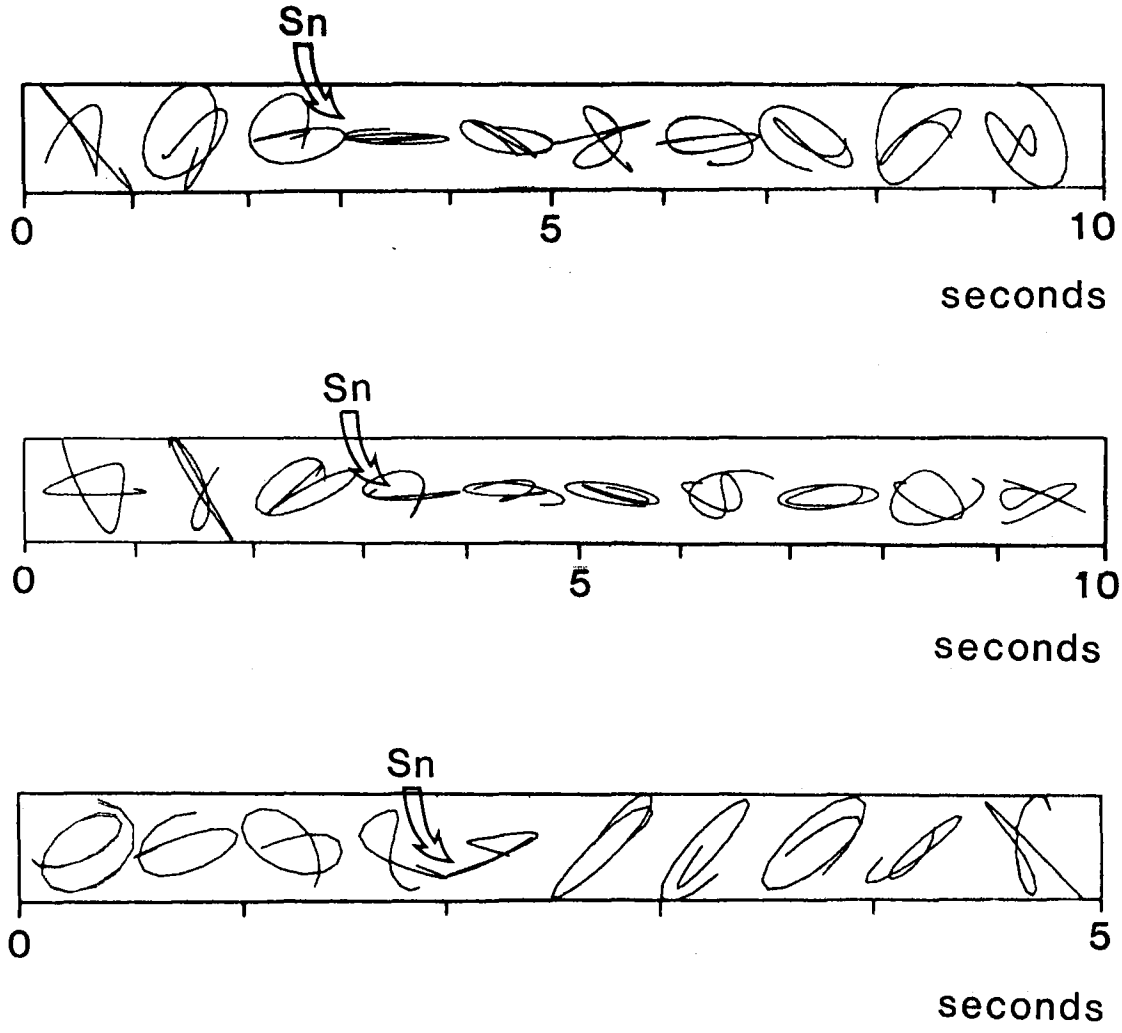

Fig. VII.2.5 Particle motion in the vertical-radial plane of SV, for S_n from three different regional events.

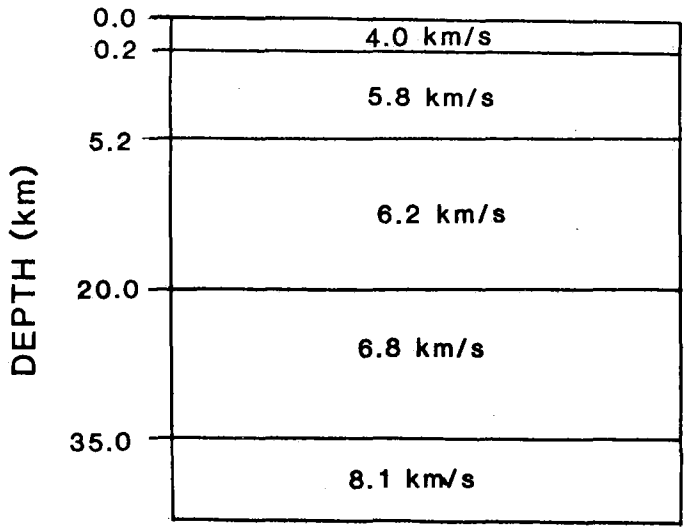

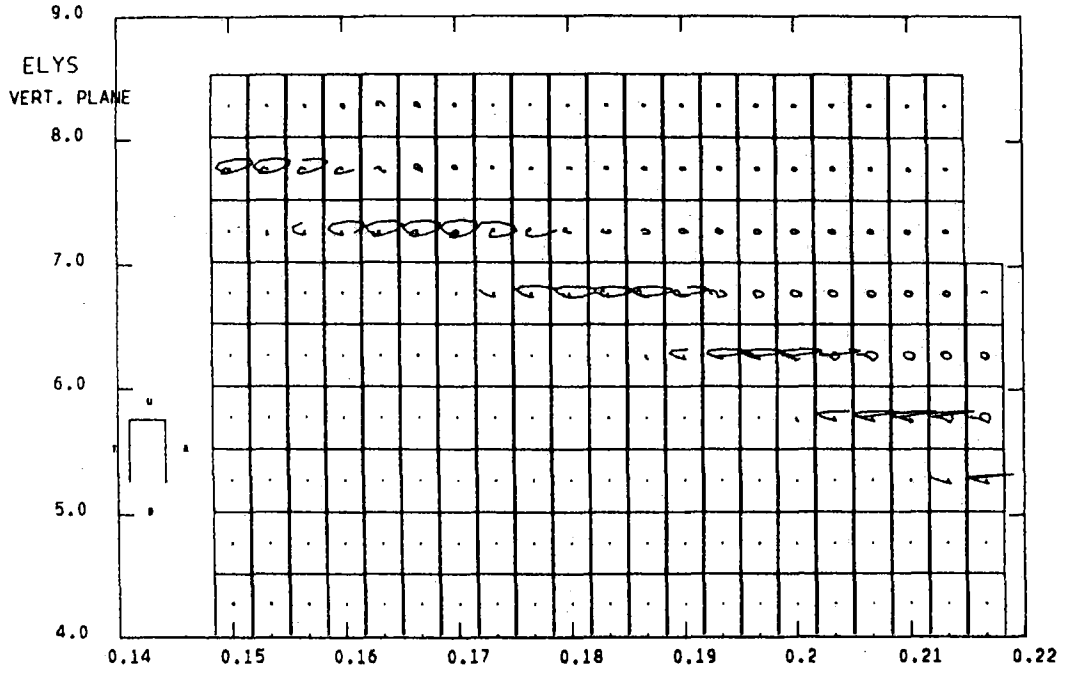

Fig. VII.2.6 a) Crustal model used to generate synthetic S_n.
b) Particle motion in the vertical-radial plane of SV, in response to incident plane SV wave in the model of a).

VII.3 Applicability of horizontal components for detection and phase discrimination

In the report 'On three component slowness analysis of secondary phases (Kværna and Doornbos, 1986), one conclusion was that the horizontal components may have some potential for detection of regional S_n. This statement was based on the fact that for several events recorded on NORESS, larger amplitudes were observed on the radial and transverse components than on the vertical. On the other hand, for Lg, the trend was that most energy was confined to the vertical and transverse components.

If the above mentioned assumpions on the distribution of energy are generally valid, the amplitude or energy ratio between the vertical and radial components should be a possible discriminator between S_n and Lg.

To test these hypotheses, 17 regional and and local events were subjected to a detailed detection and amplitude ratio analysis. The selected events represented 13 different source regions, and spanned a wide range of SNR.

Detection analysis

In the current online processing of NORESS data, the incoherent beamforming technique, (see Ringdal et al., 1975) is applied for detection of secondary phases. This method provides better detectability than coherent beamforming for such phases (Ringdal, 1985), so in this study we chose to follow this concept by forming incoherent beams applying different filters and array subconfigurations. The specific subconfigurations were:

1) AOZ, CRING and DRING
2) AOZ, BRING, CRING and DRING
3) All horizontal components

4) All north components
5) All east components
6) AOZ, CRING, DRING and all horizontal components
7) AOZ, BRING, CRING, DRING and all horizontal components.

For each subconfiguration the following bandpass filters were applied to the individual channels prior to incoherent beamforming:

1) 0.5 - 1.5 Hz
2) 1.0 - 2.0 Hz
3) 1.5 - 2.5 Hz
4) 2.0 - 3.0 Hz
5) 2.5 - 3.5 Hz
6) 3.0 - 4.0 Hz
7) 3.5 - 4.5 Hz
8) 4.0 - 5.0 Hz

The maximum STA/LTA values in the respective incoherent beams were computed for each phase, filter band and subconfiguration and stored for further analysis. For evaluation, it was in addition necessary to convert the observed SNR's to values that were directly comparable for detection purposes. For example, an SNR of 5.0 is more significant on an incoherent beam consisting of AOZ, BRING, CRING and DRING than on a beam formed from just the 8 horizontal components, because the noise variance is smaller in the first case and we can therefore operate at a lower threshold without increasing the false alarm rate.

A confidence measure D' of a given detection can be obtained by transforming the maximum observed SNR (SNR_{MAX}) as follows:

$$D' = \frac{SNR_{MAX} \cdot \overline{D}}{\sigma}$$

where D is mean STA/LTA ($\simeq$ 1) and σ is the noise standard deviation, i.e., the STA/LTA applied to representative noise samples.

The incoherent beam consisting of AOZ, CRING and DRING had the best detection characteristics when only taking the vertical channels into account. Including the ARING caused correlated noise to be added to the beam at most frequency bands, thereby increasing the noise standard deviation. Slight improvements were seen only at the highest frequencies.

We had earlier found that the correlation between the different components of 3-comp. sensors was low, so we expected to reduce the noise variance if we added the horizontal components to the already defined vertical subconfigurations. Also in that case, the ARING in subconfiguration number 7 reduced the detectability by introducing correlated noise in most frequency bands. The beams consisting of only NORTH or EAST horizontal components in some cases gave the best observed SNR, either as the radial component of Sn or as the transverse component of Lg. But we found the noise variance suppression obtained by those four instruments to be too small to match the performance of beams with more stations included.

Based on the argumentation above, we selected three different beam deployments for direct comparison: These were numbers 1), 3) and 6) in the list above, respectively. Configuration 1) was used as a reference. In the following figures, the filled squares mark the ratios between SNR for configurations 3 and 1, whereas the crosses refer to ratios between configurations 6 and 1.

From Fig. VII.3.1 it is obvious that the horizontal components in most cases will give higher SNR than only the verticals for the S_n phase. For example, if we had to choose between an equal

number of horizontal or vertical stations for detection of S_n, it would be wise to choose the horizontals.

When turning to the instrument selection possible from the NORESS configuration, we have to take into account the fact that with more instruments included, the noise variance is reduced. In Fig. VII.3.2 we have displayed the corrected SNR values (D') for the atual configurations. The horizontal beam in two cases was considerably better than the reference beam, whereas the the beam with both horizontal and vertical components in most cases was the best.

As expected, the SNR contributions from the horizontals was less for the Lg than for the Sn phase, (Fig. VII.3.3), but some of the events still had the highest SNR on the horizontal beam. The corrected values in Fig. VII.3.4 show that the horizontal beam in only one case was the best, and the improvement by the mixed beam was marginal.

In conclusion, there is a gain to be achieved by incoherent beamforming using both horizontal and vertical components together, especially for S_n detection. This gain must be weighted against the increased computer requirements involved.

Amplitude ratio analysis

After rotation of the horizontal components of each three-component station to create the radial and transverse traces, all permutations of component ratios were calculated for each station in the different detection filter bands. Both max. amplitude and energy ratios, and mean ratios over all stations were computed.

In Fig. VII.3.5, we have displayed the Z/R ratios in the frequency band with highest SNR. The values are averaged over all four three-component stations, because the ratios may differ as much as 20 percent from station to station. Even though we have not obtained full separa-

tion between the phases, 25 out of 29 phases were correctly classified if we set the critical ratio to 1.0. We also found that the improvement of applying energy ratios instead of amplitude ratios was marginal, and that the ratios Z/T or R/T did not give any pattern as applicable for phase discrimination as Z/R.

Thus we conclude that the Z/R test applied together with other types of information like apparent velocity and frequency content, is likely to improve the possibility of correctly identifying S_n and Lg phases, and thereby increase the reliability of regional event location.

T. Kværna

References

Kværna, T., and D.J. Doornbos (1986): On three-component analysis of secondary phases, This Volume.

Ringdal. F. (1985): Initial results from NORESS detection processing, Final Technical Report, 1 Apr - 30 Sep 1985, NORSAR Sci. Rep. No. 1-85/86, Kjeller, Norway.

Ringdal. F., E.S. Husebye, and A. Dahle (1975): P-wave envelope representation in event detection using array data, in Exploitation of Seismograph Networks, K. G. Beauchamp, Editor, Nordhoff-Leiden, The Netherlands, 353-372.

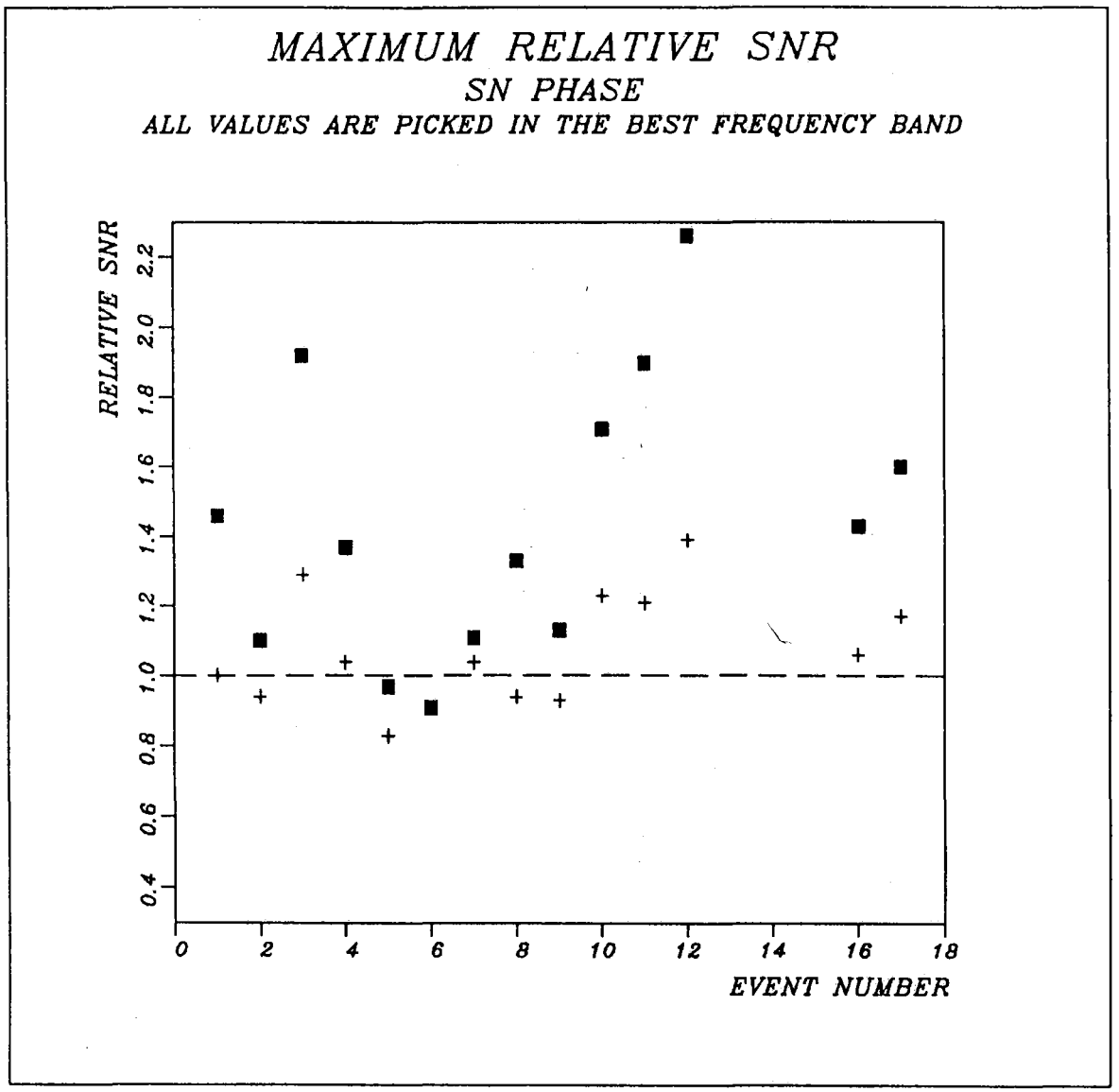

Fig. VII.3.1 Maximum SNR relative to the maximum of the AOZ, CRING and DRING configuration. The filled squares represent the beam of eight horizontal components. The crosses show the relative values of the beam with AOZ, CRING, DRING and the horizontal components, whereas the AOZ, CRING and DRING values are indicated by the dashed line at the 1.0 level.

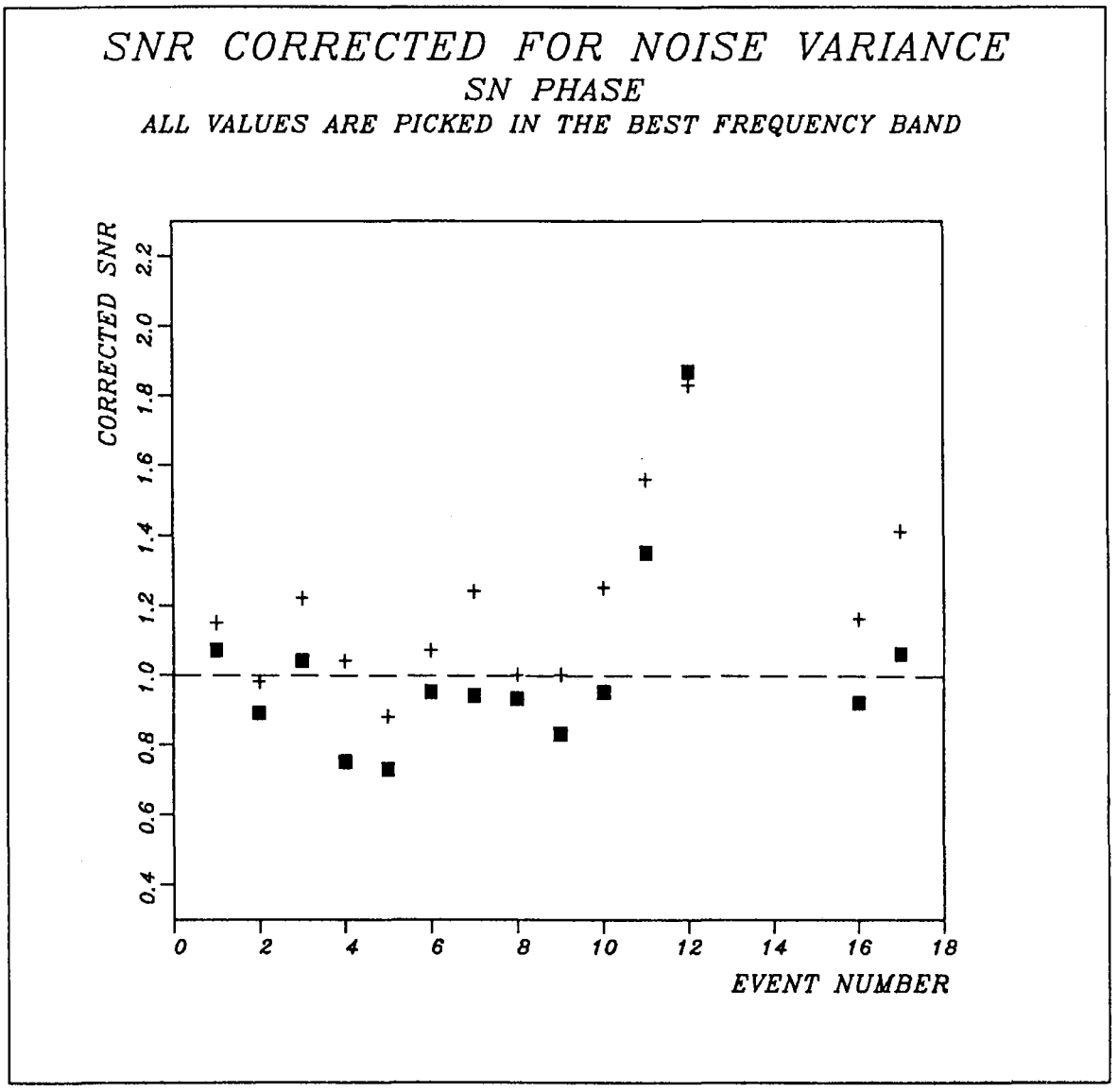

Fig. VII.3.2 Maximum corrected SNR relative to the corrected maximum of the AOZ, CRING and DRING configuration. The filled squares represent the beam of eight horizontal components. The crosses show the relative values of the beam with AOZ, CRING, DRING and the horizontal components, whereas the AOZ, CRING and DRING values are indicated by the dashed line at the 1.0 level.

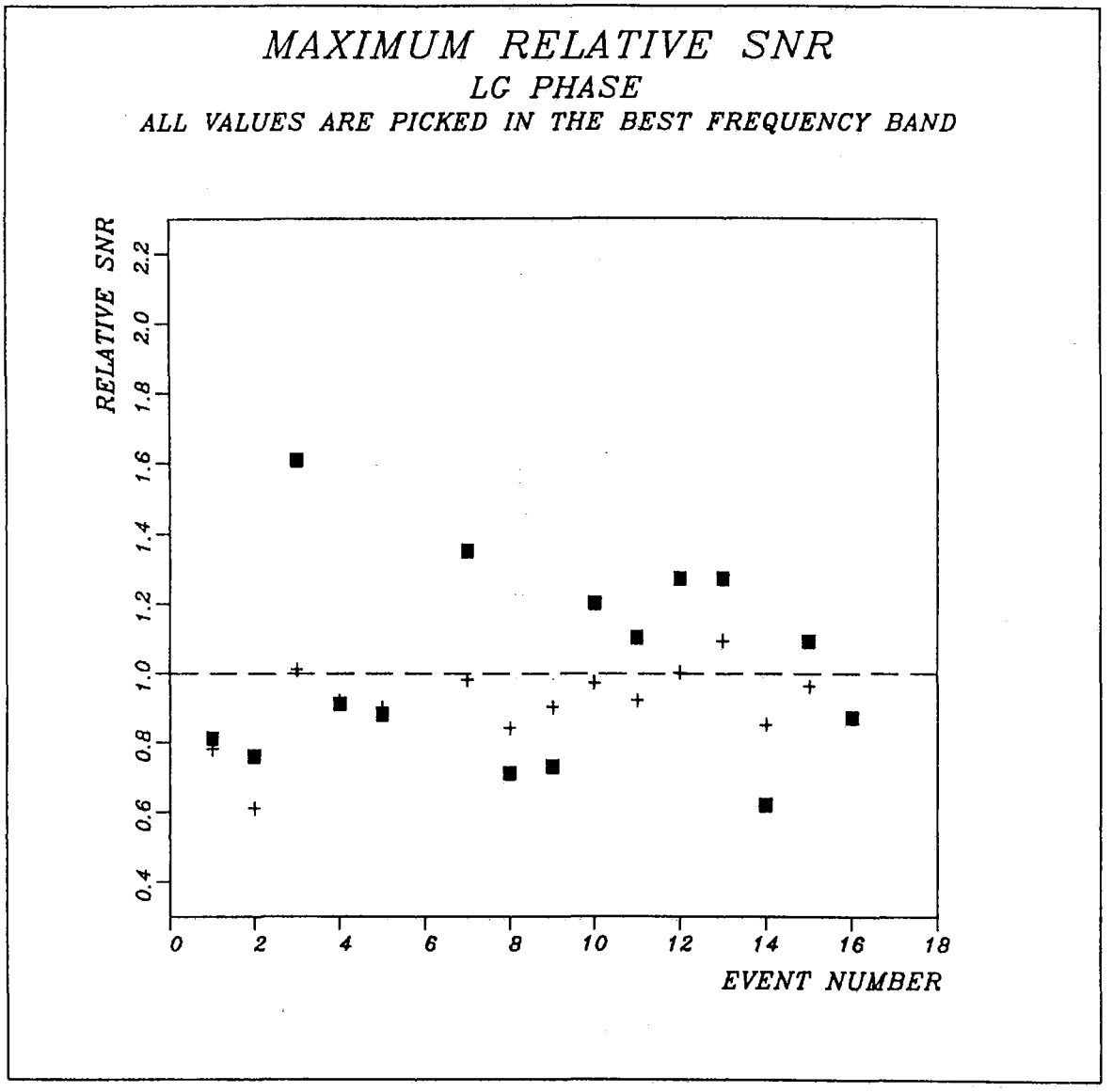

Fig. VII.3.3 Maximum SNR relative to the maximum of the AOZ, CRING and DRING configuration. The filled squares represent the beam of eight horizontal components. The crosses show the relative values of the beam with AOZ, CRING, DRING and the horizontal components, whereas the AOZ, CRING and DRING values are indicated by the dashed line at the 1.0 level.

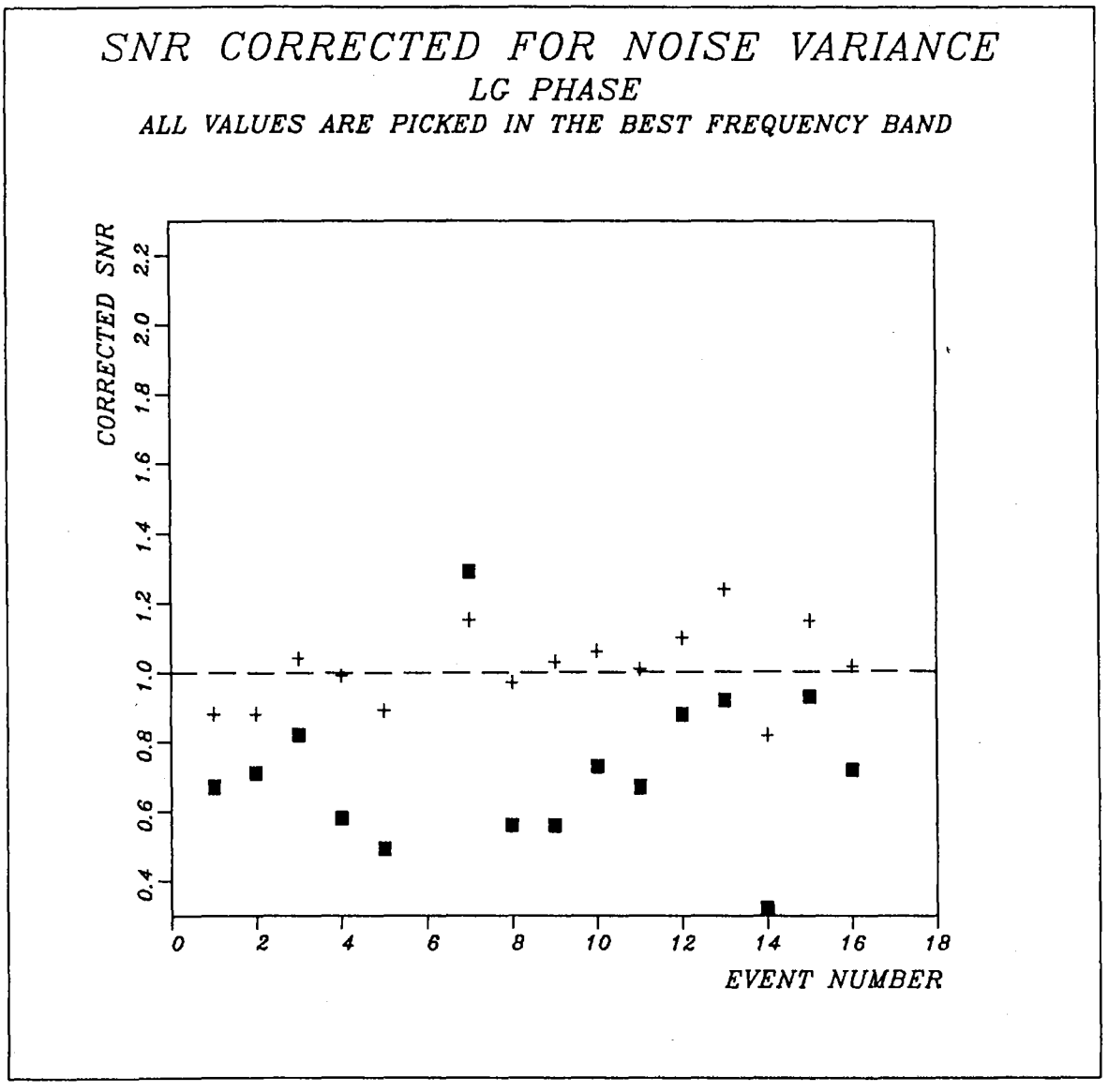

Fig. VII.3.4 Maximum corrected SNR relative to the corrected maximum of the AOZ, CRING and DRING configuration. The filled squares represent the beam of eight horizontal components. The crosses show the relative values of the beam with AOZ, CRING, DRING and the horizontal components, whereas the AOZ, CRING and DRING values are indicated by the dashed line at the 1.0 level.

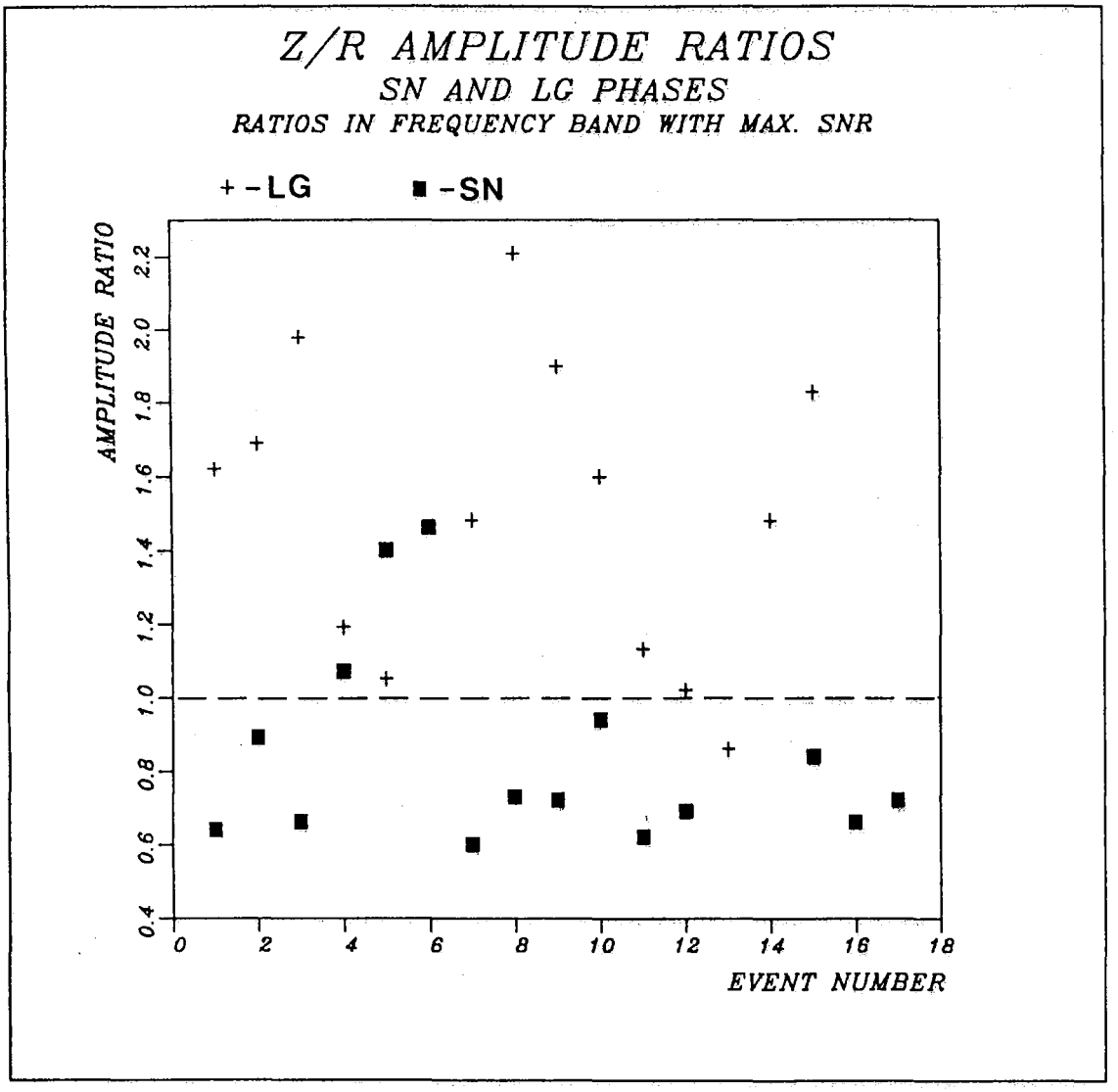

Fig. VII.3.5 Mean vertical / radial amplitude ratios for S_n and Lg phases. Only values corresponding to actually detected phases are plotted.

VII.4 Optimum beam deployment for NORESS P-wave detection

In order to realistically assess the potential of the NORESS array for event detection, it is necessary to compute the actual beamforming gain for a variety of representative seismic signals. In previous investigations (Mykkeltveit et al, 1985; Fyen, 1986) we focussed on the noise suppression obtained for various NORESS subgeometries. This contribution deals with the signal loss (by beamforming) in addition to the noise suppression, and the two quantities are combined to obtain the beamforming gain.

The main objective of this study is the recommendation of an optimum set of beams for the detection of regional and teleseismic P-waves at NORESS. This requires that for each frequency band we must find the subgeometry that gives the best beamforming gain. For each frequency band it is also necessary to determine whether one single vertical (infinite velocity) beam is adequate. Alternatively, steered beams with delays corresponding to several slownesses and azimuths are needed. Because of the potential for reduction in computation time, it is important to identify the classes of signals for which vertical beams will do.

Analysis method

Under the condition of approximately equal signal and noise amplitudes at each sensor, we can express the beamforming gain G by the normalized zero-lag cross-correlations via the formula:

$$G^2 = \sum_{i,j=1}^{N} w_i w_j c_{ij} \Big/ \sum_{i,j=1}^{N} w_i w_j \rho_{ij} \qquad (1)$$

where c_{ij} is the signal correlation between sensors i and j and ρ_{ij} is the corresponding noise correlation. N is the number of sensors used

and w_i are sensor weights. The signal loss and noise suppression are related to the numerator and denominator, respectively, of the above fraction:

$$\text{Signal loss} = \Big[\sum_{i,j=1}^{N} w_i w_j \Big / \sum_{i,j=1}^{N} w_i w_j c_{ij} \Big]^{\frac{1}{2}}$$

$$\text{Noise suppression} = \Big[\sum_{i,j=1}^{N} w_i w_j \Big / \sum_{i,j=1}^{N} w_i w_j \rho_{ij} \Big]^{\frac{1}{2}}$$

and hence

$$\text{Gain} = \text{Noise suppression} / \text{Signal loss}$$

We are now faced with the task of computing the beamforming gain for a variety of different weighting schemes for each signal in our data base. The investigation is restricted to the seven frequency bands 1.0-3.0 Hz, 1.5-3.5 Hz, 2.0-4.0 Hz, 2.5-4.5 Hz, 3.0-5.0 Hz, 4.0-8.0 Hz and 8.0-16.0 Hz. These are the frequency bands currently utilized in the detection processing part of the NORESS online processor (RONAPP). The gain is computed for all possible weighting schemes for which all elements of each ring of the NORESS geometry (see Fig. VII.4.1) have either weight 1 or weight 0. The central element A0 counts as a 'ring' in this regard. We are thus restricitng our search to symmetrical sub-geometries, which ensure equal detection capability in all directions. With five rings in the NORESS geometry there are 31 different sub-geometries, for which the gain is computed. For a given frequency, it is a priori obvious that certain geometries will be clearly inferior to others. Nevertheless, we compute the gain for the whole range of geometries for all frequency bands, because of consistency and because

the complete results give useful insight with respect to the properties of signals and noise.

For each of the seven partly overlapping frequency bands, we have selected up to four high SNR regional and/or teleseismic P-wave signals. We have chosen events with peak signal frequencies close to the lower cutoff of that band. This is done in order to ensure that the signal is analyzed in the band for which the SNR for that signal attains its maximum value. The approach chosen will satisfy this requirement since the noise amplitudes are monotonically decreasing with increasing frequencies in the range 1.0-16.0 Hz.

Results

The gains are computed both for a vertical beam and for a beam steered to the broadband slowness vector of the signal (for details on the broadband frequency-wavenumber algorithm used, see section VII.1 of this Semiannual Technical Summary). Before computing the gains for the steered beams, the signals are resampled at 200 Hz (the sampling rate for NORESS data is 40 Hz). The signal loss is computed for a 1-second data window at the signal peak and within 3 seconds from the arrival onset time. The data window length of 1 second is chosen to match the STA window length of the online detector. The noise suppression estimates are based upon 100 seconds of noise ahead of the signal, and are made for the appropriate beams. Finally, we estimate the mean noise suppression for four beams, each with an apparent velocity of 8.0 km/s and steered to azimuths of 0, 90, 180 and 270 degrees. In the following, we give results in terms of beamforming gains for each of the seven frequency bands.

1.0-3.0 Hz

Results for one event are given in Table VII.4.1. For each beam type (infinite velocity or steered), the gain, signal loss (Sloss) and noise suppression (Nsupp) are computed for all possible weighting

schemes as detailed above. The best gain obtained and the corresponding weighting scheme are given in the first row of each table within Table VII.4.1. The remaining eight configurations below the top row remain fixed for all tables. All gains, etc., are given in decibels. Nsupp8 is the mean noise suppression for the four 8 km/s beams. A0wgt, Arwgt a.s.o. denote the weights applied to A0, the A ring a.s.o.

It is seen from Table VII.4.1 that the steered beams are at best only marginally better than the infinite velocity beams, and the overall best result is in fact obtained for an infinite velocity beam. Results for the other events with peak signal frequencies slightly above 1.0 Hz show that the infinite velocity beam signal losses are generall modest and less than 1 dB for all weighting schemes considered, so the gain is really controlled by the noise suppression that can be achieved. The beam including A0 and the sensors of the C and D rings (altogether 17 sensors) gives the best overall performance, with a gain typically 4 dB above what is obtained using all 25 sensors of the array. So the recommendation is for an infinite velocity beam for this subgeometry, to cover teleseismic signals with peak signal frequencies between 1.0 and 1.5 Hz satisfactorily.

For this frequency band we also show in the bottom part of Table VII.4.1 gains obtained after having extended our weighting scheme. Here, we have allowed weights 0., 0.5 and 1.0 for each ring and computed the gain for all 242 combinations. We see from the table that a very marginal gain improvement is obtained by this extension of the weighting scheme. From these results it is seen that giving weight 0.5 to A0 is better than both omitting A0 and giving it a weight of 1.0. Still, our general finding after checking all frequency bands is that weights different from 0 and 1 at the very best contribute 1.0 dB over the 0/1 weighting scheme, and the best results are obtained for weighting schemes that vary strongly from event to event. Due to these variations, it is found not to be possible to generalize these

results, and in the following we confine our discussion and results to the 0/1 weighting scheme.

1.5-3.5 Hz

The geometry including A0, the C and D rings again gives the best gain for nearly all runs (there is one event for which the gain is improved for the steered beam by omitting A0 from the above geometry). Signal losses for the infinite velocity beams are slightly larger than for the 1.0-3.0 Hz band, and steered beams give from 0.5 to 1.2 dB gain improvement relative to the infinite velocity beams. This is a fairly modest improvement, so again the recommendation is for an infinite velocity beam including A0, the C and D rings, basically to capture the signals with peak frequencies in the range 1.5 to 2.0 Hz, the majority of which will be teleseismic.

2.0-4.0 Hz

In order to recommend a beam deployment for this frequency band, one must deal with the question of where low SNR events with peak signal frequencies in the range 2.0 to 2.5 Hz originate. There are certainly many teleseismic events of this kind, and the results are that these will be adequately covered by an infinite velocity beam using again the central element (A0) and the sensors of the C and D rings. For regional events, however, the signal losses are now becoming appreciable for the vertical beams, and one must consider steered beams for such signals. Again, it is the same subgeometry that gives the best gains, and the recommendation is for a number of beams of apparent velocity 8.0 km/s, and with azimuths to cover the circle adequately, either by an even spacing, or by pointing to source regions of particular interest.

2.5-4.5 Hz

We now observe a tendency that the B ring is becoming all more important for the gain, whereas the D ring is of lesser importance. We see from Table VII.4.2 that the signal losses for the infinite velocity beams are considerable for all geometries including the D ring, while on the other hand, the noise suppression is not much improved through inclusion of the D ring. The best single infinite velocity beam includes A0, the B and C rings. The results indicate that for both regional and teleseismic signals the gain can be further improved by up to 4 dB for optimally steered beams. The best configuration for steered beams appears to be A0, the B, C and D rings.

3.0-5.0 Hz

The geometry consisting of A0, the B and C rings is the best one for all tests in this frequency band, irrespective of beams being vertical or steered. For regional and teleseismic events, the gain can be improved by up to 2-3 dB in going to steered beams. The recommendation is then to deploy one infinite velocity beam for the teleseismic events including the 13 sensors of A0, the B and C rings and in addition, a number of pointed beams, including the same 13 sensors, and shifts corresponding to 8 km/s, to adequately cover regional events.

4.0-8.0 Hz

The events analyzed for this frequency band demonstrate that there is no longer one particular subgeometry with a superior performance, as was found for all frequency bands hitherto considered. This is clearly demonstrated by Table VII.4.3, where it is seen that 4 to 5 different geometries give gains that are within 1.5 dB of the highest gain achieved, both for the infinite velocity beams and for the steered beams.

Among signals with peak frequencies in the lower part of this band, we find events at far regional and short teleseismic ranges. One would like to select one infinite velocity beam for detection of these events, but it is not evident which one should be chosen. For local and regional signals in the entire passband 4.0-8.0 Hz, it seems appropriate to choose the geometry A0, B ring and C ring and deploy 8 steered beams of velocity 8 km/s evenly distributed around the circle. The beam pattern of this geometry suggests that 8 beams are sufficient for adequate coverage. Our results indicate that gains of the order of 10 dB could be realistically expected. In consistency with these beams, the one vertical beam could be formed using the same sensors.

The column labelled 'Nsupp8' in the tables is included to indicate what noise suppressions should be expected when typical regional beams of velocity 8 km/s are formed. From the three tables given, it is seen that this noise suppression almost matches the one obtained for vertical beams, with some exceptions for results given for the 2.5-4.5 Hz band (Table VII.4.2). Taking all events in our data base into consideration, it is found that the noise suppression for the 8 km/s steered beams is generally within 1-2 dB of the corresponding infinite velocity beam noise suppression.

8.0-16.0 Hz

Vertical beams make no sense in this frequency band. The interest in detection in this band is limited to local and regional signals, and the detection beams must be steered to the Pn phase velocity of 8.0 km/s, with a minimum of 8 beams to ensure adequate coverage. A good choice of geometry might be the 8 sensors A0, the A and B rings. A good alternative might be the deployment of one so-called incoherent beam, see below.

Summary and recommendations

The main results of this study are summarized in Figs. VII.4.2 and VII.4.3. Fig. VII.4.2 shows the average beam gains as a function of the lower cutoff frequency of the 7 bands, for 4 selected geometries. This figure comprises both regional and teleseismic events. Fig. VII.4.3 shows, for teleseismic events only, the difference between the gains for steered beams and for the corresponding infinite velocity beams. We see that for 2 Hz and below these differences are very modest but then increase rather abruptly at 2.5 Hz for several of the geometries, indicating the importance of steered beams from this frequency upwards. By combining the two figures, it is seen that vertical beams for at least one of the two subgeometries 1) A0, C and D ring and 2) A0, B and C ring provide more than 10 dB gain for teleseismic events with peak frequencies in the bands with lower cutoff up to and including 3.0 Hz. For higher frequencies steered beams are required in order to achieve 10 dB gain for teleseismic signals.

To achieve similar gains for the regional signals, even more steered beams must be deployed. A viable alternative here is the use of incoherent beams, which are already used by RONAPP for the detection of secondary phases, see Ringdal (1985). The use of a few such beams in the detection of high frequency regional P phases may reduce substantially the number of coherent beams otherwise needed. The recommendations for coherent beam deployment as resulting from this study are summarized in Table VII.4.4.

The results obtained in this study have been compared to SNR gains computed directly in the time domain, with measurements of maximum noise and signal amplitudes. The results confirmed the findings in this investigation.

T. Kværna
S. Mykkeltveit

References

Fyen, J. (1986): NORESS noise spectral studies, preliminary report. Semiannual Technical Summary, 1 October 1985 - 31 March 1986, NORSAR Sci. Rep. No. 2-85/86, Kjeller, Norway.

Mykkeltveit, S., D.B. Harris and T. Kværna (1985): Preliminary evaluation of the event detection and location capability of the small-aperture NORESS array. Semiannual Technical Summary, 1 October 1984 - 31 March 1985, NORSAR Sci. Rep. No. 2-84/85, Kjeller, Norway.

Ringdal, F. (1985): Initial results from NORESS detection processing. Final Technical Report, 1 April - 30 September 1985, NORSAR Sci. Rep. No. 1-85/86, Kjeller, Norway.

1.0-3.0 Hz

Results for infinite velocity beams:

AOwgt	Arwgt	Brwgt	Crwgt	Drwgt	Gain	Sloss	Nsupp	Nsupp8
1	0	0	1	1	13.21	0.35	13.56	12.40
1	1	1	1	1	9.64	0.26	9.90	9.63
1	0	0	0	1	10.56	0.54	11.10	10.46
1	0	0	1	1	13.21	0.35	13.56	12.40
1	0	1	1	1	11.21	0.16	11.37	11.06
1	1	1	1	0	6.16	0.00	6.16	6.02
1	0	1	1	0	7.17	0.00	7.17	6.94
1	1	1	0	0	2.53	0.00	2.53	2.62
1	1	0	0	0	0.89	0.00	0.89	0.92

Results for steered beams:

AOwgt	Arwgt	Brwgt	Crwgt	Drwgt	Gain	Sloss	Nsupp
1	0	0	1	1	12.99	0.00	12.99
1	1	1	1	1	9.77	0.00	9.77
1	0	0	0	1	11.04	0.09	11.13
1	0	0	1	1	12.99	0.00	12.99
1	0	1	1	1	11.21	0.00	11.21
1	1	1	1	0	6.24	0.00	6.24
1	0	1	1	0	7.22	0.00	7.22
1	1	1	0	0	2.63	0.00	2.63
1	1	0	0	0	0.91	0.00	0.91

Results for infinite velocity beams, extended weighting scheme:

AOwgt	Arwgt	Brwgt	Crwgt	Drwgt	Gain	Sloss	Nsupp
0.5	0.0	0.0	1.0	1.0	13.27	0.35	13.62
0.0	0.0	0.0	1.0	1.0	13.15	0.35	13.50
0.5	0.0	0.0	0.5	1.0	13.13	0.37	13.50
1.0	0.0	0.0	0.5	1.0	13.00	0.38	13.38
1.0	0.0	0.5	0.5	1.0	11.99	0.35	12.34

Table VII.4.1 Gain results for one of the events analyzed in this frequency band. The signal had a peak frequency of 1.4 Hz, an SNR (online) of 91.8, apparent velocity 16.37 km/s and arrival azimuth of 14.7 degrees. See the text for explanation of abbreviations.

2.5-4.5 Hz

Results for infinite velocity beams:

AOwgt	Arwgt	Brwgt	Crwgt	Drwgt	Gain	Sloss	Nsupp	Nsupp8
1	0	1	1	0	13.18	1.11	14.29	11.70
1	1	1	1	1	9.67	3.88	13.55	9.63
1	0	0	0	1	-0.55	9.90	9.35	10.17
1	0	0	1	1	7.18	6.02	13.20	13.56
1	0	1	1	1	10.00	4.44	14.44	13.97
1	1	1	1	0	10.79	0.92	11.71	9.62
1	0	1	1	0	13.18	1.11	14.29	11.70
1	1	1	0	0	4.87	0.26	5.13	4.58
1	1	0	0	0	1.36	0.08	1.44	1.31

Results for steered beams:

AOwgt	Arwgt	Brwgt	Crwgt	Drwgt	Gain	Sloss	Nsupp
1	0	1	1	1	13.98	0.54	14.52
1	1	1	1	1	12.78	0.45	13.23
1	0	0	0	1	8.87	1.01	9.89
1	0	0	1	1	13.00	0.63	13.63
1	0	1	1	1	13.98	0.54	14.52
1	1	1	1	0	11.14	0.00	11.14
1	0	1	1	0	13.58	0.00	13.58
1	1	1	0	0	4.72	0.00	4.72
1	1	0	0	0	1.33	0.00	1.33

Table VII.4.2 Gain results for one of the events analyzed in this frequency band. The signal had a peak frequency of 2.6 Hz, an SNR (online) of 238.4, apparent velocity 13.36 km/s and arrival azimuth of 89.1 degrees.

4.0-8.0 Hz

Results for infinite velocity beams:

A0wgt	Arwgt	Brwgt	Crwgt	Drwgt	Gain	Sloss	Nsupp	Nsupp8
1	0	1	0	0	7.69	1.31	9.00	7.96
1	1	1	1	1	3.90	9.90	13.80	13.56
1	0	0	0	1	-4.97	14.89	9.92	10.17
1	0	0	1	1	-5.58	17.72	12.14	12.77
1	0	1	1	1	2.36	12.04	14.40	13.98
1	1	1	1	0	7.23	4.15	11.38	11.06
1	0	1	1	0	7.08	5.04	12.12	12.04
1	1	1	0	0	6.35	1.01	7.36	7.13
1	1	0	0	0	2.32	0.27	2.59	2.73

Results for steered beams:

A0wgt	Arwgt	Brwgt	Crwgt	Drwgt	Gain	Sloss	Nsupp
0	1	1	1	1	12.00	1.94	13.94
1	1	1	1	1	11.49	1.83	13.32
1	0	0	0	1	5.56	4.01	9.57
1	0	0	1	1	9.63	2.62	12.25
1	0	1	1	1	11.97	2.05	14.02
1	1	1	1	0	10.56	0.54	11.10
1	0	1	1	0	11.86	0.54	12.40
1	1	1	0	0	6.41	0.18	6.59
1	1	0	0	0	2.39	0.08	2.47

Table VII.4.3 Gain results for one of the events analyzed in this frequency band. The signal had a peak frequency of 4.6 Hz, an SNR (online) of 264.1, apparent velocity 11.10 km/s and arrival azimuth of 166.3 degrees.

Frequency band Hz	Configuration	Velocity km/s	Azimuths
1.0-3.0	A0 C D	∞	
1.5-3.5	A0 C D	∞	
2.0-4.0	A0 C D	∞	
	A0 C D	8.0	(i)
2.5-4.5	A0 B C	∞	
	A0 B C D	8.0	(i)
3.0-5.0	A0 B C	∞	
	A0 B C	8.0	(i)
4.0-8.0	several possibilities	∞	
	A0 B C	8.0	(ii)
8.0-16.0	A0 A B	8.0	(ii)

(i) : These beams could be pointed to source regions of particular interest, or alternatively, distributed evenly around the circle.

(ii) : 8 beams spaced at 45 degrees intervals are recommended.

Table VII.4.4 Recommendation for deployment of coherent beams for optimum detection of P waves on NORESS.

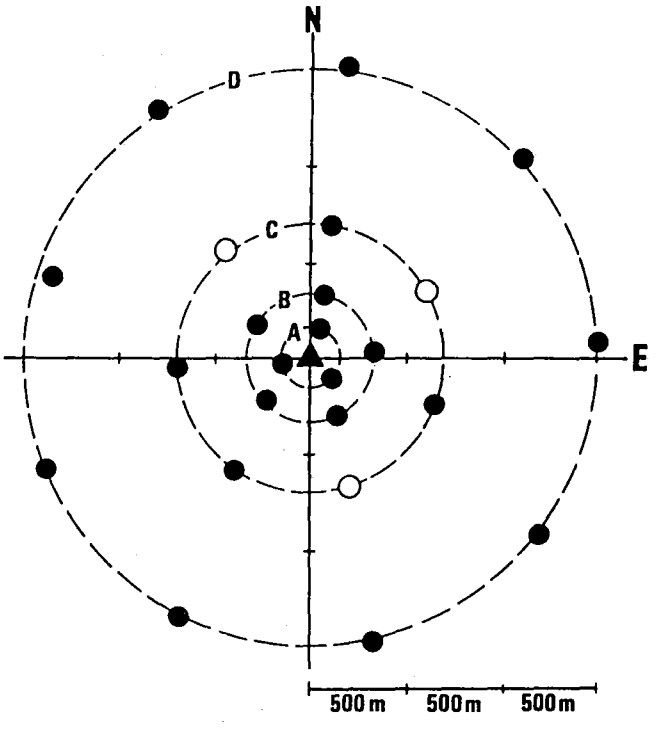

LEGEND:

● VERTICAL SHORT PERIOD

○ 3-COMPONENT SHORT PERIOD

▲ 3-COMPONENT BROAD BAND
AND 3-COMPONENT SHORT PERIOD

Fig. VII.4.1 The geometry of the NORESS array. The instrument at the center is denoted A0. This investigation deals with data from the vertical short period array, comprising one sensor at each of the 25 instrument sites.

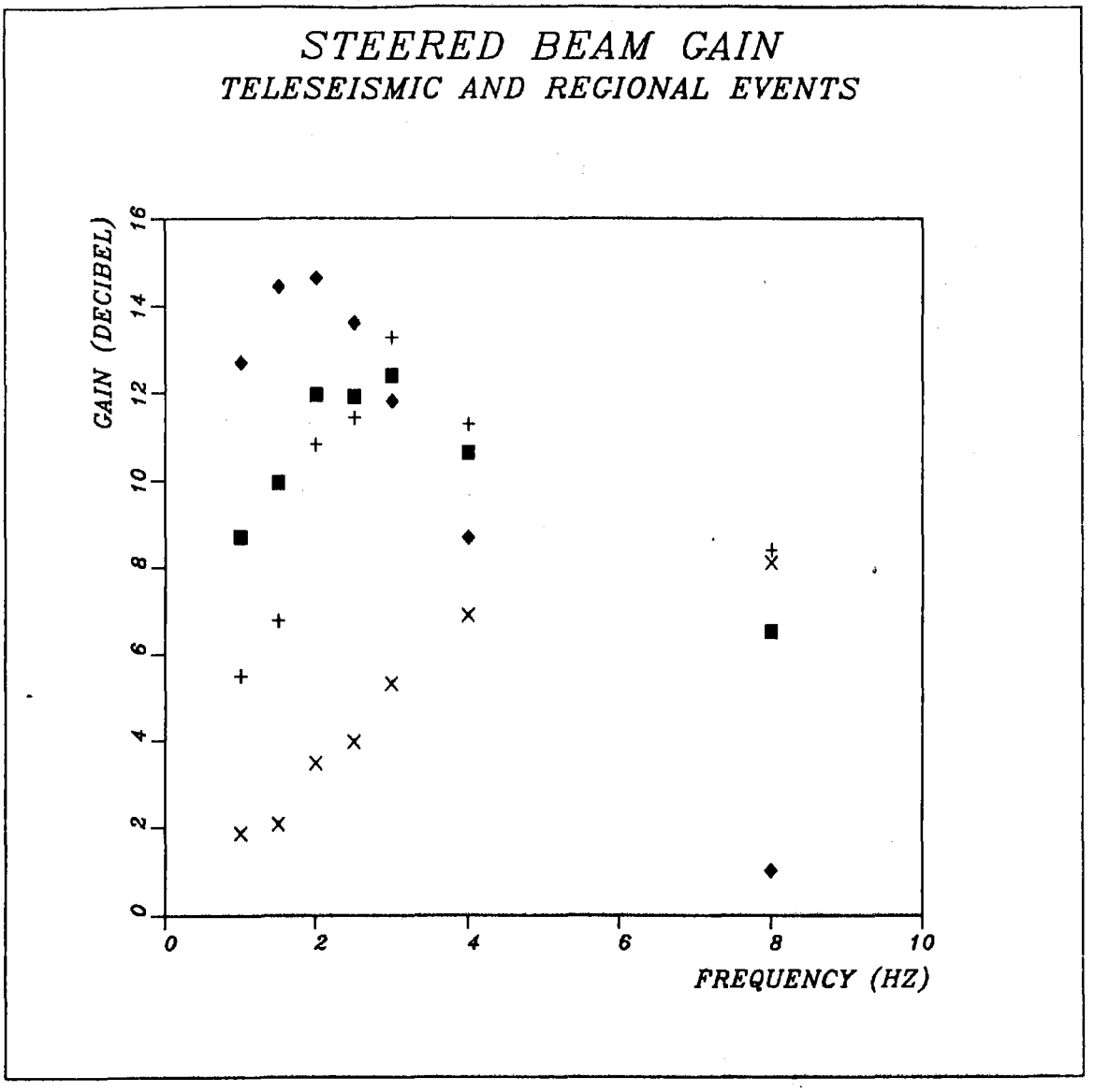

NORESS subgeometries:

◆ A0, C ring, D ring

\+ A0, B ring, C ring

■ All sensors

× A0, A ring, B ring

Fig. VII.4.2 Gains for optimally steered beams as a function of lower cutoff frequency for the 7 passbands considered in this study, for 4 selected NORESS subgeometries. For each geometry and frequency, the gain is the average for all events analyzed, both regional and teleseismic.

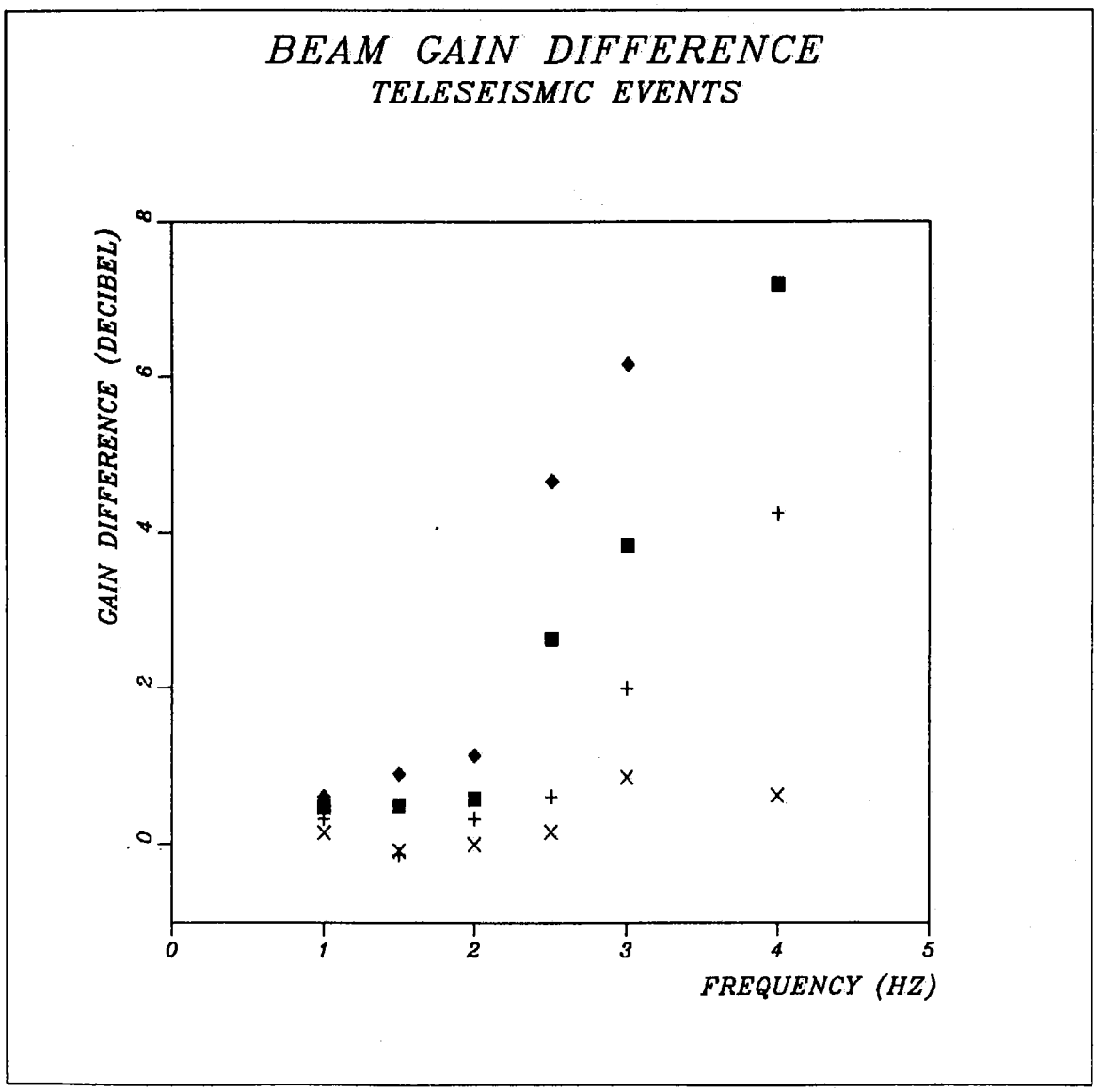

Fig. VII.4.3 The figure shows the differences between the gains for optimally steered beams and for the corresponding vertical beams. Only signals of apparent velocities above 11 km/s have been used. Symbols correspond to the ones in Fig. VII.4.2.

VII.5 NORESS noise spectral studies - system description

The NORESS noise spectral recording system has been developed to run unattended on the NORESS data recording computer, in parallel with the RONAPP processor (IBM 4341 with VM/CMS).

The idea behind the system is to systematically observe noise frequency spectra in order to determine characteristic features of noise over short and long periods of time. Moreover, the system will be able to observe noise beam suppression for different array configurations.

After some initial testing it was decided to use one minute of NORESS SPZ data to estimate noise spectrum and beam suppression, and to conduct the estimation on an hourly basis. As a procedure for spectral estimation we adopted the method described by Kværna et al in NORSAR Scientific reports nos. 2-84/85 and 1-85/86. The background for this was discussed in NORSAR Sci. rep. no 2-85/86.

A number of programs and procedures has been developed for this purpose. Overall, the spectral recording system is divided into 4 steps :

1. Search for one minute of noise data at a specified time.
   This involves checking NORESS recording status, NORESS recording gap statistics and RONAPP event processing results.
2. Calculate spectra for individual channels and selected beams, and record the results.
3. Analyze the observed data and compile statistics.
4. Do regular backup of the observed data on tape.

Step 1. Search for noise intervals

To be sure to find a one-minute data interval of noise without interfering signals or data errors, 5 programs (CMS procedure language REXX) have been developed.

NORREC - reports NORESS recording time intervals. It may also be used to see whether a wanted time interval has been recorded.

NRSINT - reports NORESS current recording statistics and RONAPP processing times. It is also used to see whether a wanted time interval has been processed by RONAPP.

NORGAP - reports NORESS recording gaps. Gaps are of typical length 1 to 4 seconds. It is here used to see whether a wanted time interval has any recording gaps.

NORDET - reports RONAPP processing results, and detection lists. It is here used to see whether a wanted time interval has any reported detections. If so, the time is adjusted to avoid such signals.

NORSTL - reports NORESS communication statistics and other data quality statistics. It is used to see whether any individual channels should be avoided for a given time interval.

NRSONLIN is the main driving procedure. The previous time of spectral computation is read and is used to find a new time interval, one hour later, and on the hour. All the procedures above are then run to see whether the data interval is acceptable. If not, the selected time is incremented by three minutes, and the tests are run over again. When a time interval has been found, all the necessary inputs to the spectral system are created, and the procedure NRSSPC is executed. If the tests result in incrementation of time passed current RONAPP processed time, then the NRSONLIN procedure go to 'sleep' for a preset number of hours. When the wait time has elapsed, the procedure resumes all the checking procedures. The NRSONLIN procedure is programmed to either find noise after these

criteria, or detections. It has also been used to control programs that execute on detected signals only.

Step 2 . Calculate power spectra

NRSSPC is developed for calcualtion of power spectra for individual NORESS SPZ channels or beams. The calculation of spectra using the method of Kværna et al is performed in pratice by linking the NRSSPC and DISPAT programs together. DISPAT is the interactive analysis program described by Harris and Kværna in NORSAR Sci.rep. No 2-84/85. The DISPAT program includes the use of macros to do specific calculation procedures. This has been adopted by the spectral system in such a way that data is presented to DISPAT together with name of the macro to be used for spectrum estimation. In this way we obtain flexibility in the calculation process.

The input to the spectral system program is mainly start time of analysis, length of data (one minute), channels and/or beams to use. An input file is easily set up to define the actual beam configurations. Velocity and azimuth may be given, and the velocity used so far is 999.9 km/sec which give zero delays (vertical beam or direct sum). The input file may give a name to each beam configuration, and list the channels to use. The beams currently used are as follows:

BRING - 9 sensors, AOZ plus A-ring instruments plus B-ring SPZ instruments.
CRING - 13 sensors, AOZ plus B-ring plus C-ring.
TELEV - 17 sensors, AOZ plus C-ring plus D-ring.
HIFRQ - 16 sensors, AOZ plus A-ring plus B-ring plus C-ring.
INTER - 22 sensors, AOZ plus B-ring plus C-ring plus D-ring.
ALLV - 25 sensors, All SPZ instruments.

Before doing any calculations, NRSSPC inspects whether the NRSONLIN process reported any channel as bad. If so, the configurations are automatically adjusted, leaving out possible bad data channels. Thereafter RMS is calculated for each individual SPZ channel. The individual values are compared to the mean value, and if a channel is more than two standard deviations from the mean, then that channel is excluded from analysis. The next step is estimating power spectra for each individual SPZ. The arithmetic average of all accepted SPZ channel spectra is called 'MEANZ'. The individual spectra are compared to the mean spectrum point for point (total 512 points in one spectrum). If 250 of the values for one channel is outside two standard deviations from the mean, then that channel is declared an outlier, and a new MEANZ is calculated. An outlier channel is also excluded from the beamforming. This technique of data quality control successfully masks outliers due to near-field weak events, bad data due to electronics failures and channels with numerous spikes. A channel with one spike (or few single spikes) will not be detected by this procedure, which has been in effect since day 154/1986.

After the masking procedure has been performed, all the selected beams are formed and spectra calculated. The program then record the data on disk files. The disk file names follow the general NORSAR rules for data files, where the name of the file defines both the content of the file and the time and date of the data. NORESS spectra files are denoted for example by SPC86277 1201350, where SPC identifies the content as spectra data, and the data were observed day 277, 1986 at 12.01.35.0.

During some time periods the borehole instrument FOZ has been used instead of AOZ. Until day-of-year 176, 1986 we recorded all the individual spectra. At present (november 1986), only MEANZ spectrum plus the beam spectra are recorded. In addition, spectra of the high frequency system NORESS HFSE, and the three component stations A0, C4 and C7 are recorded.

Step 3. Analyze the observed data and compile statistics

To find the characteristics of the data we have developed the program SPC. This program allows the analyst to plot any of the spectra for any time interval, and calculate noise suppression. Noise suppression is defined as the function BEAM/MEANZ, where BEAM is the spectrum of the actual beam.

All measurements are here reported in dB relative to one quantum unit squared, as sampled by the NORESS system. No corrections are done to determine ground motion, since the features we want to extract are the relative noise variations over time and beam noise suppression.

To report the content of this data, a standard procedure has been adopted. For every week we plot the following data, where the term 'versus time' mean that we plot exactly one week of data , and x-axis is 7*24 hours. The standard plots are:

1 Average noise RMS for NORESS SPZ instruments versus time.
2 NORESS HUB temperature versus time.
3 NORESS HUB average wind speed and maximum wind speed over one hour, plotted versus time.
4 MEANZ for selected frequencies versus time. Frequency bands are 0.4 - 0.6 Hz, 1.9 - 2.1 Hz, 5.9 - 6.1 Hz, 9.9 - 10.1 Hz, 14.9 - 15.1 Hz.
5 MEANZ for selected frequencies versus time. Frequency bands are 0.9 - 1.1 Hz, 2.9 - 3.1 Hz, 6.9 - 7.1 Hz,11.9 - 12.1 Hz, 16.9 - 17.1 Hz.
6 BRING noise suppression versus frequency. All observations within week.
BRING noise suppression average and standard deviation.
7 CRING noise suppression versus frequency. All observations within week.
CRING noise suppression average and standard deviation.
8 CRING noise suppression for frequencies within 3.4 - 3.7 Hz versus time.
9 TELEV noise suppression versus frequency. All observations within week.
TELEV noise suppression average and standard deviation.
10 TELEV noise suppression versus frequency. Only observations from 00 GMT.
11 TELEV noise suppression versus frequency. Only observations from 08 GMT.
12 TELEV noise suppression for frequencies within 1.9 - 2.1 Hz versus time.
13 INTER noise suppression versus frequency. All observations within week.
INTER noise suppression average and standard deviation.
14 HIFRQ noise suppression versus frequency. All observations within week.
HIFRQ noise suppression average and standard deviation.
15 ALLV noise suppression versus frequency. All observations within week.
ALLV noise suppression average and standard deviation.

16 All HFZ power spectra for the week.
17 All HFN power spectra for the week.
18 All HFE power spectra for the week.
19 HFZ power spectra for 00 GMT hours only.
20 HFZ power spectra for 12 GMT hours only.
21 HFZ for selected frequencies versus time. Frequency bands are
4.8 - 5.2 Hz, 14.8 - 15.2 Hz, 47.3 - 47.6 Hz.
22 HFZ for selected frequencies versus time. Frequency bands are
5.8 - 6.2 Hz, 17.8 - 18.2 Hz.
23 HFZ for selected frequencies versus time. Frequency bands are
29.4 - 29.7 Hz, 19.9 - 20.2 Hz.
24 HFZ for selected frequencies versus time. Frequency bands are
0.8 - 1.1 Hz, 11.8 - 12.1 Hz, 34.9 - 35.2 Hz.
25 HFZ for selected frequencies versus time. Frequency bands are
0.3 - 0.7 Hz, 24.9 - 25.2 Hz.
26 HFZ for selected frequencies versus time. Frequency bands are
41.9 - 42.1 Hz, 2.9 - 3.2 Hz.
27 HFZ for selected frequencies versus time. Frequency bands are
49.8 - 50.1 Hz, 3.9 - 4.2 Hz.

The selected frequency bands have been chosen as a representative set.

Backup

Standard procedures for VM/CMS disk file backup are used to store the observed data on tapes.

The NORESS noise spectral recording system as described here, has now been running since March 7, 1986.

Figs. VII.5.1a&b show the recording statistics for the spectral system.

J. Fyen

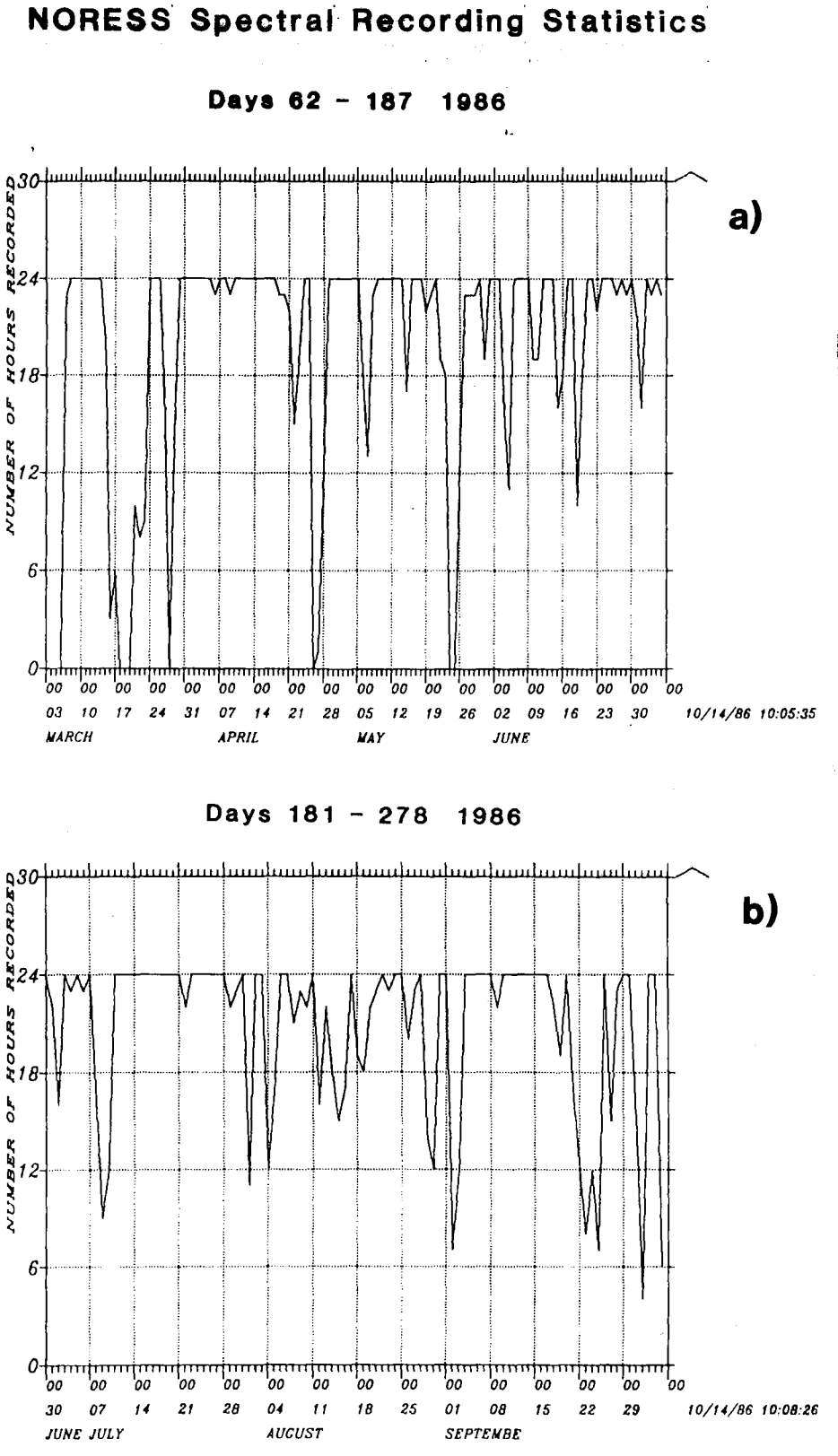

Fig. VII.5.1 NORESS noise spectral system recording statistics. The points plotted are number of hours recorded per day.

VII.6. NORESS noise spectral studies - beam suppression

We refer to section VII.5 for description of the NORESS noise spectral system.

The objective of the system is to collect, on a regular basis, data that are relevant to the detection algorithms. In this report we will draw some conclusions based upon 6 months of data, during which period we have recorded noise spectra for NORESS short period instruments and beams every hour. We will also go into some of the data in more detail to document the outcome of the huge amount of processing that has been done.

The production scheme listed in section VII.5 gives a far too large amount of plots to be documented in this summary, and will therefore be the subject of a separate report. Rather, we have chosen to show a few examples which illustrate our conclusions, based on 4-6 months of data.

We have chosen week 30, 1986, as reference for this report, due to good recording statistics that week.

Beam suppression spectrum S(f) is defined as the ratio between the beam power spectrum B(f) to the average SPZ power spectrum ('MEANZ'). This ratio is expected to reach the value 1/N for random uncorrelated noise, or $1/\sqrt{N}$ for noise amplitudes.

In this report we have plotted the function SUPP(f) defined by:

$$S(f) = B(f)/MEANZ(f),\ SUPP(f) = 10\log(S) = 10\log(B) - 10\log(MEANZ)$$

For TELEV beam, SUPP(f) is expected to obtain the value -12.3 dB.

Figs. VII.6.1-2 display the observed TELEV beam suppression spectra for week 30. The number of spectra in the figure is 166, i.e., 7*24 minus 2 hours with no recording. The -10log(N) line is denoted $\sqrt{N}$ in all figures concerning beam suppression. In Fig. VII.6.2 we show the arithmetic mean of the beam suppression spectra together with plus/minus one standard deviation.

All average spectra that are displayed in this report have been corrected for outliers in the following way:

For each frequency the mean value and standard deviation is calculated. If an individual spectrum at one point is more than two standard deviations from the mean, then that spectrum is given one outlier score. If the value is among the 15% highest or lowest values it is also given one score. Then, if a spectrum obtains more than 250 scores (one spectrum is 512 points), that spectrum is excluded from the final estimate of average and standard deviation.

From Figs. VII.6.1 and VII.6.2 we observe that on an average the theoretical $\sqrt{N}$ noise suppression is obtained for all frequencies above 1.3 Hz using the TELEV configuration. Lower frequencies are not suppressed as much by this beam configuration, since noise for these lower frequencies becomes more coherent within the NORESS array. For frequencies above 4 Hz, the beam suppression spectrum follows the expected results for normally distributed stochastic processes. Between 1.3 and 4.0 Hz the TELEV beam configuration clearly demonstrates a better suppression than expected. At 2.13 Hz the average suppression is -17.5 dB, which corresponds to a theoretical number of instruments of 56.

Morever, this 'extra' suppression has been consistently observed during our recording period. As an illustration of this, Figs. VII.6.3 and VII.6.4 show the spectra for GMT hours 00 and 08 only. We may here conclude that the minima are the same for night-time and day-time, but

the extra suppresion is narrower for day-time periods. This feature is to some extent observed throughout this reporting period.

Fig. VII.6.5 displays frequencies between 1.9 and 2.1 Hz plotted versus time during week 30. We see that the TELEV extra suppression is mostly independent of time-of-day and week-day. The variation is ± 1.5 dB. We are not able to see any characteristic features that correlate with time of observation.

There is a 'bump' in the spectrum at 7.3 Hz which is more pronounced on night-time observations during week 30. This effect, however, is not systematically observed for other time periods.

In Figs.VII.6.6 - 13 we have displayed the features of the other beam configurations, and only the average values with standard deviations are plotted.

Fig. VII.6.6 shows that the BRING configuration (A0Z - A3Z plus B1Z - B5Z, Fig. VII.6.6) approaches the theoretical suppression for frequencies above 5.3 Hz. Moreover, the suppression obtained is on an average more than expected.

Fig. VII.6.7 shows the CRING configuration (A0Z , B1Z - B5Z, C1Z - C7Z). This beam shows additional suppression for frequencies between 2.5 and 7.7 Hz, which is systematically observed. Again the minima are independent of time of observation, as seen in Fig. VII.6.8.

The HIFRQ configuration has no pronounced extra suppression, at least not of the same dimension as TELEV and CRING. Still, a very consistent pattern is however observed. These remarks also apply to the INTER and ALLV configurations.

The consistency of observations is shown in Figs. VII.6.12 - 13 where we have average beam suppression for CRING and TELEV. These are averages of observations made at 02 local time only, and over the period day 062 through day 187 (4 months). We see that there is not much variance in the observation of beam suppression. Single case studies may actually give a good measure of a beam suppression spectrum.

Conclusions for the configuration study are shown in Fig. VII.6.14. Comparing with the bold curve for ALLV configuration we see that the TELEV and the INTER configuration has better noise suppression characteristics than using all the instruments in the array:

TELEV is 'best' up to 2.8 Hz.
INTER is 'best' from 2.8 Hz and up to 3.9 Hz.

The results based upon more than 5000 noise spectra for each array configuration can be summarized as follows:

Better than $\sqrt{N}$ suppression can be consistently achieved at selected frequencies and subconfigurations, and a subgeometry can outperform the full array.

ALLV - Full array geometry: A0, A, B, C, D rings, 25 instruments. Noise suppression of $\sqrt{N}$, 14 dB is consistently achieved in the band 3.0 - 20.0 Hz.

TELEV - Geometry: A0, C, D rings, 17 instruments. Noise suppression better than $\sqrt{N}$, 12.3 dB is consistently achieved in the band 1.3 - 4.0 Hz. This subgeometry is superior to the full array for all frequencies below 3 Hz.

CRING - Geometry: AO, B, C rings, 13 instruments.
Noise suppression better than $\sqrt{N}$, 11.1 dB is consistently achieved in the band 2.4 - 7.5 Hz.

BRING - Geometry: AO, A, B rings, 9 instruments.
Noise suppression better than $\sqrt{N}$, 9.5 dB is achieved in the band 5.3 - 20.0 Hz, however not as consistent as TELEV. The geometry responds with smaller noise suppression for spurious local noise extremums.

HIFRQ - Geometry: AO, A, B, C rings, 16 instruments.
Noise suppression of $\sqrt{N}$, 12.0 dB is achieved in the band 3.0 - 20.0 Hz. Better than $\sqrt{N}$ is observed, but inferior to TELEV.

INTER - Geometry: AO, B, C, D rings, 22 instruments.
Noise suppression of $\sqrt{N}$, 13.4 dB is achieved in the band 2.0 - 20.0 Hz.
This subgeometry is superior to the full array for all frequencies below 4 Hz.

These studies indicate that there are considerable benefits to be obtained using narrow band filters and selecting array subconfigurations for optimum noise suppression. In addition, the signal beam loss must be studied to determine the best configuration for array beamforming signal-to-noise gain (see Section VII.4).

J. Fyen

86 WEEK 30 TIME 202: 0 208.23

Telev Beam Power - Average SPZ Power

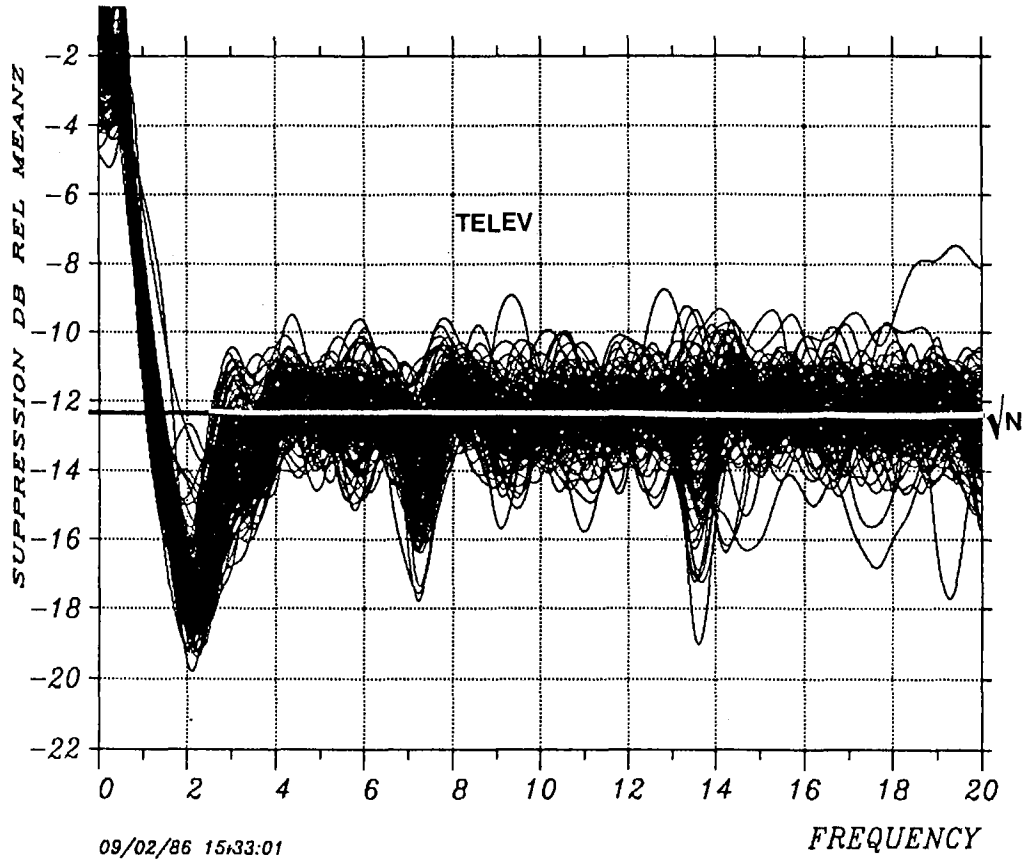

Fig. VII.6.1 Noise suppression for TELEV subgeometry week 30, 1986. The plot contains 166 curves, which are all hourly observed noise suppression spectra for TELEV during week 30.

86 WEEK 30 TIME 202: 0 208.23

Telev Beam Power - Average SPZ Power

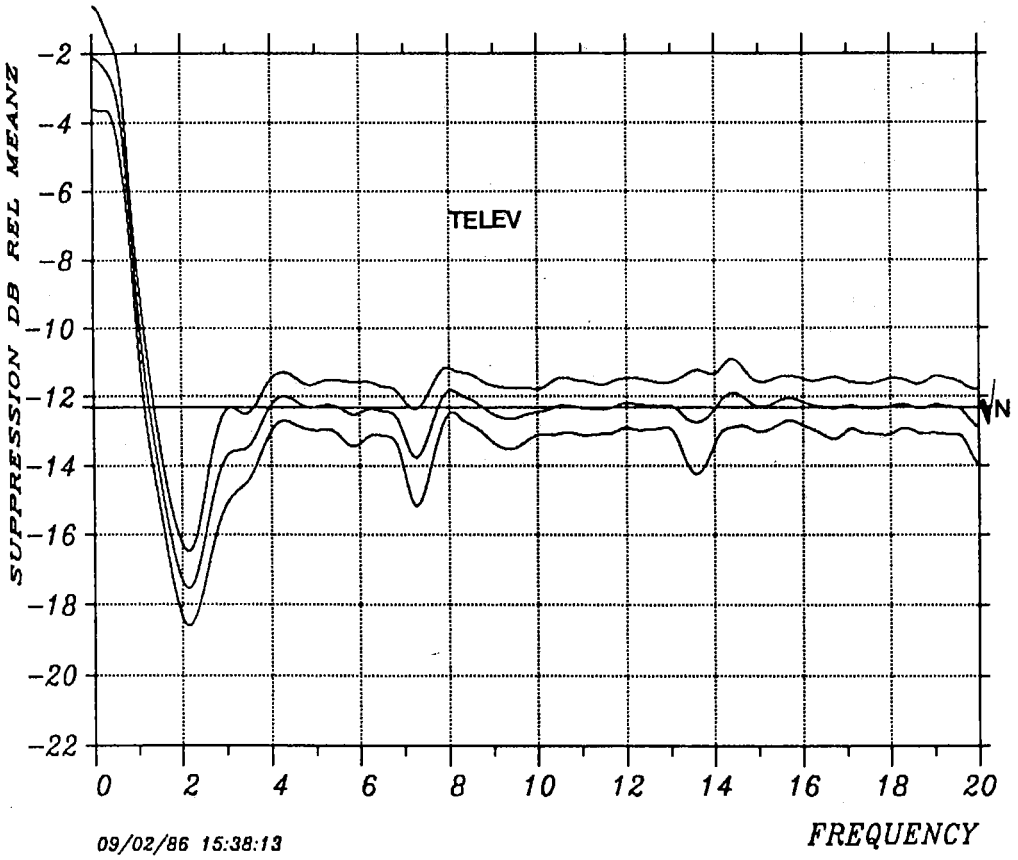

Fig. VII.6.2 Noise suppression for TELEV subgeometry week 30, 1986. The curves plotted are average noise suppression spectrum together with plus/minus one standard deviation.

86 WEEK 30 TIME 202: 0 208.23 00 GMT

Telev MEANZ

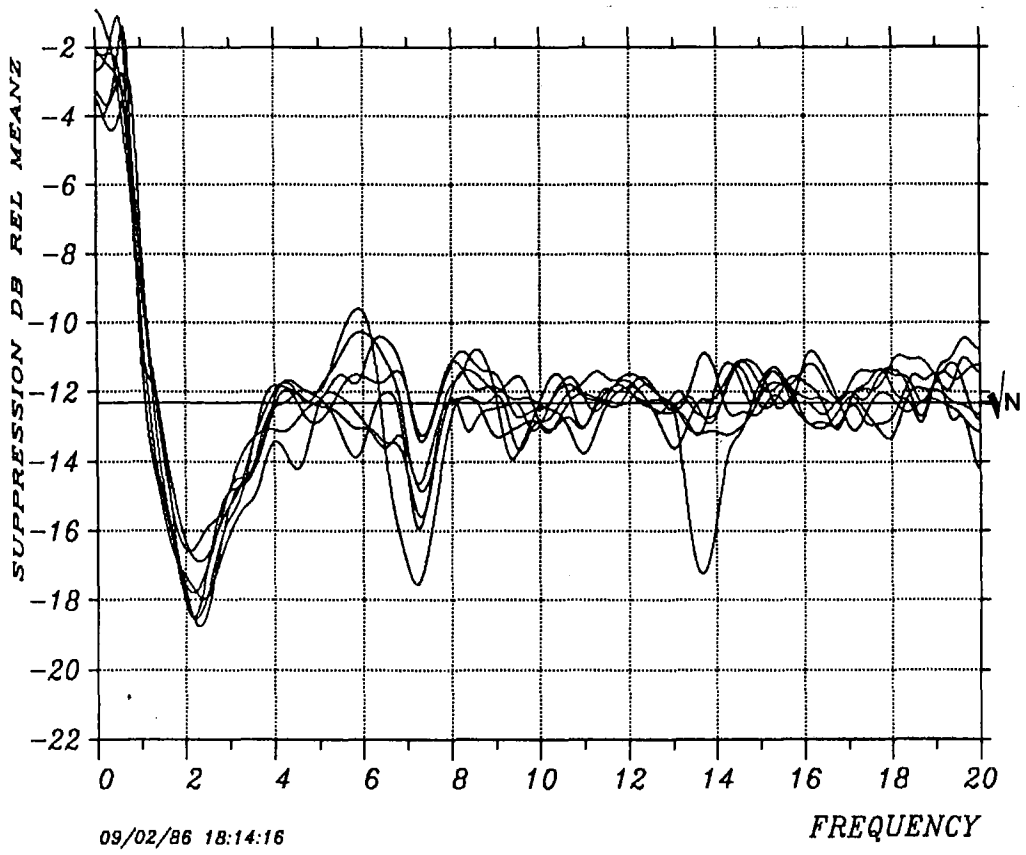

Fig. VII.6.3 Noise suppression for TELEV subgeometry week 30, 1986. The curves plotted are all noise suppression spectra observed at 00 GMT by the NORESS noise spectral system.

86 WEEK 30 TIME 202: 0 208.23 08 GMT

Telev MEANZ

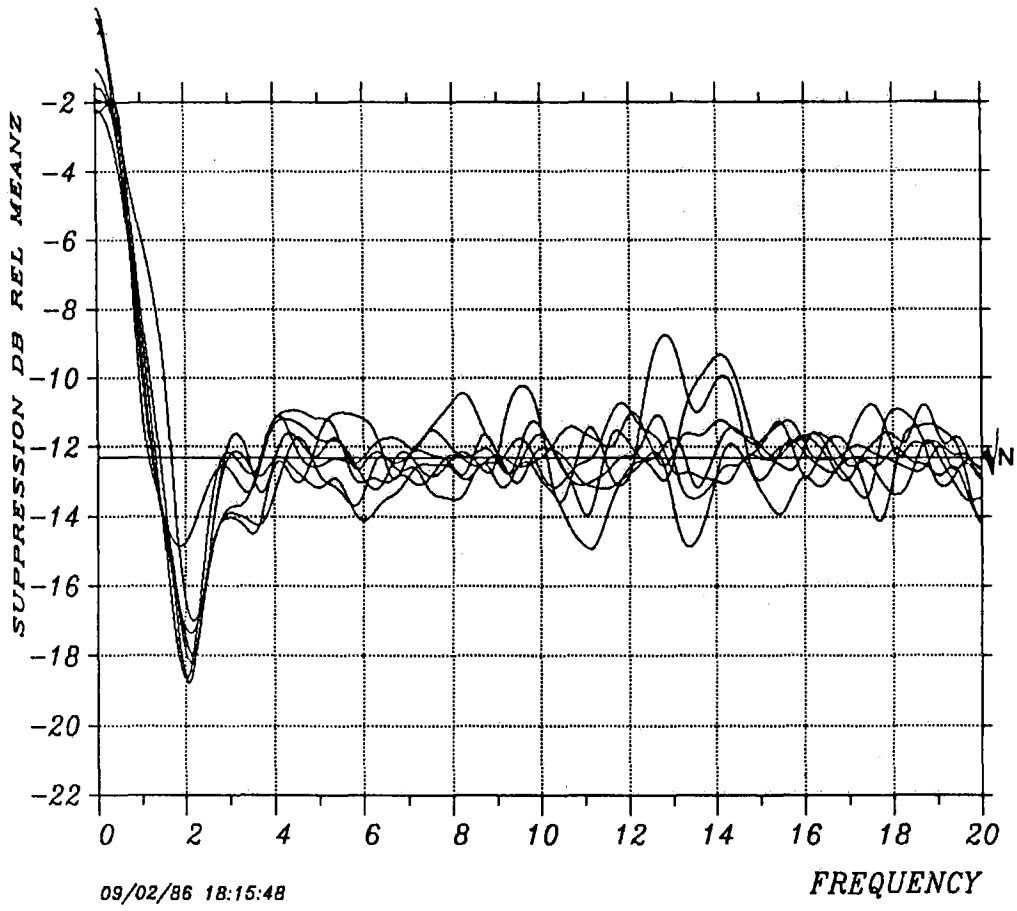

Fig. VII.6.4 Noise suppression for TELEV subgeometry week 30, 1986. The curves plotted are all noise suppression spectra observed at 08 GMT by the NORESS noise spectral system.

86 WEEK 30 TIME 202: 0 208.23

Telev Beam Power - Average SPZ Power 1.9 - 2.1 Hz

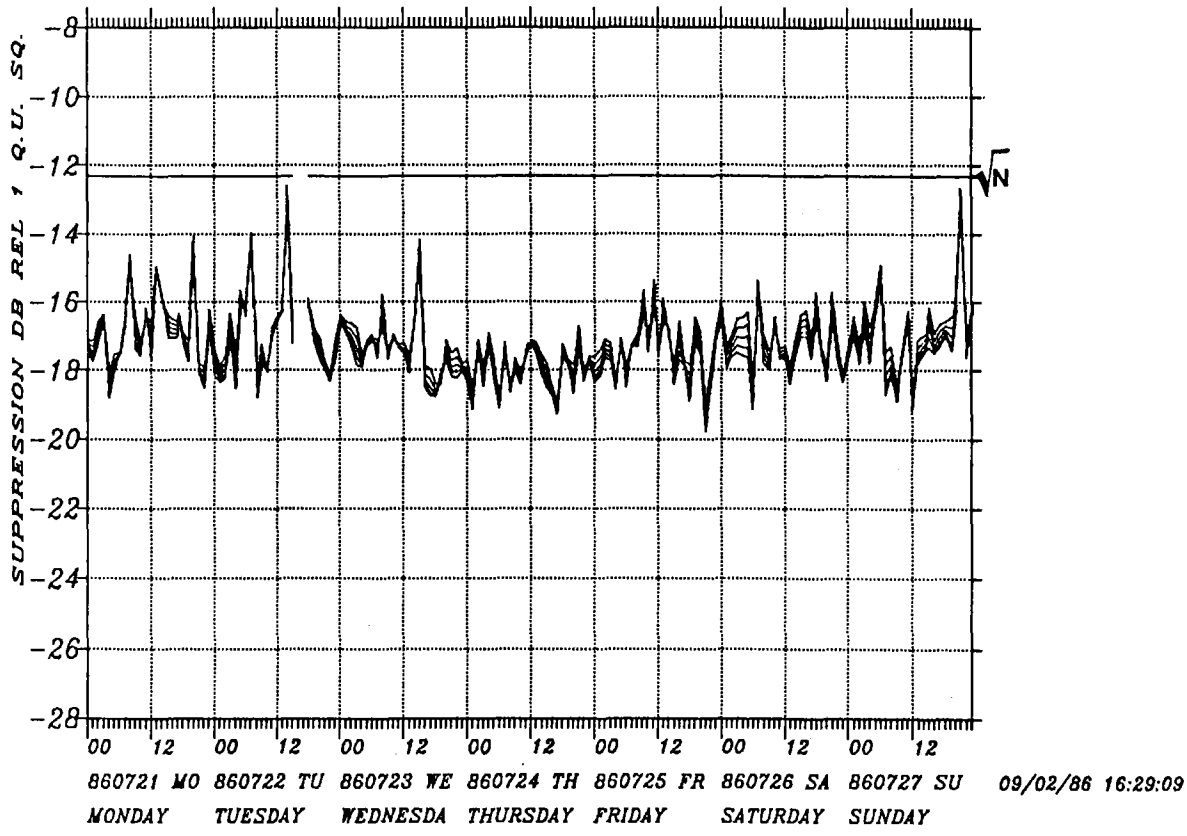

Fig. VII.6.5 Noise suppression for TELEV subgeometry week 30, 1986. The curves plotted are the hourly observed noise suppression values for frequencies between 1.9 and 2.1 Hz.

86 WEEK 30 TIME 202: 0 208.23

BRING Beam Power - Average SPZ Power

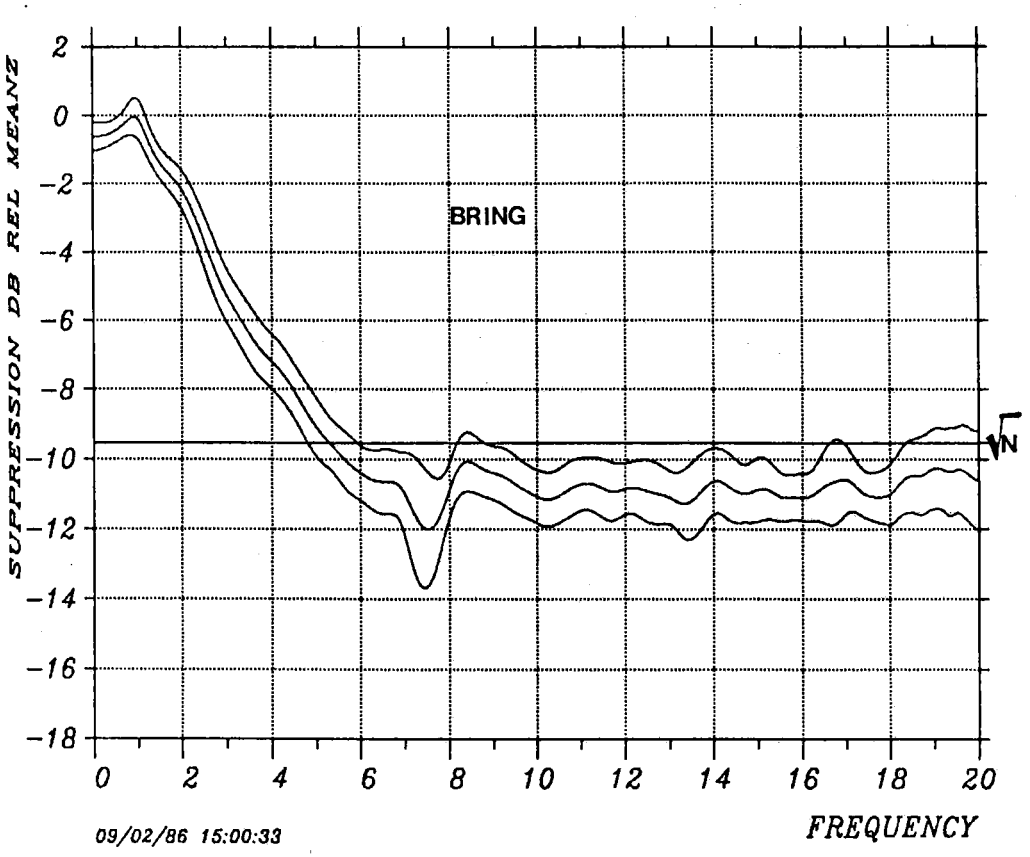

Fig. VII.6.6 Noise suppression for BRING subgeometry week 30, 1986. The curves plotted are average noise suppression spectrum together with plus/minus one standard deviation.

86 WEEK 30 TIME 202: 0 208.23

CRING Beam Power - Average SPZ Power

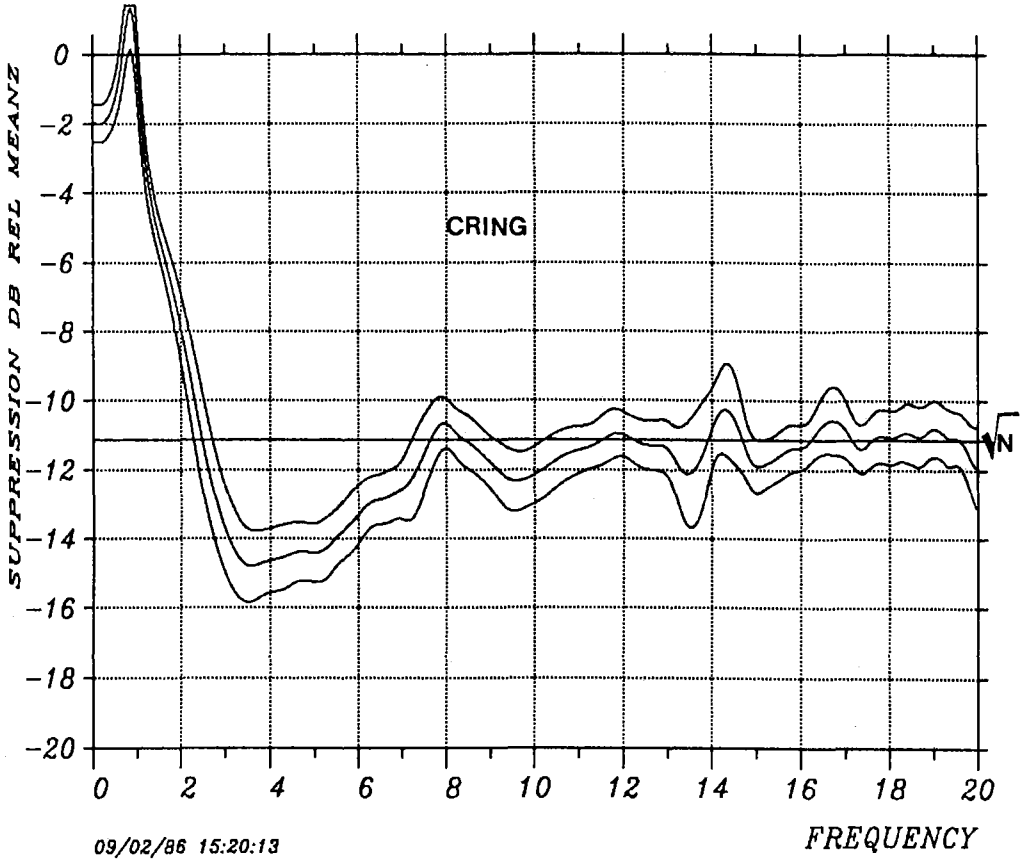

Fig. VII.6.7 Noise suppression for CRING subgeometry week 30, 1986. The curves plotted are average noise suppression spectrum together with plus/minus one standard deviation.

86 WEEK 30 TIME 202: 0 208 .23

CRING Beam Power - Average SPZ Power 3.4 - 3.7 Hz

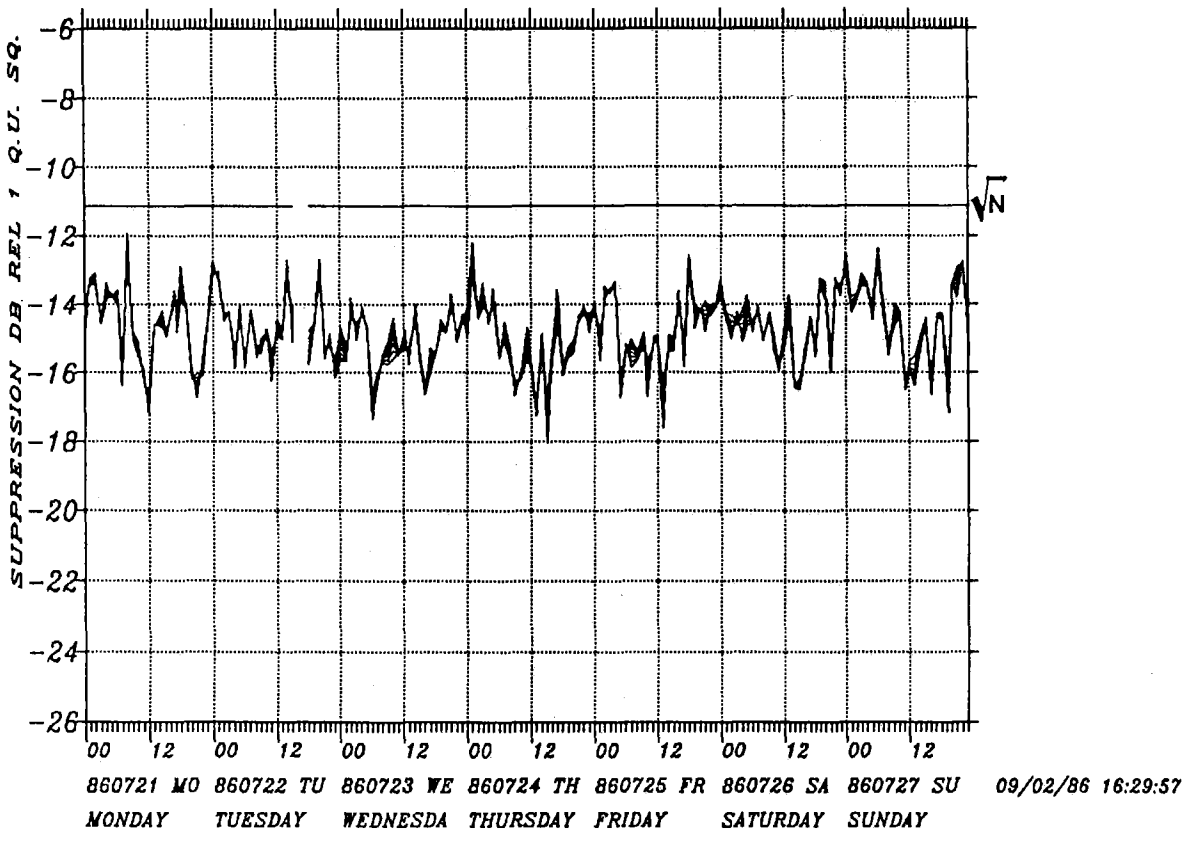

Fig. VII.6.8 Noise suppression for CRING subgeometry week 30, 1986. The curves plotted are the hourly observed noise suppression values for frequencies between 3.4 and 3.7 Hz.

86 WEEK 30 TIME 202: 0 208.23

HIFRQ Beam Power - Average SPZ Power

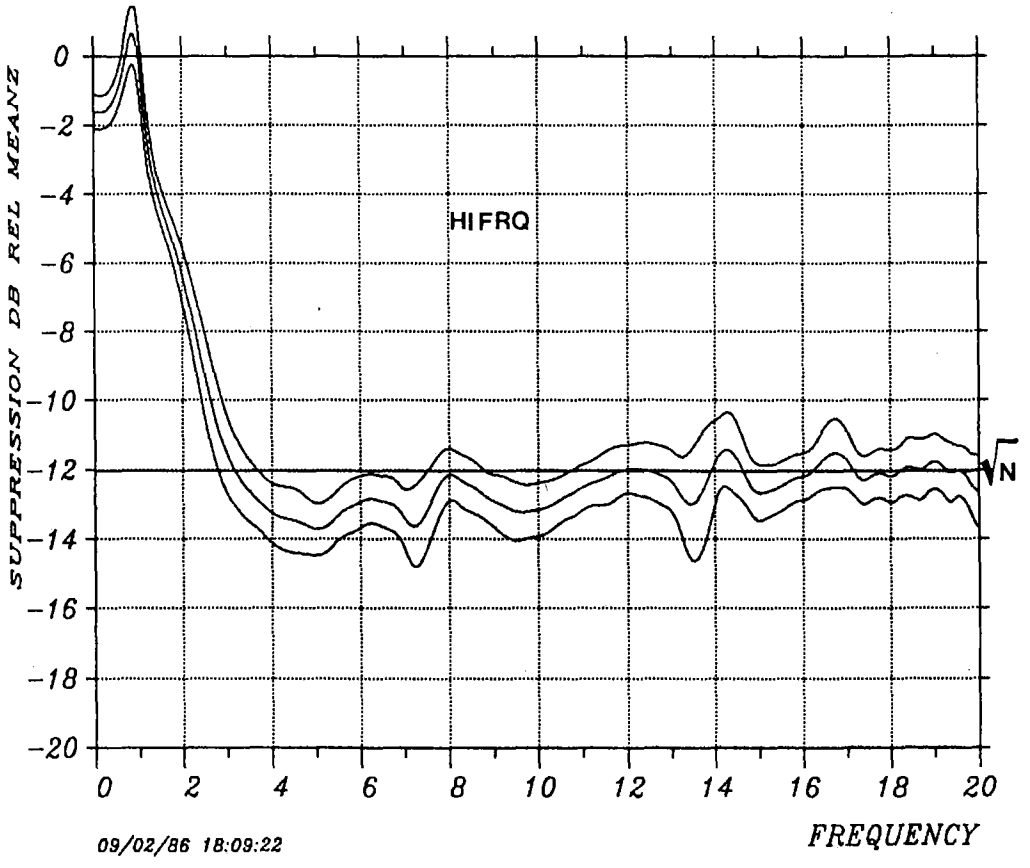

Fig. VII.6.9 Noise suppression for HIFRQ subgeometry week 30, 1986. The curves plotted are average noise suppression spectrum together with plus/minus one standard deviation.

86 WEEK 30 TIME 202: 0 208.23

INTER Beam Power - Average SPZ Power

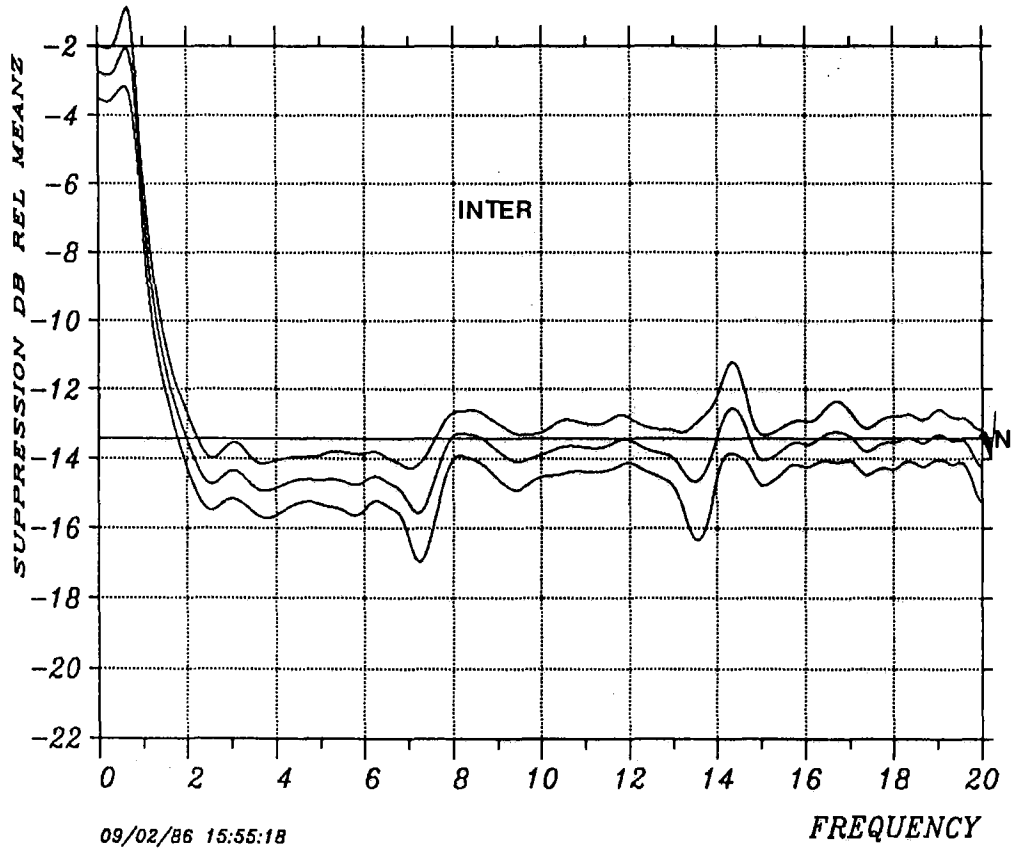

Fig. VII.6.10 Noise suppression for INTER subgeometry week 30, 1986. The curves plotted are average noise suppression spectrum together with plus/minus one standard deviation.

86 WEEK 30 TIME 202: 0 208.23

ALLV Beam Power - Average SPZ Power

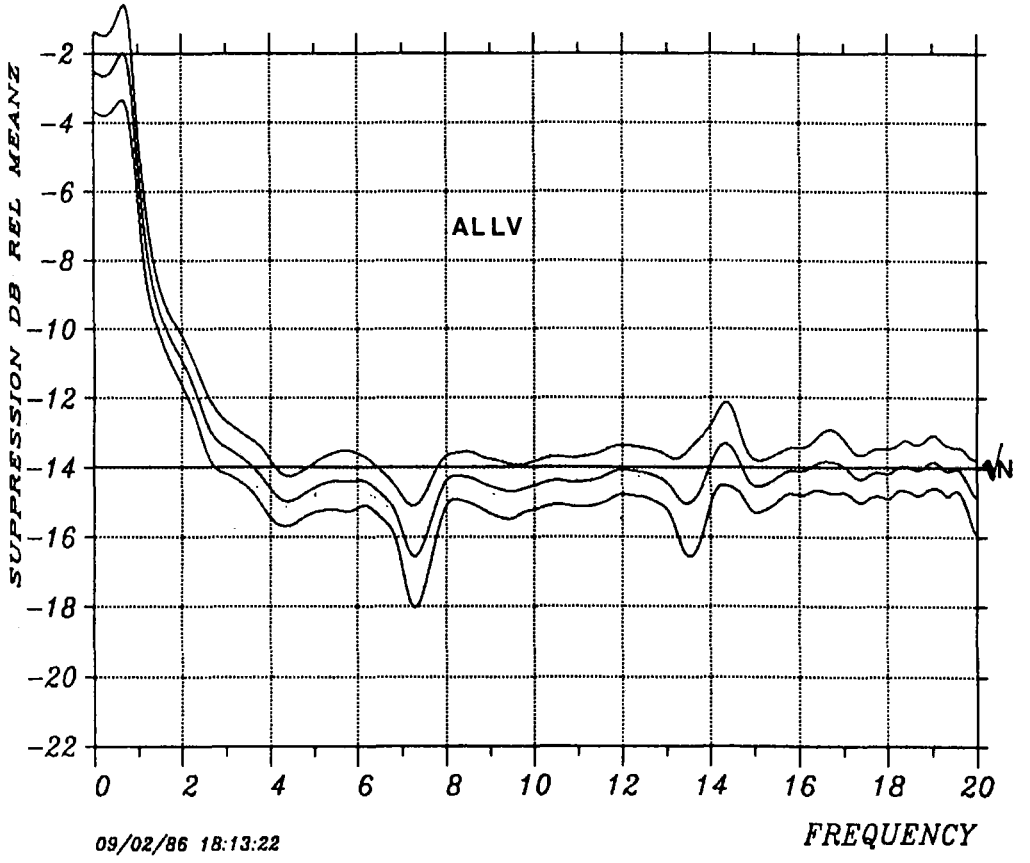

Fig. VII.6.11 Noise suppression for full array geometry week 30, 1986. The curves plotted are average noise suppression spectrum together with plus/minus one standard deviation.

86 TIME 062:00 187:23 (02 LOCAL)

7 CRING Beam Power - Average SPZ Power

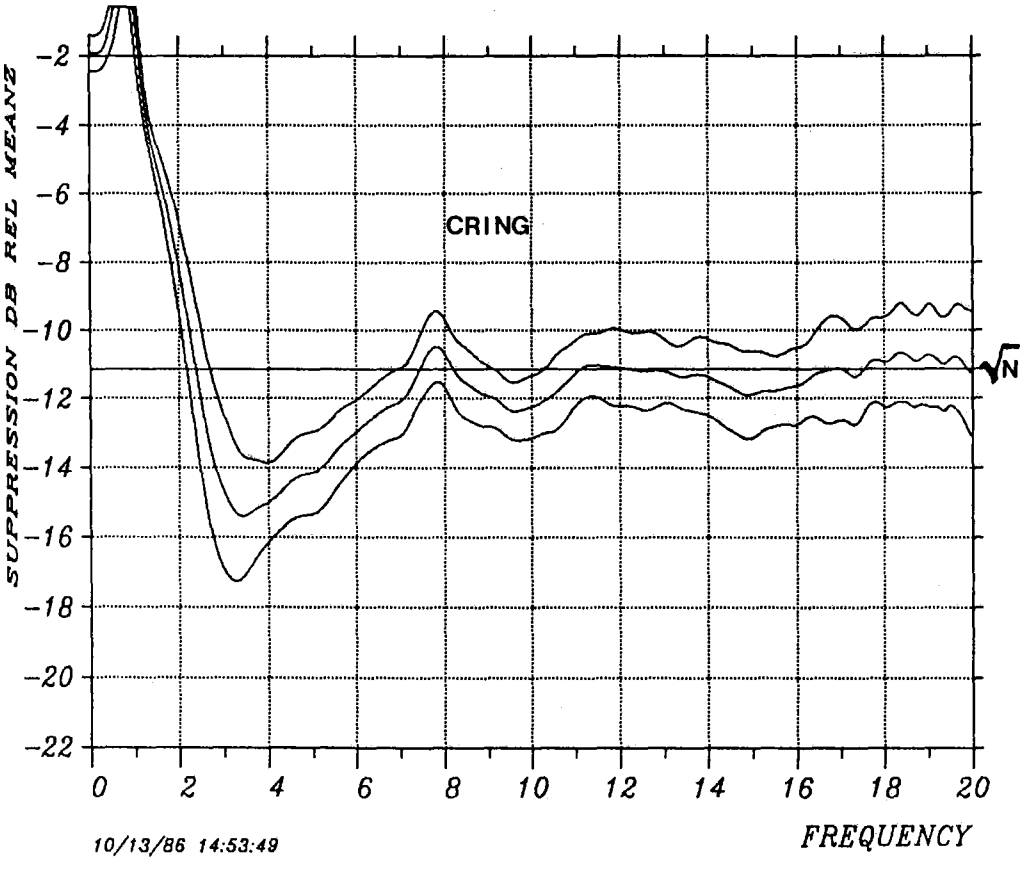

Fig. VII.6.12 Noise suppression for CRING subgeometry observed during the period day 062 through 187 for local times 02 only. The curves plotted are average noise suppression spectrum together with plus/minus one standard deviation.

86 TIME 062:00 187:23 (02 LOCAL)

9 TELEV Beam Power - Average SPZ Power

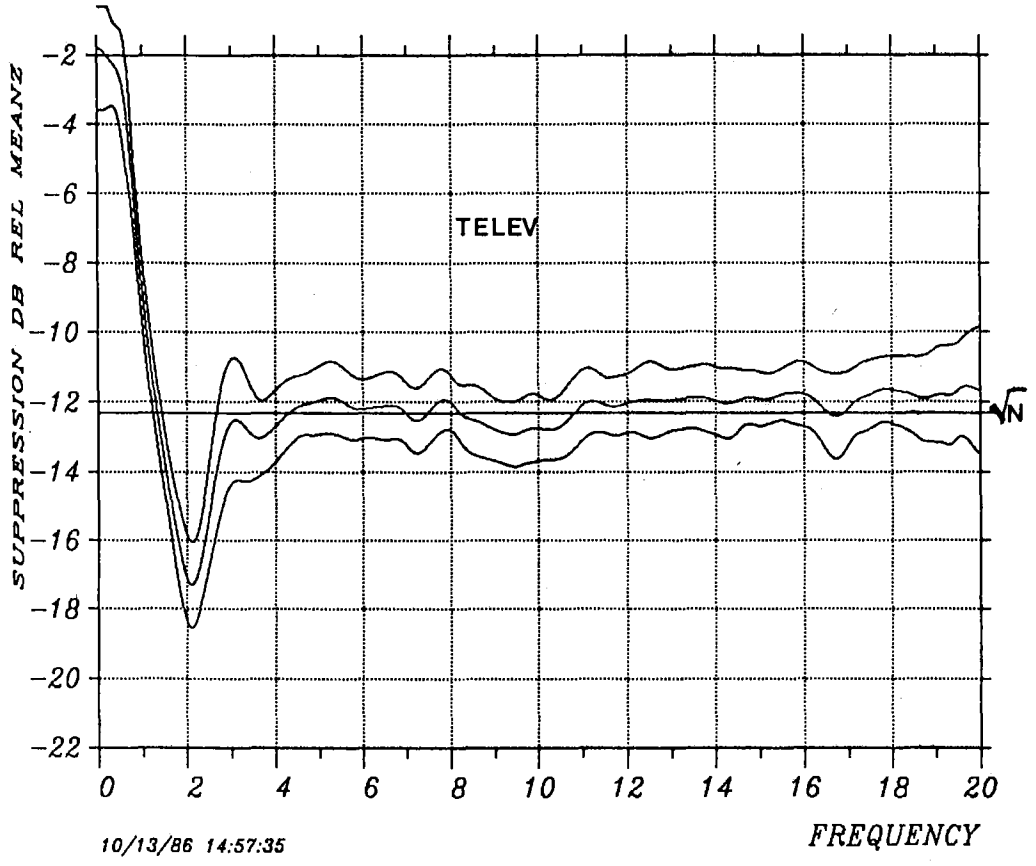

Fig. VII.6.13 Noise suppression for TELEV subgeometry observed during the period day 062 through 187 for local times 02 only. The curves plotted are average noise suppression spectrum together with plus/minus one standard deviation.

WEEK 30, 1986, AVERAGE NOISE SUPPRESSION

BRING CRING TELEV INTER HIFRQ ALLV

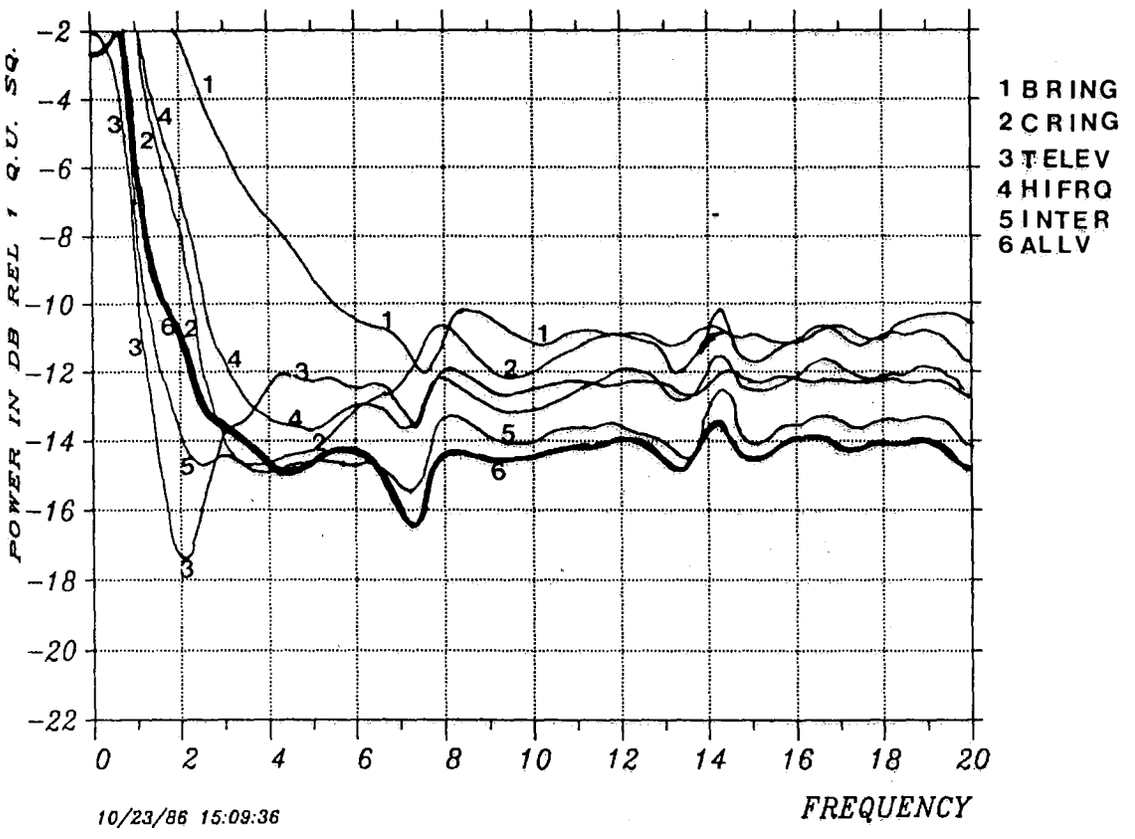

Fig. VII.6.14 Noise suppression for 6 different NORESS array geometries based on week 30, 1986. The curves plotted are average noise suppression spectrum for each geometry. The bold line is the full array, ALLV.

VII.7 NORESS noise spectral studies - noise level characteristics

We refer to section VII.5 for description of the NORESS noise spectral system.

In this part of the NORESS noise studies, we will report the characteristic features of the seismic background noise with respect to diurnal and seasonal variations, especially at frequency ranges from 2 Hz and up. For lower frequencies a number of earlier studies are available, and microseismic long period background noise will therefore not be discussed in this summary. The features that will be emphasized in particular are those relevant to detection capability.

Figs. VII.7.1 through VII.7.3 are selected to illustrate the diurnal noise variation at NORESS. The figures show NORESS average SPZ power (MEANZ) versus time of week, for selected frequency bands. The center frequencies are identified on the plot and the bandwidth is 0.2 Hz. The weeks we have chosen as representative are week 15 , week 30 and week 31 of 1986. Week 30 is the last week of a three-week vacation period in Norway. Nearly all industry close during this period. Therefore week 30 and 31 represent summertime observations without and with industry activities, respectively. On the other hand, week 15 represent near winter-time conditions, as there is still frost in the ground during that week.

The figures show that at frequencies above 2 Hz there are pronounced peaks during working hours, whereas at lower frequencies no strong correlation with working hours can be found. Our experience is that the 0.5 Hz frequency noise level correlates well with the average unfiltered noise root-mean-squeare of SPZ instruments, thus illustrating the overall noise level.

When correlating the variations in noise power in the 0.5 Hz band, with power variations for frequencies above 2.0 Hz, we see that large fluctuations in the noise level (5 dB and more) at 0.5 Hz are not reflected at the higher frequencies. This pattern is observable for each of the three weeks displayed in Figures VII.7.1 - VII.7.3.

The typical noise pattern during working days, for most frequencies above 2 Hz, is a raise in noise power of 5 - 8 dB during normal working hours. The noise power is at a minimum level during the GMT hours 23 - 04. Then the power increases to a maximum lasting 6 - 8 hours. Thereafter, the noise power decays down to the night-time minimum.

A different pattern is seen for the frequencies 6, 12 and 18 Hz. It is down to a minimum for the same hours, but increases much more steeply to a maximum which lasts for 8 - 16 hours. In NORSAR Scientific report No. 2-85/86 we identified this as energy coming from a sawmill 15 km east of the NORESS center. In that report, details of the first working day of week 15 were plotted.

We have checked our observations against the operational times of the sawmill, and their statistics concerning days with and without activity, days with 8 and 16 hours operation, respectively, have all shown excellent correlation with our data. The sawmill operates 2 vertical ram saws, each with a mass of 5000 kg oscillating 365 times per minute (6.08 HZ). A neighboring factory also operates heavy heat-producing equipment all night through, but not during weekends. This latter information may explain the fact why the night-time minima we observe between working days always are somewhat higher than weekend minimum values.

Looking at week 30 (Fig. VII.7.2), at which time both of the above-mentioned plants have been closed, we still see a noise increase, presumably due to cultural activities, during working hours. Moreover, by comparing week 30 and 31 (Figs. VII.7.2 and VII.7.3), we note that the noise patterns are practically identical, except for the 6, 12, and 18 Hz bands and frequencies below 2 Hz. We also see that night-time minima during week 30 are closer to weekend minima.

Saturdays also indicate some day time noise increase, and this has been consistent during the reporting period. We may for some weeks also see some increase in noise level on Sundays.

The interpretation of all the data is that the NORESS noise is influenced by cultural activities during working hours, and that the pattern, when excluding the mentioned sawmill, is similar during both active and vacation periods of the nearby industry.

The noise level is increased 5 - 8 dB during 6 - 8 hours of a working day, and the sawmill 15 km east of NORESS contributes with additional 4 - 5 dB noise level increase for 6 , 12 and 18 Hz only, and extends the period to 16 hours (during periods where the sawmill has enough timber to operate two shifts).

Heavy traffic on roads may explain some of the daily cultural activity. This is not easily confirmed by the observations we have here, but we will make some comments to this source of noise: Car traffic is expected to reach maxima on mornings and around end of working hours. The noise power observed show, however, a maximum value which last for 6 hours during the middle of the working day. Car traffic is particularly heavy on the second day of Easter. Inspecting this day, we have seen that noise level for frequencies above 2 Hz increases by 3 dB during day time, whereas total noise level decreases about 3 dB,

which indicates that the increase in noise level at higher frequencies may be due to peak traffic.

Noise level on Saturdays has a peak level before 12 GMT, whereas noise level on Sundays has a peak after 12 GMT (if a peak at all can be seen). This sunday afternoon effect may support the assertion that the cultural noise source is weekend traffic. However, looking at noise pattern on Friday afternoons and comparing with other days, we see no indications for weekend traffic. Thus, any correlation between car traffic and NORESS noise level, is likely to be marginal.

Seasonal variations

We have indicated that the noise level above 2.0 Hz show rather small variation when compared to the overall noise level. Figs. VII.7.4 - VII.7.6 have been chosen to document this fact.

In Fig. VII.7.4 we have plotted average SPZ noise power (MEANZ) for the selected frequencies, but only observations made at local time 02. (GMT 00 or 01). The points are connected, so lacking observations are not shown as gaps in this plot. Fig. VII.7.5 shows average SPZ noise observed at 08 local times only.

The interpretation of the data is as follows: Comparing June data with March, we may conclude that summertime observations show up to 5 dB higher noise level for frequencies above 2 Hz. Again we see that higher frequencies do not follow the larger variations in total noise level, and there is in fact a general decline in the noise level at low frequencies during summer. These effects will be investigated in more detail when a full year of observations have been collected.

A major feature of the plots is the great increase in noise power late April. This apparently is due to ice-melting in rivers close to NORESS. The effect is most clear on Fig. VII.7.6 where data for D3Z

and D8Z is shown. About 100m from D8Z is a small river, and we see the highest power increase on this instrument. At the point furthest away from the river, D3Z, the power for frequencies above 5 Hz does not show this pattern. However, the data for the 3.0 Hz band show nearly the same pattern on both sides of the array. Thus, we are apparently dealing with two different noise sources, and the 3 Hz behavior is possible tied to the water flow of the large river Glomma, about 18 km east of the NORESS array.

Inspecting details of all frequencies for this time period, we have found that there is a clear minimum in the noise level at the 1st of June. Thereafter the noise increases again. The increase in noise level is more dominant on the east side of the array (D3Z), and more dominant in the frequency band 2.0 - 5.0 Hz. (Peak at 3.0 Hz). On the west side we see the same pattern, but a second increase in the noise level after June 1st is seen at all frequencies. Moreover, the increase in noise level is smaller for the lower frequencies. We have correlated these observations with operational statistics made by the staff at two electrical power plants by the larger river. At the 1st of June, the river was indeed down to a minimum level. Thereafter the water flow tripled in just 5 days. Moreover, both of the plants were out of operation June 2 through 4, during which period the water flowed through a natural water fall rather than through the turbins.

NORESS High frequency element - HFSE

Figs. VII.7.7 - VII.7.8 are selected to show characteristic features of the high frequency system. Fig. VII.7.7 shows power as a function of time, while Fig. VII.7.8 shows all Z-component spectra for GMT hours 00 and 12, respectively, during week 15. The high frequency element is located in the NORESS central vault and therefore close to the local road. Daily activities in the area are shown very clearly on this system. Spurious high frequency noise (or near-field events) are

for the NORESS array averaged out by using the average of up to 25 instruments, and excluding instruments which are outliers as compared to the other instruments. For the one HFSE instrument the data will naturally show greater variability.

As seen from Fig. VII.7.8, this may result in "outliers" among the noise spectra for HFZ. The peaks around 21 and 29 Hz are apparently due to fans in the vault. A peak resulting from the 50 Hz power supply is also commonly seen on these data.

The HFSE data confirm the results from NORESS SPZ instruments with regard to daily and seasonal variations in the noise level. Furthermore, we can see diurnal noise level variations due to cultural activities for frequencies up to around 50 Hz. (Fig. VII.7.7). In Fig. VII.7.9, this is shown by displaying power spectra for A0Z, D3Z, D8Z and HFZ corrected for system response. The data is from day 318, 00 GMT.

The studies presented here will be further expanded as more data is accumulated. In particular, we plan to evaluate in detail seasonal and diurnal noise level charactersistics at the very high frequency end of the spectrum.

J. Fyen

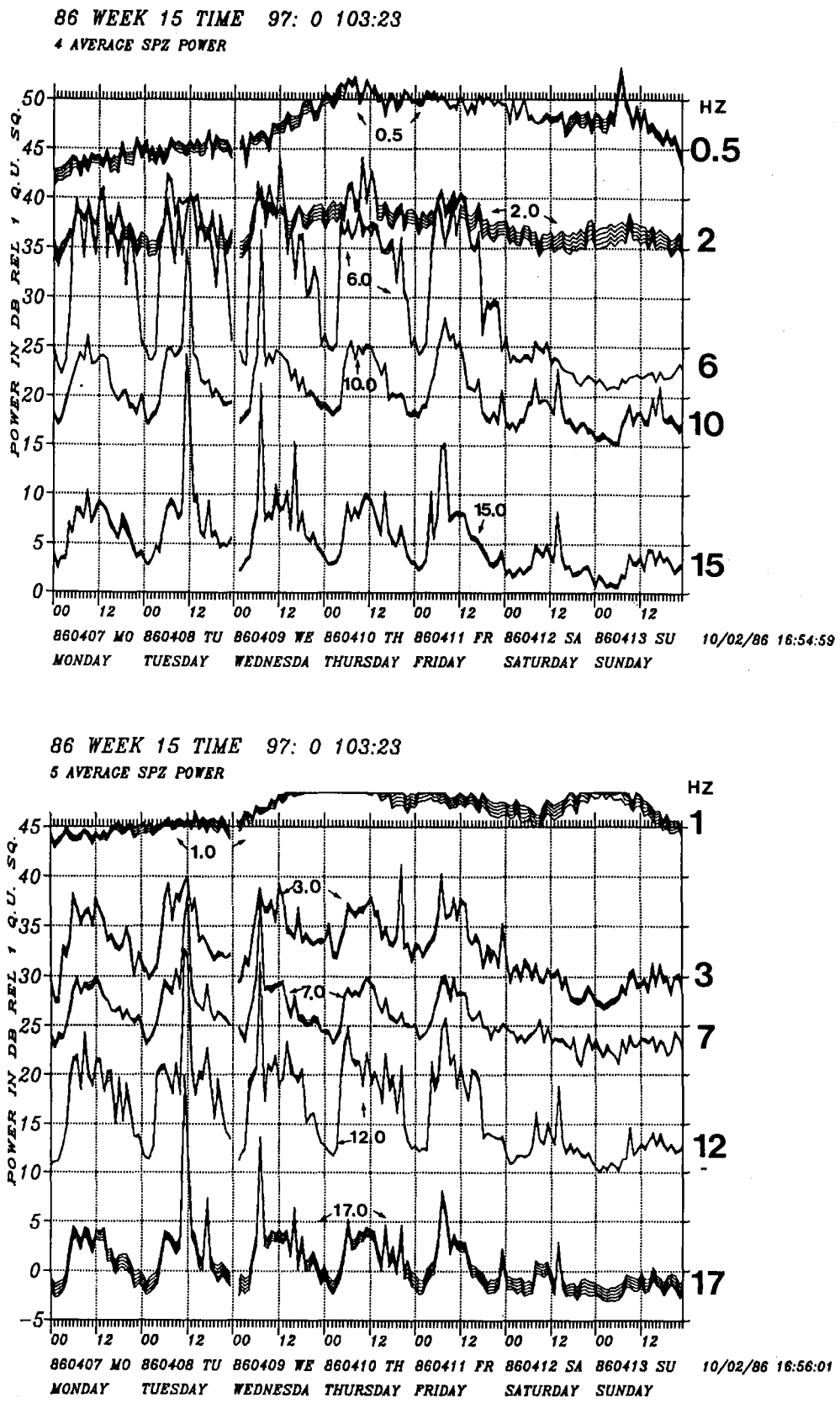

Fig. VII.7.1 Average NORESS SPZ spectral levels plotted on an hourly basis for a one-week period (week 15, 1986). The plots show a sequence of narrow frequency bands (+/- 0.1 Hz around the indicated center frequency). For better legibility, the data are shown in two separate diagrams, (top and bottom) with 5 frequency bands in each.

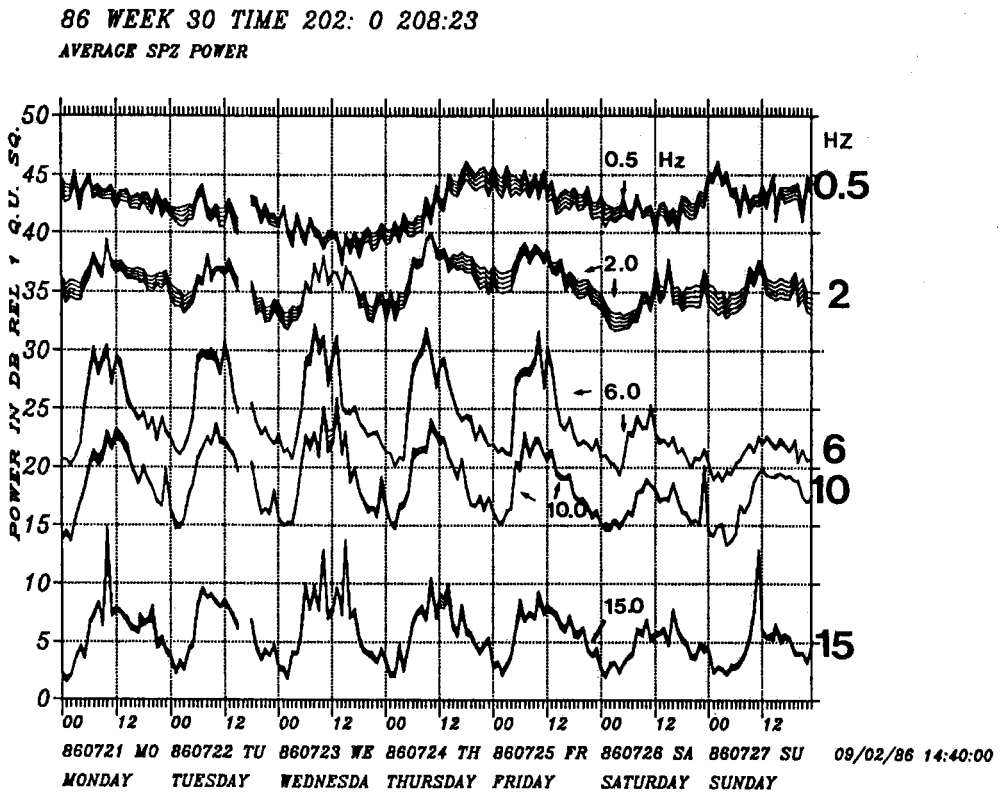

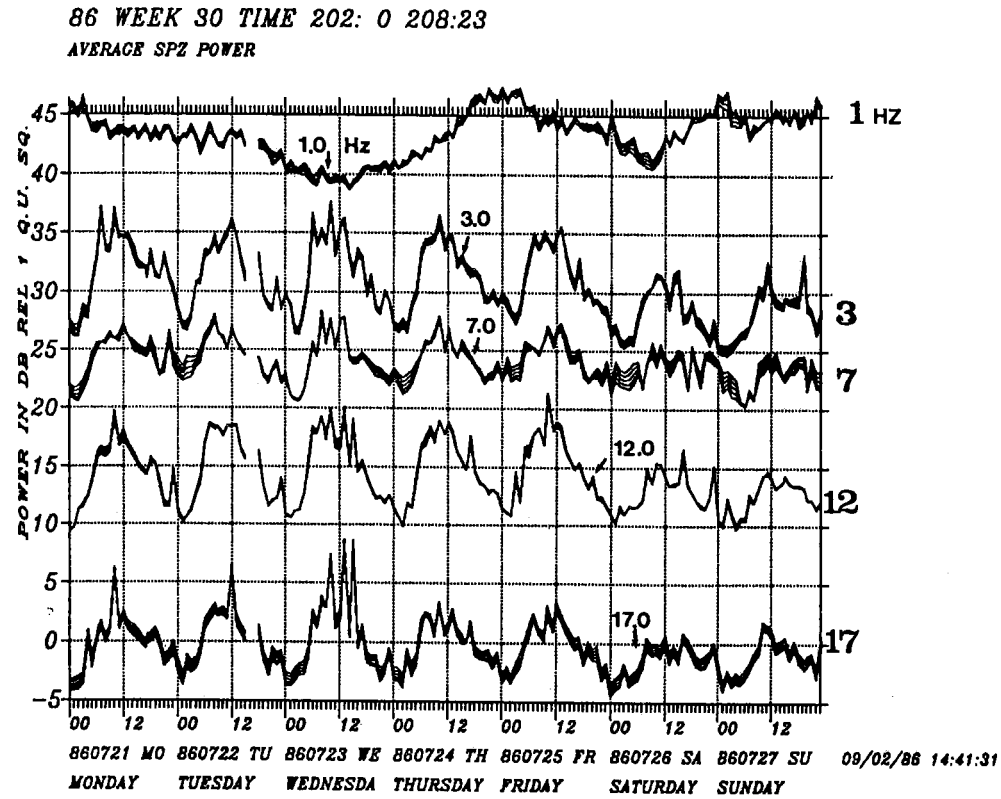

Fig. VII.7.2 NORESS average SPZ power as in Fig. VII.7.1, but for week 30, 1986. Note that week 30 is during industry vacation period.

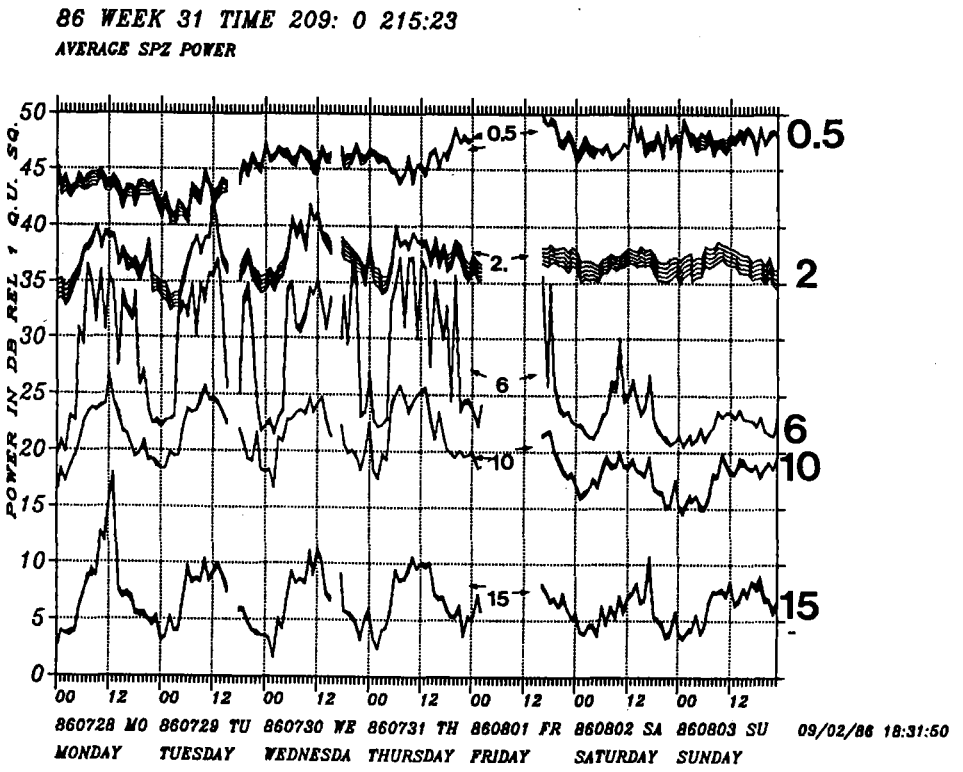

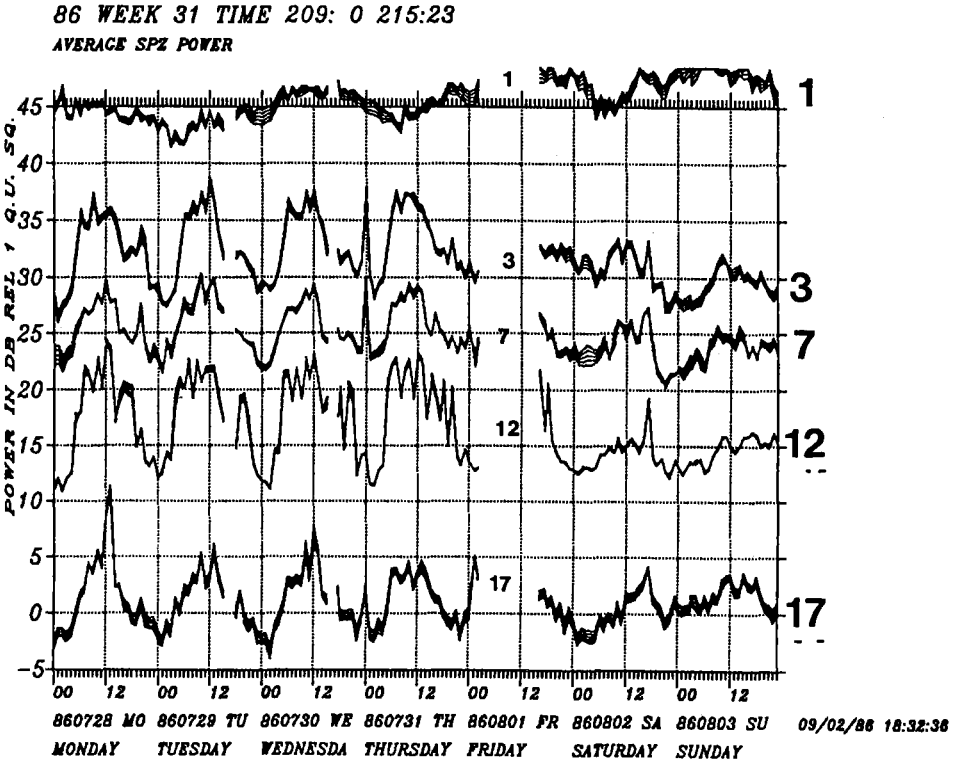

Fig. VII.7.3 NORESS average SPZ power as in Fig. VII.7.1, but for week 31.

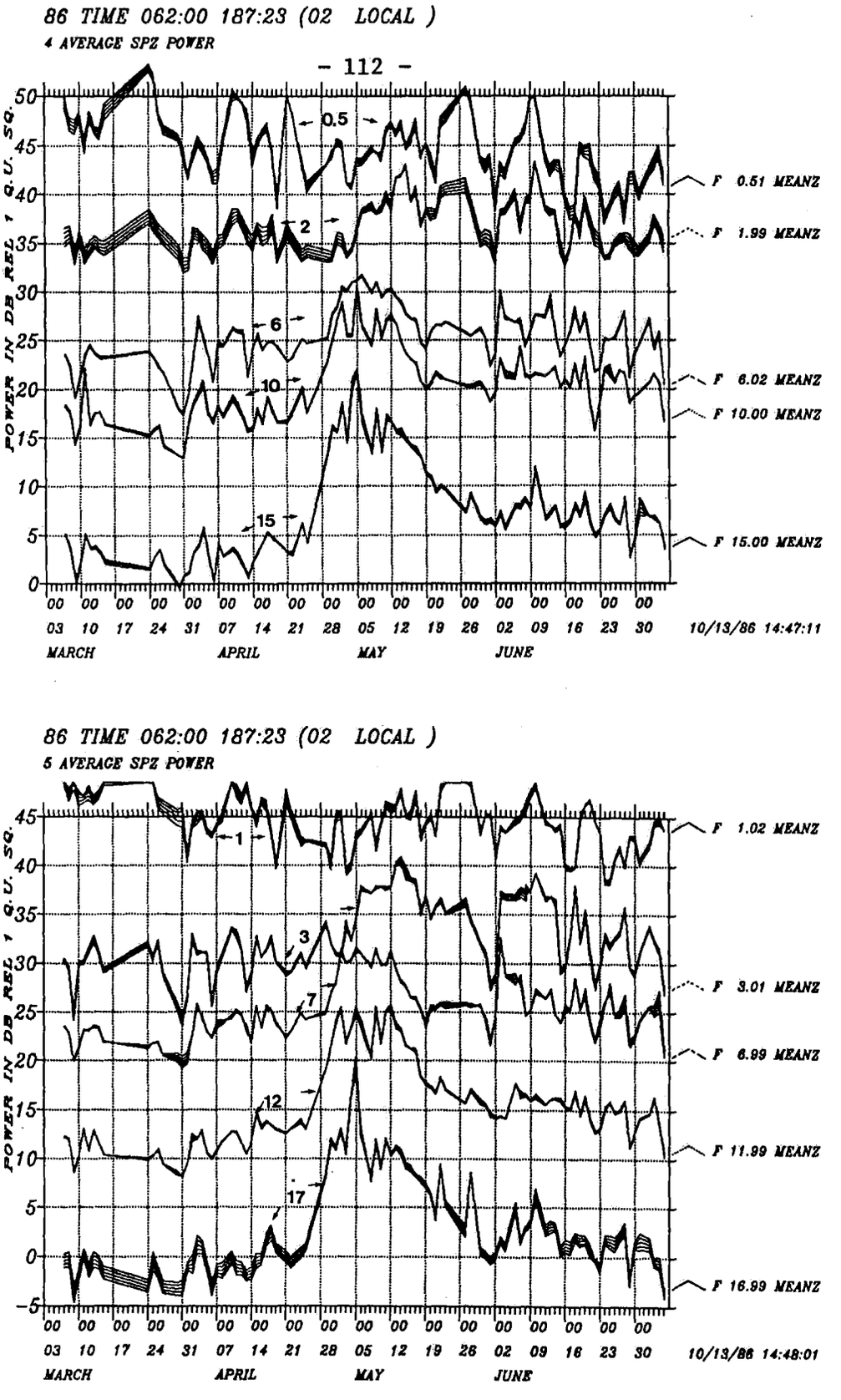

Fig. VII.7.4 NORESS average SPZ power observed at 02 local hours only, for the period day-of-year 062 through 187. There is one data point per day. Minor ticks on time axis is one day. The numbers identify frequency in Hz and the data is observed at these frequencies +/- 0.1 Hz. Points are connected, so lacking observations are not shown. The upper and lower parts of the figure corresponds to different sets of frequencies.

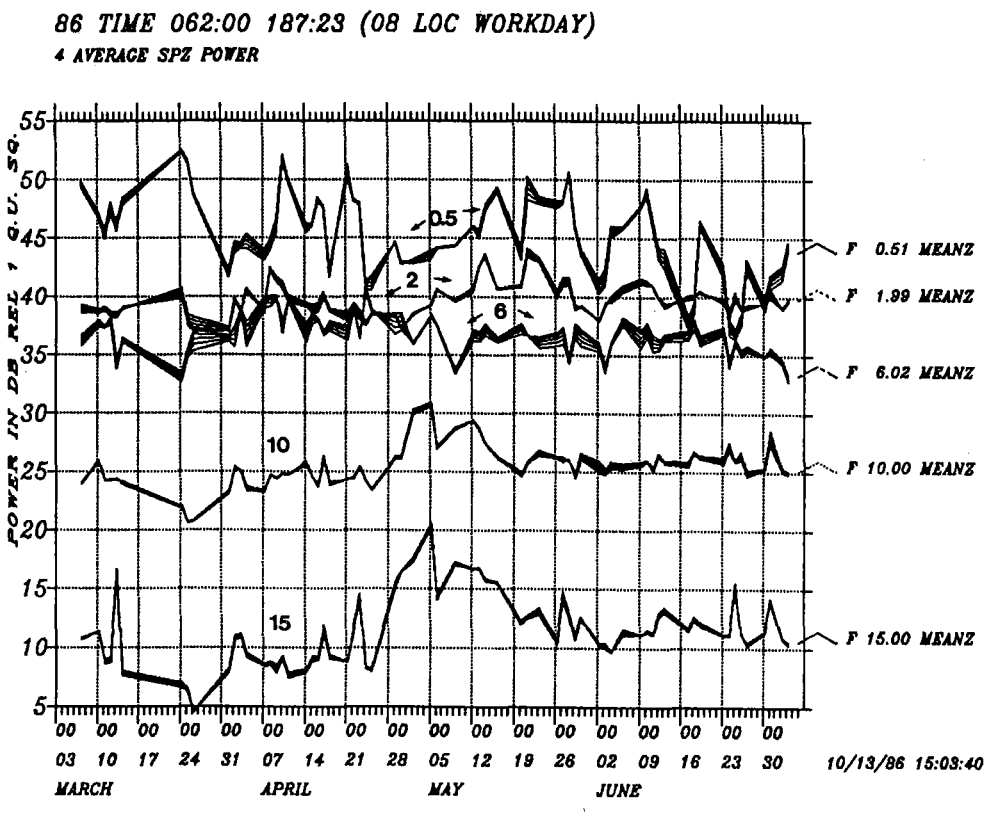

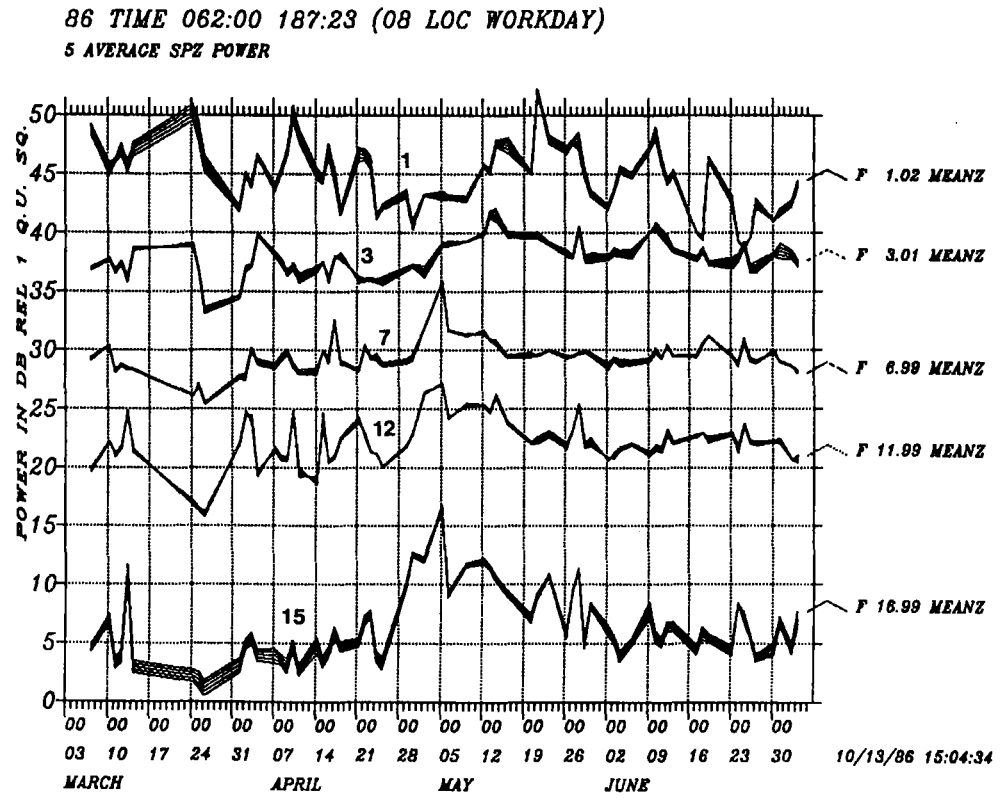

Fig. VII.7.5 NORESS average SPZ power as in Fig. VII.7.4, but observed at 08 local hours only.

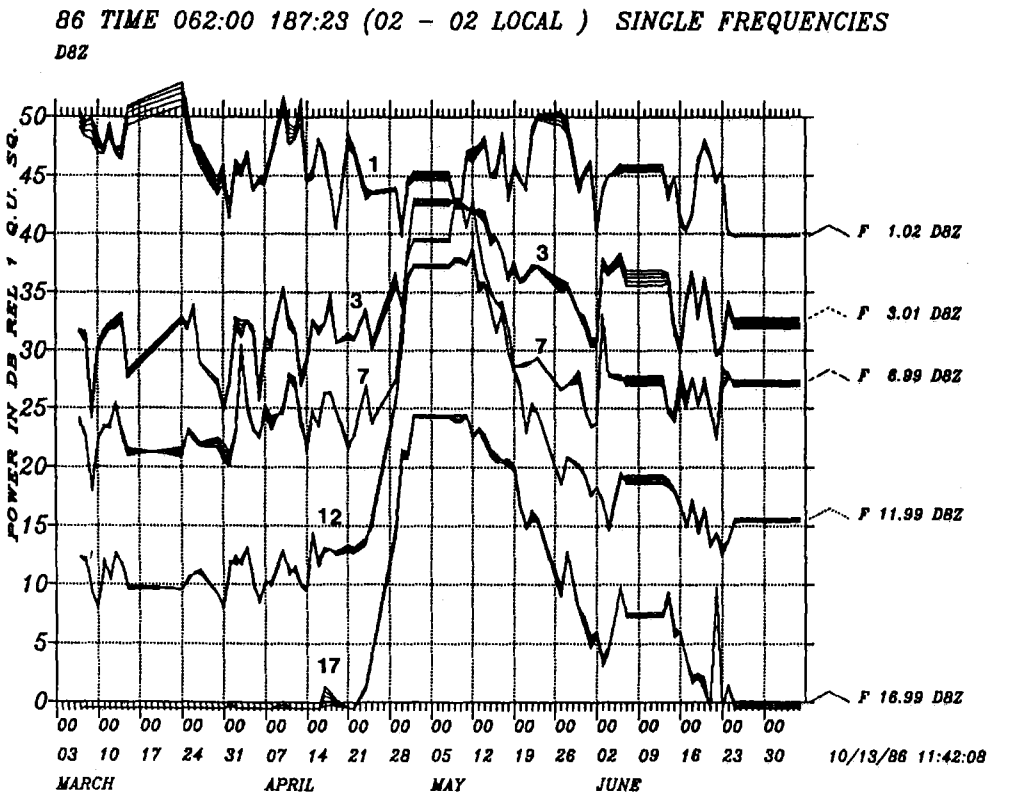

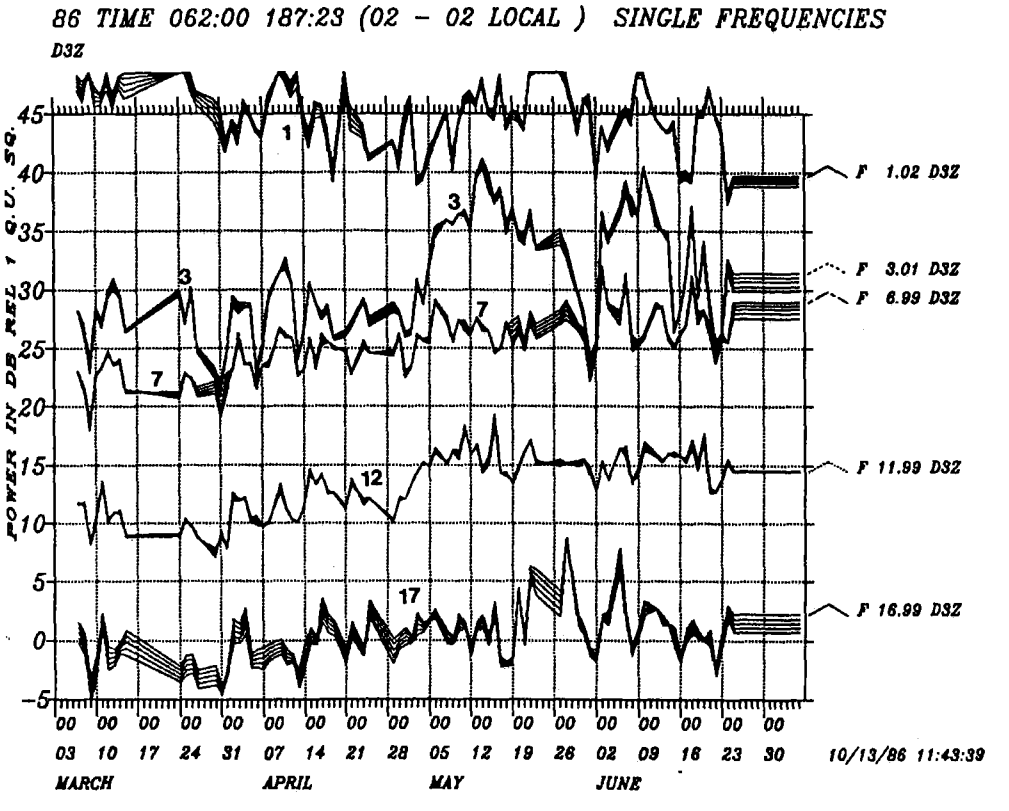

Fig. VII.7.6 NORESS SPZ power for two instruments: D8Z (top) and D3Z (bottom) observed at 02 local hours only.

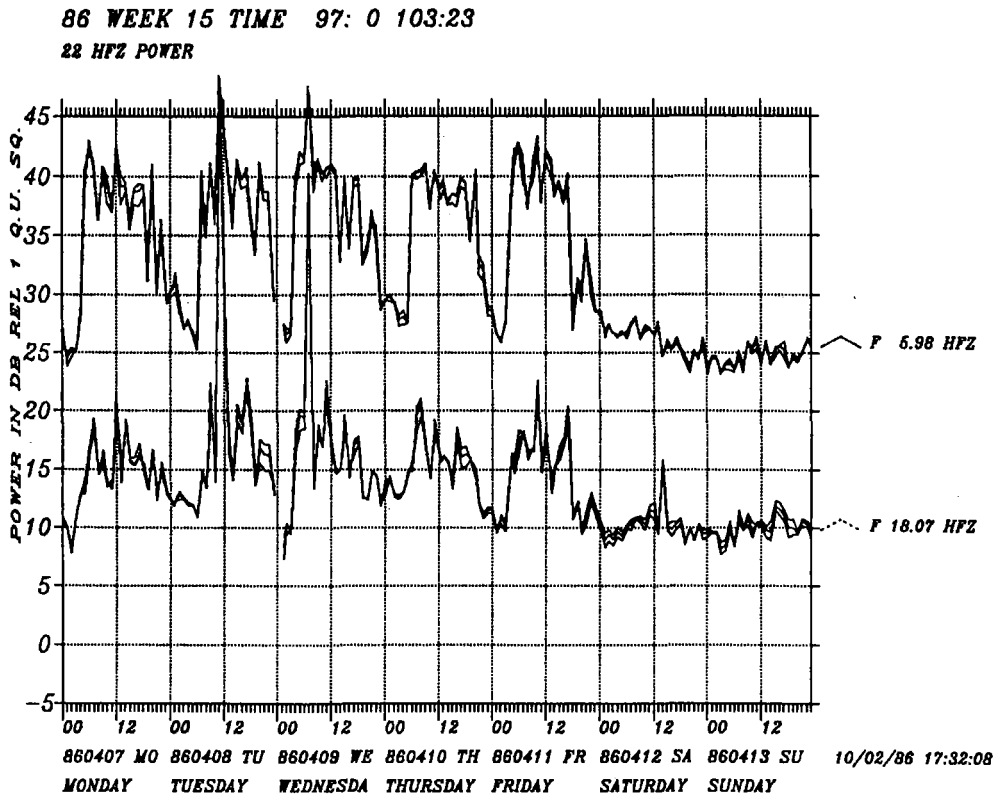

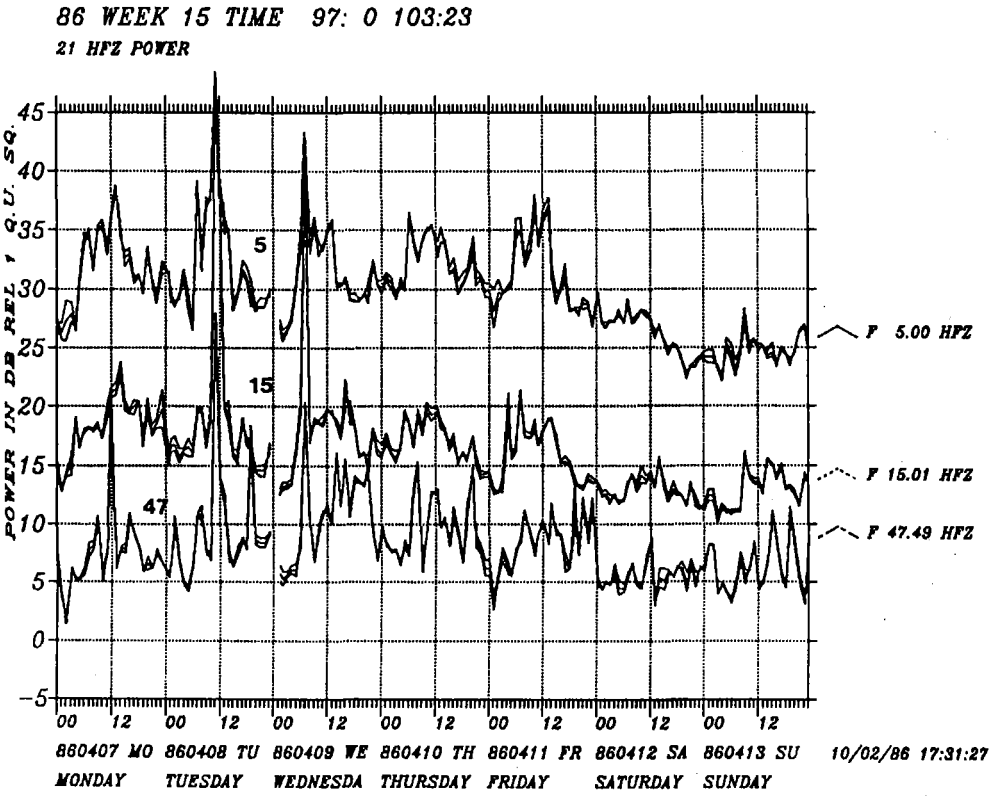

Fig. VII.7.7 NORESS HFSE Z-component power observed during week 15. See the text of Fig. VII.7.1.

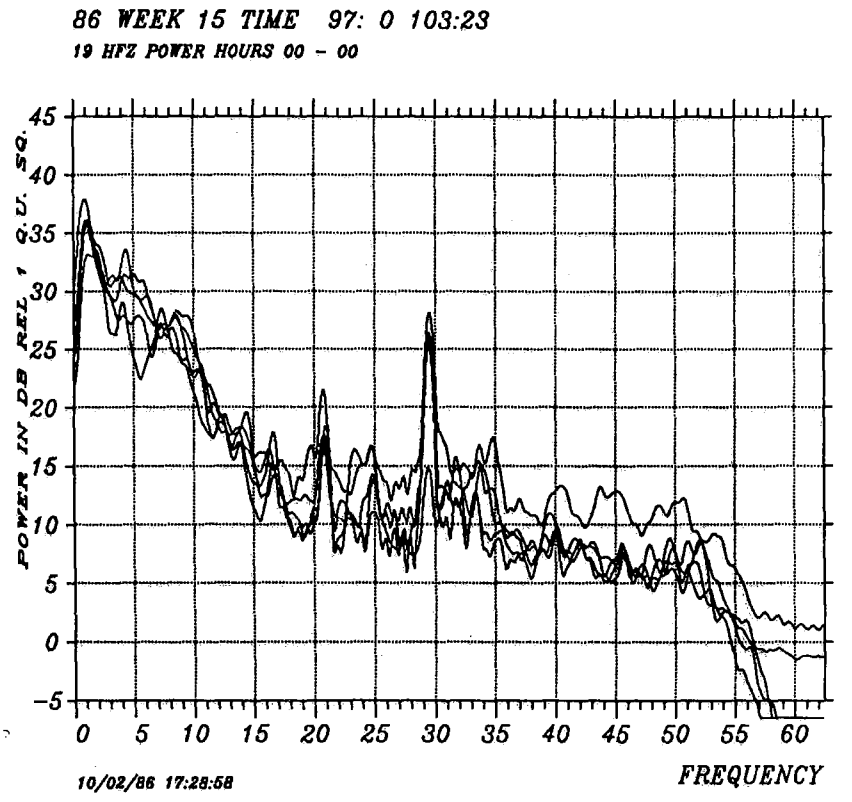

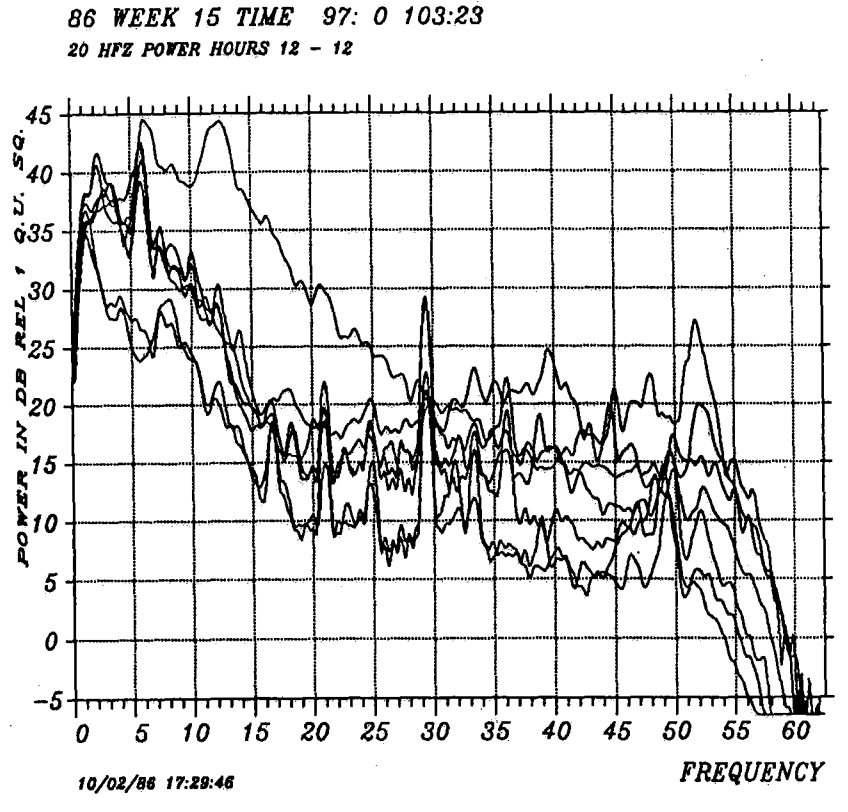

Fig. VII.7.8 NORESS HFSE Z-component spectra observed at two fixed times of day, during week 15, 1986. The top part corresponds to 00 hours GMT, the bottom part to 12 hours GMT.

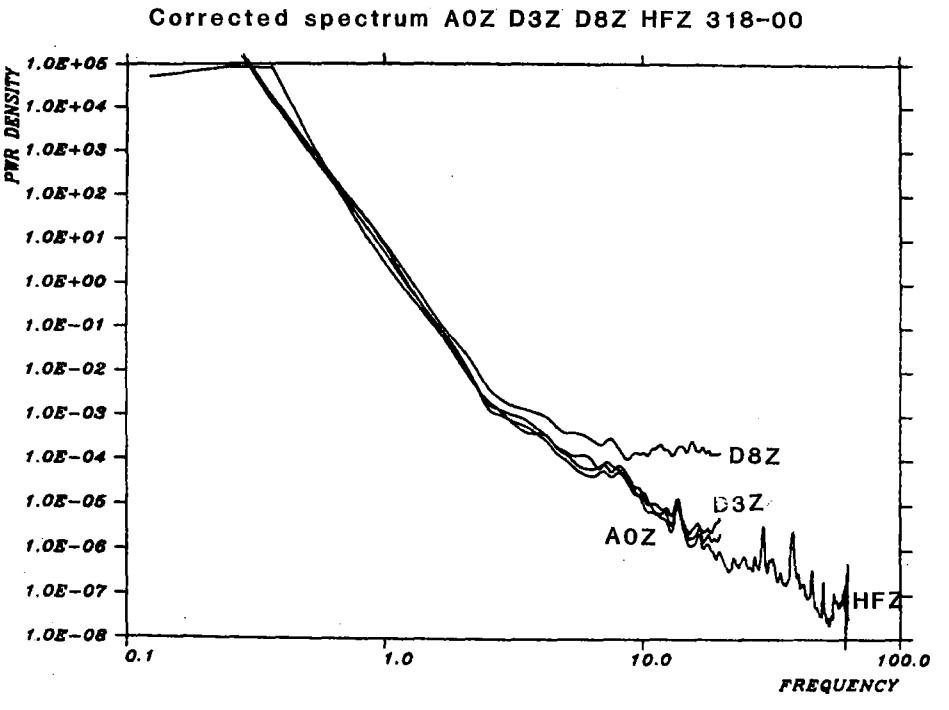

Fig. VII.7.9 Corrected noise spectra for A0Z, D3Z, D8Z, HFZ observed day 318 at 00 GMT. The power density unit is nm^2/Hz.